Selective Covalent Targeting of BFL-1 by Cysteine-Reactive Stapled Peptide Inhibitors to Reactivate Apoptosis in Cancer

Selective Covalent Targeting of BFL-1 by Cysteine-Reactive Stapled Peptide Inhibitors to Reactivate Apoptosis in Cancer

A dissertation presented

by

Rachel Maria Guerra

to

The Division of Medical Sciences

in partial fulfillment of the requirements

for the degree of

Doctor of Philosophy

in the subject of

Biological Chemistry and Molecular Pharmacology

Harvard University

Cambridge, Massachusetts

April 2018

Dissertation Advisor: Dr. Loren Walensky Rachel Maria Guerra

Selective Covalent Targeting of BFL-1 by Cysteine-Reactive Stapled Peptide Inhibitors to Reactivate Apoptosis in Cancer

ABSTRACT

Apoptosis is a highly conserved form of programmed cell death that is essential for organismal development and homeostasis. BCL-2 family proteins regulate mitochondrial apoptosis through homo- and hetero-oligomeric protein interactions. Anti-apoptotic proteins inhibit cell death by trapping the critical □-helical BH3 domain of pro-apoptotic proteins in a surface groove, thereby blocking their conformational activation and mitochondrial poration. Cancer cells hijack this system by overexpressing anti-apoptotic members, resulting in cellular immortality and treatment resistance. Thus, drugging BCL-2 family anti-apoptotic proteins is a high-priority therapeutic goal. Venetoclax is a BCL-2 inhibitor that selectively induces apoptosis in BCL-2-dependent cancers, and it is inspiring the design of next-generation compounds that target individual, subsets, or all anti-apoptotic proteins. BFL-1/A1 is an anti-apoptotic protein implicated in the pathogenesis and chemoresistance of melanoma, lymphoma, and leukemia, but it remains undrugged. As an alternative to small-molecule development, we applied hydrocarbon stapling to transform natural BH3 sequences into □-helical peptide probes and prototype therapeutics to respectively dissect and target the BCL-2 family signaling network. Motivated by the natural juxtaposition of two unique cysteines

at the binding interface between the NOXA BH3 helix and the BFL-1/A1 binding pocket, we developed stapled BH3 peptides bearing acrylamide warheads to irreversibly inhibit BFL-1/A1 through covalent targeting. The cysteine-reactive stapled peptides demonstrate exquisite selectivity for BFL-1/A1 as well as the capacity to trigger more rapid and potent apoptosis of BFL-1-driven cancers compared to their non-reactive analogs. Thus, we present design principles and proof-of-concept validation for covalent stapled peptide inhibitors as a novel therapeutic modality to reactivate apoptosis in cancer.

TABLE OF CONTENTS

ACKNOWLEGEMENTS

The completion of this dissertation would not have been possible without the continued support of many mentors, colleagues, friends, and family. I would like to thank the members of my dissertation advisory committee, Drs. Andi McClatchey, Steve Gygi, and Nika Danial, for your feedback and advice concerning my research during my time in graduate school. I would also like to thank Drs. Andi McClatchey, Wolfram Goessling, Karen Cichowski, and Penny Beuning for kindly agreeing to serve on my dissertation defense committee.

I have been so fortunate to have fantastic mentors to turn to for guidance during these challenging years in pursuit of my thesis. I cannot express enough thanks to my thesis advisor, Dr. Loren Walensky, for his unwavering support and optimism. Any time that I worked late into the night on a paper, grant, or patent, Loren was always up even later working on it too; such example of dedication and drive has been critical in sharpening my own focus when times got tough. Loren's enthusiasm, compassion, commitment to his trainees, and perseverance has truly made this lab a special place to work and learn. I would also like to thank Andi McClatchey, who has served on both my DAC and thesis defense committees; I have been lucky to be able to turn to her for advice and encouragement ever since interning in her lab for a summer as an undergrad. Also I would like to thank Kevin Rice, who provided me with my very first research opportunity as a freshman at Colby College, and who has been such a wonderful mentor and friend for almost a decade now.

The members of the Walensky lab, both past and present, have been so influential in making this lab such a welcoming and supportive community. I have so

valued everyone's advice, support, collaboration, and camaraderie over years. I want to thank in particular Dr. Greg Bird, for all of his brainstorming sessions, insightful discussions, and peptide synthesis. I would also like to acknowledge Dr. Susan Lee for her help with mass spectrometry and mouse protocols. Of course, I must also sincerely thank our lab manager Marina Godes for keeping all lab operations running smoothly. In addition to making this environment so intellectually stimulating and exciting, I want to thank everyone for keeping things lighthearted to balance out the inevitable stress of grad school. I have so many fun memories with the lab, from learning to water ski on lab lake trips to our fantastic yearly holiday dinners.

I cannot thank my close friends enough for their love and support during the ups and downs of this journey. Jess, Cara, and Theresa – you have been such amazing roommates, travel companions, pub trivia teammates, elaborate dinner party cohosts, and more. I will always cherish all of our laughter and memories over the past five years. I also want to express my deepest gratitude to my parents and brothers. Ricky, thanks for keeping me grounded and always providing an understanding and listening ear as you also make your way through grad school in the BBS program. Mark, thanks for your youthful and refreshing outlook on life. I have been lucky to live so close to my family during this time; I am so grateful for being able to make frequent visits home for Sunday family dinners and puppy therapy with Georgie and Grayson. Above all, thank you to my parents, Rose and Rick, for your unconditional love and encouragement. I could not have done this without you.

Chapter I

Introduction

BCL-2 Family Regulation of Apoptosis

Programmed Cell Death in Homeostasis and Development

The lifespan of each cell is governed by a complexity of intersecting signaling networks. These life and death decisions are crucial for maintaining organismal health and homeostasis. The conserved process of programmed cell death, or apoptosis, regulates this equilibrium throughout all metazoa[1]. Apoptosis is genetically-defined, and morphologically and mechanistically distinct from death by necrosis, the autolytic cell death that occurs in response to injury. Each day, approximately 60 billion cells in the average human body die by apoptosis in an effort to counterbalance the 100,000 cells undergoing mitosis every second[1]. Apoptosis plays a major role in development, from sculpting structures in organogenesis, like the interdigital space in vertebrates, to deleting sex-specific structures, such as the removal of Mullerian ducts in males[2,3]. In addition to culling cell numbers, apoptosis is a defensive mechanism, as it eliminates defective and damaged cells that can pose danger, such as auto-reactive immune cells[4].

The concept of programmed natural cell death was first described in 1842 by Carl Vogt who observed dying neuronal cells during the development of toad embryos[5]. In 1885, Walter Flemming, a pioneer of mitosis research, developed histological methods to stain tissues, allowing for the first morphological description of apoptosis, with his drawings depicting cell shrinkage, nuclear fragmentation, and apoptotic body formation[6]. Nearly 100 years later in 1974, Kerr and colleagues formally defined programmed cell death and named it “apoptosis”[7]. Rooted in the Greek word meaning “to fall off”, apoptosis is characterized by distinct morphological features, including

nuclear condensation, membrane blebbing, phagocytosis, and lysosomal degradation. In this seminal publication, Kerr described the physiological role of apoptosis in tissue homeostasis and development, and was the first to propose that apoptosis could become deregulated in tumorigenesis[7]. In contrast to necrosis, which is cell death resulting from external injury and culminating in cell lysis and inducing inflammation, apoptosis does not damage surrounding tissue or cause an immunological response, as apoptotic bodies are rapidly cleared through phagocytosis[8].

The model organism *C. elegans* proved to be a critical system in shaping our understanding of apoptosis as a type of cell death that is genetically controlled during defined stages of development and in response to specific developmental cues. The Nobel prize-winning work of Robert Horvitz and John Sulston provided pioneering insights into the precise control of cell death in the nematode. Nematode development is strictly controlled and highly reproducible, with every individual cell having a predetermined fate[9]. Early light microscopy experiments noted that each nematode is composed of 1090 cells, and exactly 131 cells die by apoptosis over the course of maturation, mostly during embryogenesis[10]. This key observation spurred various forward genetic approaches that resulted in the identification of the cell death genes in *C. elegans*, as well as the hierarchy of the genes that regulate this process.

In screening for genes that disrupt normal cell death, *ced-4* and *ced-3* were identified as essential to the apoptotic process[11]. Further screening revealed that *ced-9* was involved in protection against cell death, and *egl-1* was an activator of apoptosis[12]. Studies characterizing the sequence and function of these genes revealed CED-4, the *C. elegans* homolog of human APAF1, as an adaptor protein that oligomerizes with

CED-3, a caspase homolog, to form the apoptosome and execute cell death through the cleavage of cellular substrates[9,11]. The anti-apoptotic protein CED-9 contains two BCL-2 homology (BH) domains and negatively regulates CED-3 and CED-4[13], and is negatively regulated itself by the BH3-containing protein EGL-1[12]. Thus, a simplified molecular model of apoptosis in *C. elegans* involves CED-9 sequestering CED-4 at the mitochondria and keeping it inactive in the absence of apoptotic stimuli. Developmental cues for cell death prompt the expression of EGL-1, which can bind CED-9 and release CED-4, allowing it to bind CED-3, form the apoptosome, and cleave substrates to execute apoptosis[14]. Interestingly, the overexpression of the human *Bcl-2* gene in *C. elegans* reduces the number of developmentally programmed cell deaths, demonstrating that BCL-2 can engage the nematode cell death machinery[15]. Thus, it became clear that a core molecular mechanism of cell death was conserved over the course of 500 million years of evolution, highlighting the critical nature of the apoptotic process in homeostasis and development.

The apoptotic pathway in mammals is controlled by a more complex signaling network than in *C. elegans*, though both culminate in the activation of caspases. The executioners of apoptosis, caspases are evolutionarily conserved cysteine proteases that cleave cellular substrates to irreversibly propagate programmed cell death[16]. The caspase substrates are incredibly diverse, targeting thousands of proteins ranging from nuclear lamins to cell cycle regulators, and through these cleavages caspases systematically ensure cellular demise[17,18]. Caspases, both initiator and executioner classes, are kept inactive in the cytosol as zymogens, and require activation through cleavage in order to drive apoptosis.

One route of caspase activation is through the extrinsic pathway, in which apoptosis is triggered by death receptors, such as the FAS or TRAIL receptor. Corresponding death ligands engage these cell surface receptors, whose intracellular death domains oligomerize and recruit FADD and pro-caspase-8 to form the death-induced signaling complex (DISC)[19] (**Figure 1.1, left**). The dimerization of pro-caspase-8 causes auto-activation through self-cleavage, allowing it to directly cleave and activate effector caspases-3, 6, and 7 to execute apoptosis[16]. This apoptotic signal can be further amplified through the mitochondria, as caspase-8 can cleave BH3-only protein BID into tBID, allowing crosstalk with the intrinsic pathway of apoptosis[20].

Alternatively, caspases can be activated through the intrinsic pathway of apoptosis, which is initiated in response to developmental cues or cytotoxic insults, such as stress, viral infection, DNA damage, or growth factor deprivation. This pathway culminates in mitochondrial outer membrane permeabilization (MOMP), irreversibly destroying the integrity of the mitochondrial network and releasing apoptogenic factors from the intermembrane space into the cytosol, including cytochrome *c* and SMAC/DIABLO[21] (**Figure 1.1, right**). Soluble cytochrome *c* can engage the scaffold protein APAF-1, which recruits and activates caspase-9 to form the apoptosome and further cleaves executioner caspases-3 and 7[22,23]. Inhibitors of apoptosis proteins (IAPs) reside in the cytosol to bind and neutralize caspases, which are in turn antagonized by SMAC/DIABLO upon its release from the mitochondria during MOMP[24,25]. MOMP is highly destructive to a cell and represents the ultimate commitment to apoptosis. Therefore, it is not surprising that MOMP is the most tightly

Figure 1.1 *The extrinsic and intrinsic pathways of apoptosis*.

The extrinsic pathway of apoptosis (left) is driven by the binding of death ligands to cell surface death receptors, resulting in intracellular clustering of receptor components, adaptor proteins, and pro-caspase-8 to form the death-inducing signaling complex (DISC). DISC formation results in the cleavage and activation of initiator caspase-8, which can further cleave executioner caspases-3/7, allowing them to proteolytically dismantle their cellular substrates and execute apoptosis. The intrinsic pathway of apoptosis (right) converges at the mitochondria and is driven by cell stress, including UV damage, infection, growth factor deprivation, and many others. The BCL-2 family controls the critical step of mitochondrial outer membrane permeabilization (MOMP), which releases cytochrome *c* and SMAC/DIABLO from the mitochondrial intermembrane space into the cytosol. Soluble cytochrome *c* binds to the adaptor protein APAF-1, thus forming the apoptosome that cleaves and activates caspase-9. Inhibitor of apoptosis proteins, such as XIAP, reside in the cytosol to inhibit caspases, but this inhibition is derepressed upon the mitochondrial release of SMAC/DIABLO, which inhibits the IAPs. Caspase-9 then cleaves executioner caspases to drive apoptosis. Although the extrinsic apoptotic pathway can operate independently from the mitochondria, amplification can occur through crosstalk with the intrinsic pathway via caspase-8-mediated cleavage of BID to tBID, which then engages BCL-2 family pathway, resulting in MOMP.

Figure 1.1 (Continued)

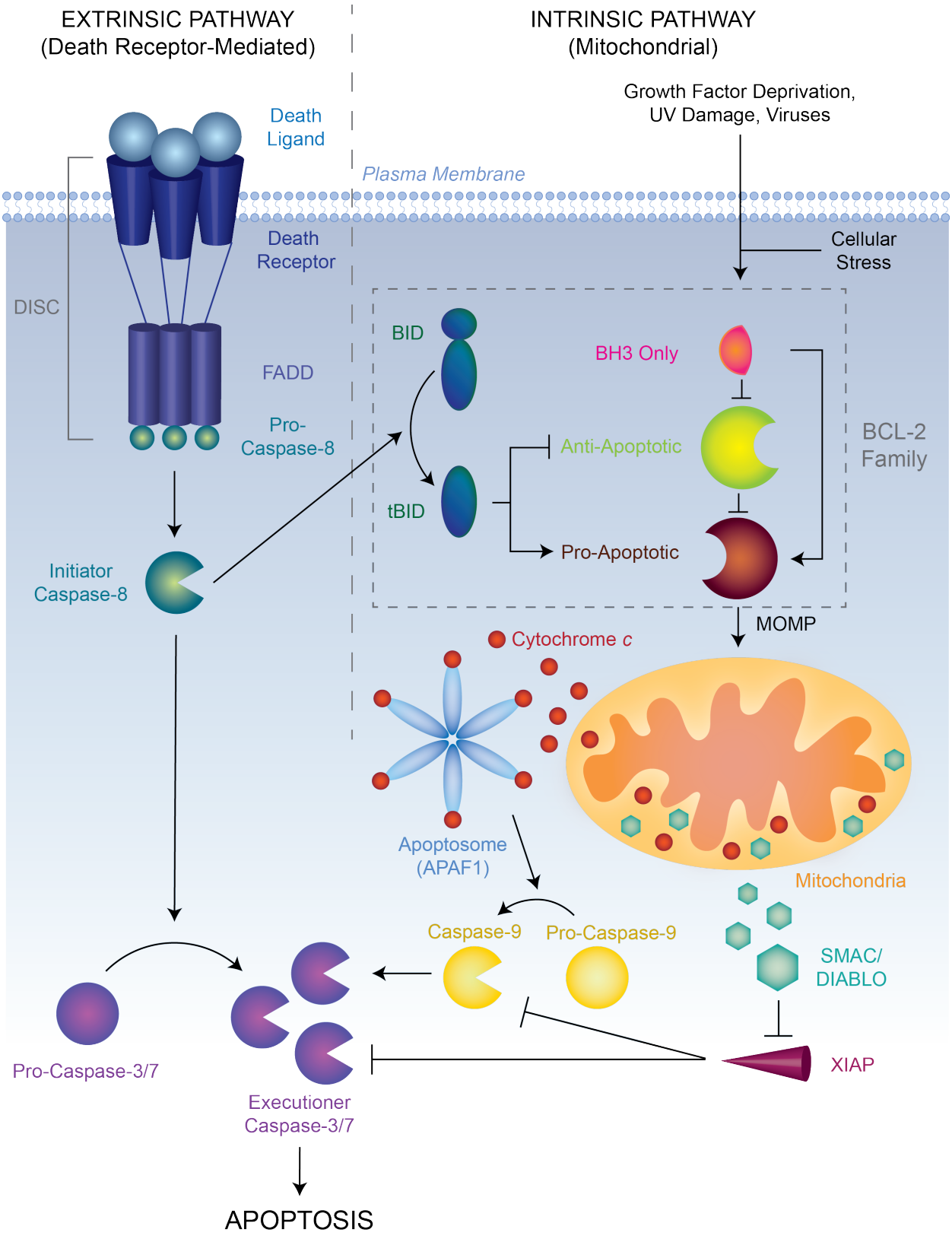

regulated step in apoptosis and is governed by complex interactions among the BCL-2 family of apoptotic regulators.

BCL-2 Family Regulation of Apoptosis at the Mitochondria

BCL-2 family proteins directly regulate apoptosis at the level of the mitochondria through protein-protein interaction. The founding member, BCL-2, was first discovered in 1985 based on cloning of the t(14;18) chromosomal breakpoint in follicular lymphoma, where fusion to the immunoglobulin gene resulted in its dramatic overexpression[26-28]. Initial efforts to functionally characterize this gene revealed that, unlike known oncogenes at the time, BCL-2 did not contribute to proliferation but rather protected against cell death in response to numerous stressors[29,30]. Further efforts revealed that BCL-2 resides at the mitochondria where it directly blocks cytochrome *c* release, thus preventing downstream caspase activation[31-33].

The mechanism of mitochondrial regulation of apoptosis slowly unfolded as a result of the discovery of homologous proteins, now classified as the BCL-2 family of proteins. BCL-2 family proteins can be subdivided into three groups based on their structure, namely the presence of BCL-2 Homology (BH) domains, as well as their function (**Figure 1.2A and 1.2B**).

The multidomain pro-apoptotic proteins, BAX and BAK, act as the mitochondrial executioners of cell death by homo-oligomerizing and forming toxic pores in the outer mitochondrial membrane, resulting in irreversible MOMP[21]. While BAK is constitutively localized to the mitochondrial outer membrane, BAX is cytosolic, where it remains inactive until stimulated by cell stress to undergo a series of conformation changes,

Figure 1.2 *BCL-2 family regulation of mitochondrial apoptosis*.

(**A**) BCL-2 family proteins share sequence and structural homology as evidenced by a series of conserved BCL-2 Homology (BH) domains and a transmembrane helix. (**B** and **C**) BCL-2 family protein interactions mediate the induction of apoptosis at the level of the mitochondria. Upon activation, the multi-domain pro-apoptotic protein BAX (grey) undergoes a series of conformational changes, resulting in mitochondrial translocation and the formation of toxic pores that cause MOMP and the release of cytochrome *c* from the mitochondria. Anti-apoptotic proteins (blue) can directly bind to and entrap the exposed BH3 domain of pro-apoptotic proteins in a hydrophobic surface groove, thereby preventing their activation. BH3-only proteins promote apoptosis through two distinct mechanisms: (1) direct activation of pro-apoptotic proteins and (2) indirect activation by targeting the surface groove of anti-apoptotic proteins, which lowers the apoptotic threshold by releasing pro-apoptotic proteins.

Figure 1.2 (Continued)

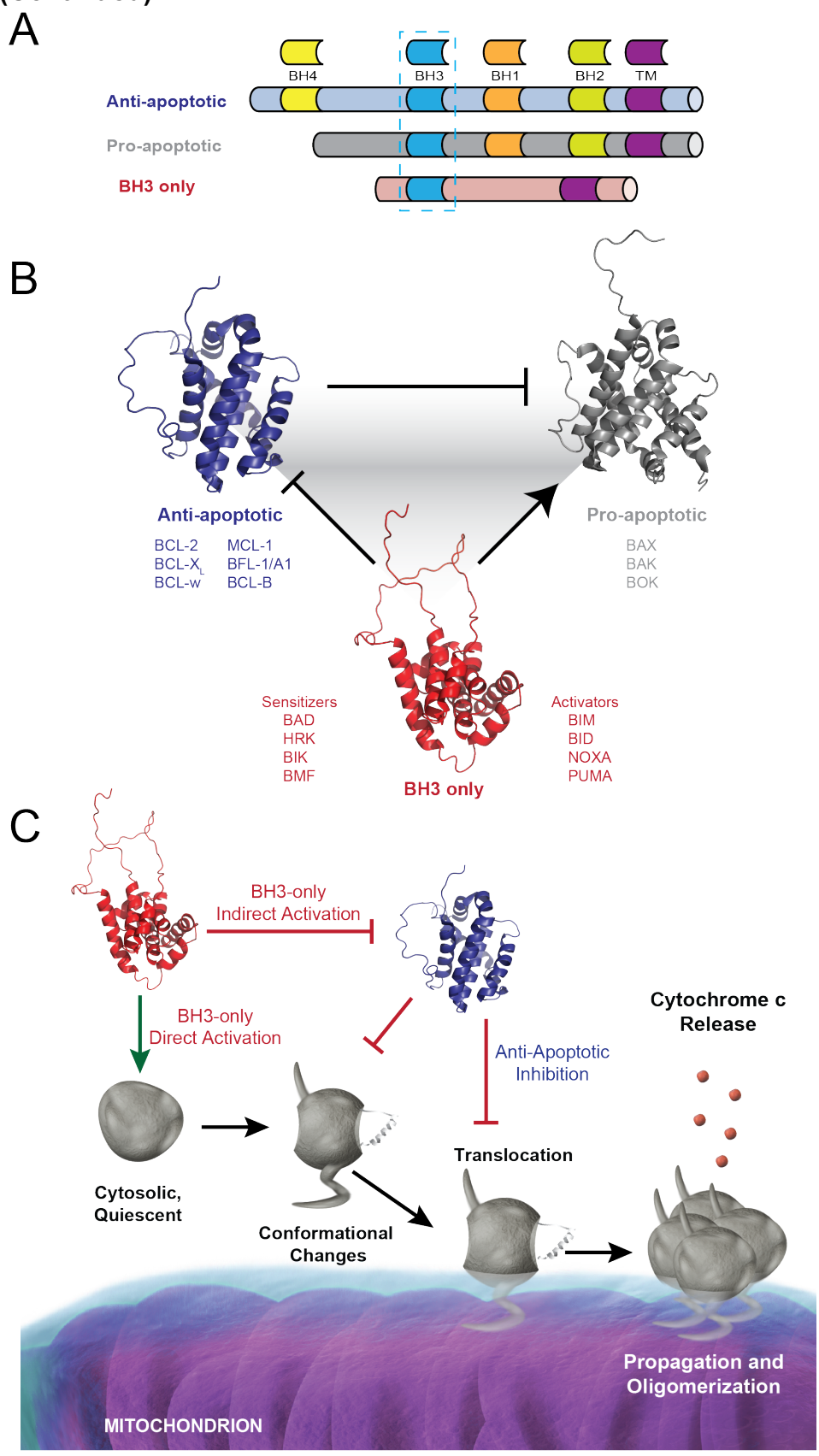

resulting in exposure of its BH3 domain and transmembrane helix, translocation to the mitochondria, oligomerization, and poration[34,35] (**Figure 1.2C**). Although the mechanisms underlying BH3-mediated initiation of BAX activation have been elucidated over the past decade[36,37], the membrane-associated structural modifications that lead to a functional pore remain unknown.

The anti-apoptotic proteins represent a second subgroup of the BCL-2 family, which includes BCL-2, BCL-X_L, BCL-w, MCL-1, BFL-1/A1, and BCL-B. The redundancy of anti-apoptotic proteins in inhibiting cell death, coupled with their differential tissue-specific expression and unique mouse knockout phenotypes, suggests that individual proteins could have tailored functions in regulating apoptotic and perhaps non-apoptotic roles in physiology[38-41]. Anti-apoptotic proteins directly bind to and neutralize the activated conformers of BAX and BAK[42]. Both pro- and anti-apoptotic proteins share structural similarities, with a globular fold comprised of nine conserved α-helices (α1-9), centered around a core hairpin (α5-α6)[43]. Additionally, they share the BH3 'LXXXGD' sequence, the most highly conserved motif of the family[44]. The NMR structure of BCL-X_L bound to the BH3 domain of BAK revealed the structural paradigm governing the regulatory interactions between pro- and anti-apoptotic BCL-2 family members[45]. Helices α2-α5 coalesce to form a hydrophobic surface groove that enables anti-apoptotic proteins to trap the exposed amphipathic BH3 helices of pro-apoptotic proteins, enforcing a formidable apoptotic blockade[45].

An additional layer of regulation is provided by the BH3-only proteins, which engage pro- and anti-apoptotic targets to modulate the apoptotic response. The BH3-only subclass, so named because they only share a single BH domain, includes

members such as BIM, BID, NOXA, BAD, and PUMA, and can promote apoptosis through two mechanisms. Firstly, BH3-only proteins can stably bind and inhibit anti-apoptotic proteins at the conserved surface groove, thus liberating pre-bound pro-apoptotic proteins for activation[46]. Additionally, BH3-only proteins such as BIM and BID can directly and transiently bind to BAX, triggering its conformational activation[36,37]. Various approaches have been taken to map the binding preferences of BH3-only proteins for their pro- and anti-apoptotic counterparts, including yeast two-hybrid analysis, biochemical binding experiments with BH3 peptides, and mitochondrial and liposomal permeabilization experiments[47-49]. BH3-only proteins act as sensors and respond to diverse stress stimuli to induce apoptosis. For example, the expression of NOXA and PUMA is induced transcriptionally by p53 in response to DNA damage, whereas growth factor deprivation can activate BIM and BAD through transcriptional upregulation and post-translational modification, respectively[50-53]. The dynamic interplay between the three subclasses of BCL-2 family interactions results in exquisite control over MOMP, and thus apoptosis induction, during homeostasis and disease.

Deregulation of Apoptosis in Disease

Because apoptosis plays such a critical homeostatic role in balancing cell proliferation and cell death, disruption of this process can result in a broad spectrum of human diseases. Tipping the scale in either direction can lead to diseases of pathologic cell death or unwanted cell survival[54]. For example, a variety of neurodegenerative disorders are characterized by premature neuronal apoptosis, such as in Huntington's, Alzheimer's, and Parkinson's diseases, and in amyotrophic lateral sclerosis (ALS)[55].

Acute tissue hypoxia, such as in ischemic stroke or myocardial infarction, produce distinct patterns of necrotic and apoptotic cell death[55,56]. Deregulated apoptosis in specific cell types can yield hallmark pathologies, such as infertility from aberrant spermatozoa cell death[57] and immunodeficiency from excessive lymphocyte death[4]. Conversely, defective apoptosis in the immune system, through failure to destroy auto-reactive B and T cells during lymphocyte maturation, can lead to autoimmunity[4].

Perhaps the best-characterized pathology due to aberrant apoptotic regulation is cancer, whereby malignant cells usurp the anti-apoptotic arm of the BCL-2 pathway to block apoptosis and enforce cellular immortality. Indeed, characterization of deregulated apoptosis in cancer led to the paradigm shift that cancer not only results from uncontrolled cell proliferation, but also from evasion of cell death[58]. Deregulated apoptosis became known as a hallmark of cancer due to the discovery of *Bcl-2* at the t(14;18) chromosomal translocation in follicular lymphoma, in which the *Bcl-2* gene is fused to the immunoglobulin heavy chain locus, resulting in pathologic overexpression of BCL-2[26-28]. Anti-apoptotic overexpression promotes oncogenesis by allowing transformed cells to withstand a diversity of insults, conferring resistance to proliferative stress, cytotoxic agents, and cancer treatments[30,59]. Indeed, blockade of apoptotic cell death is rampant in cancer and can be attributed to the diversity of anti-apoptotic BCL-2 family proteins. For example, analysis of somatic copy number alterations in over 3000 cancer specimens identified *Mcl-1* as one of the top ten most amplified genes in human cancer[60]. In addition to chromosomal translocations and gene amplifications, anti-apoptotic expression in tumors can be increased through alternate mechanisms, such

as gene hypomethylation and loss of microRNAs that normally suppress pro-survival protein expression[61,62].

Cancers can also evade apoptosis by down-regulating BH3-only proteins. Loss or silencing of BIM expression contributes to the pathogenesis of renal cell carcinoma and mantle cell lymphoma, with approximately 20% of cases displaying homozygous *Bim* deletions[63,64]. Though far less common than anti-apoptotic up-regulation, pro-apoptotic silencing is seen in certain cancer settings as well, such as frameshift mutations in *Bax* that attenuate the apoptotic response in colon cancer[65]. In addition to ensuring cell survival, deregulation of the BCL-2 family is a major contributor to cancer chemoresistance. Anti-apoptotic protein overexpression establishes a formidable roadblock to chemotherapy and radiation treatments[66]. Since BH3-only proteins, such as PUMA and NOXA, transmit pro-death signaling in the context of DNA-damage response, chemoresistance can also arise from loss of BH3-only proteins[67]. Many cancers are genetically unstable and "primed for death" and thus rely on anti-apoptotic addiction to maintain survival and chemoresistance[68]. Thus, drugs that target anti-apoptotic proteins have the potential to resensitize tumors to chemotherapy and synergize with current treatment regimens. Given their prominent role in the survival and resistance of human cancers, the BCL-2 family proteins have emerged as major drug targets for pharmacologic restoration of apoptosis in human cancer.

Structural Paradigm of BCL-2 Family Interactions Provides a Guide for Drug Discovery

Cell survival in cancer is most frequently enforced by upregulation of anti-apoptotic BCL-2 family members. Thus, one therapeutic strategy is to functionally "inhibit the

inhibitors" of apoptosis. Initial efforts to reactivate apoptosis in cancer focused on suppressing the expression of BCL-2 in leukemia through antisense RNA targeting[69]. Antisense RNA knockdown of BCL-2 seemed to improve non-Hodgkin lymphoma patient outcome in a Phase 1 clinical trial[70]. However, this strategy was abandoned due to off-target activity. Subsequent drug development efforts instead focused on small molecule targeting of BCL-2. The path to developing a small molecule BCL-2 inhibitor was enabled by the NMR structure of BCL-X_L in complex with a BAK BH3 peptide[45]. The history of BCL-2 inhibitor drug development provides a remarkable example of how structural insights can guide the discovery and clinical translation of compounds that target pathologic protein interactions.

By elucidating the BH3-in-groove interaction paradigm, Fesik and colleagues at Abbott Laboratories created a blueprint for BCL-2 inhibitor design. They applied a structure-activity relationship (SAR) by NMR approach, which led to the discovery of a potent small molecule inhibitor of the canonical BCL-2/ BCL-X_L groove[71]. This method was used to identify multiple molecular fragments that engaged neighboring sites on the protein target with relatively low affinity. However, when chemically linked together, as guided by the structural data, the composite molecule displayed strikingly high affinity due to binding energy additivity[72]. The lead compound that resulted, ABT-737, bound with subnanomolar affinity for BCL-2, BCL-X_L, and BCL-w[73,74]. ABT-737 effectively mimicked a portion of the α-helical BAD BH3 domain (**Figure 1.3A**), and demonstrated potent *in vivo* activity in xenograft models of human cancers driven by BCL-2 expression, including follicular lymphoma, acute myelogenous leukemia, chronic lymphocytic leukemia, and small cell lung carcinoma[73].

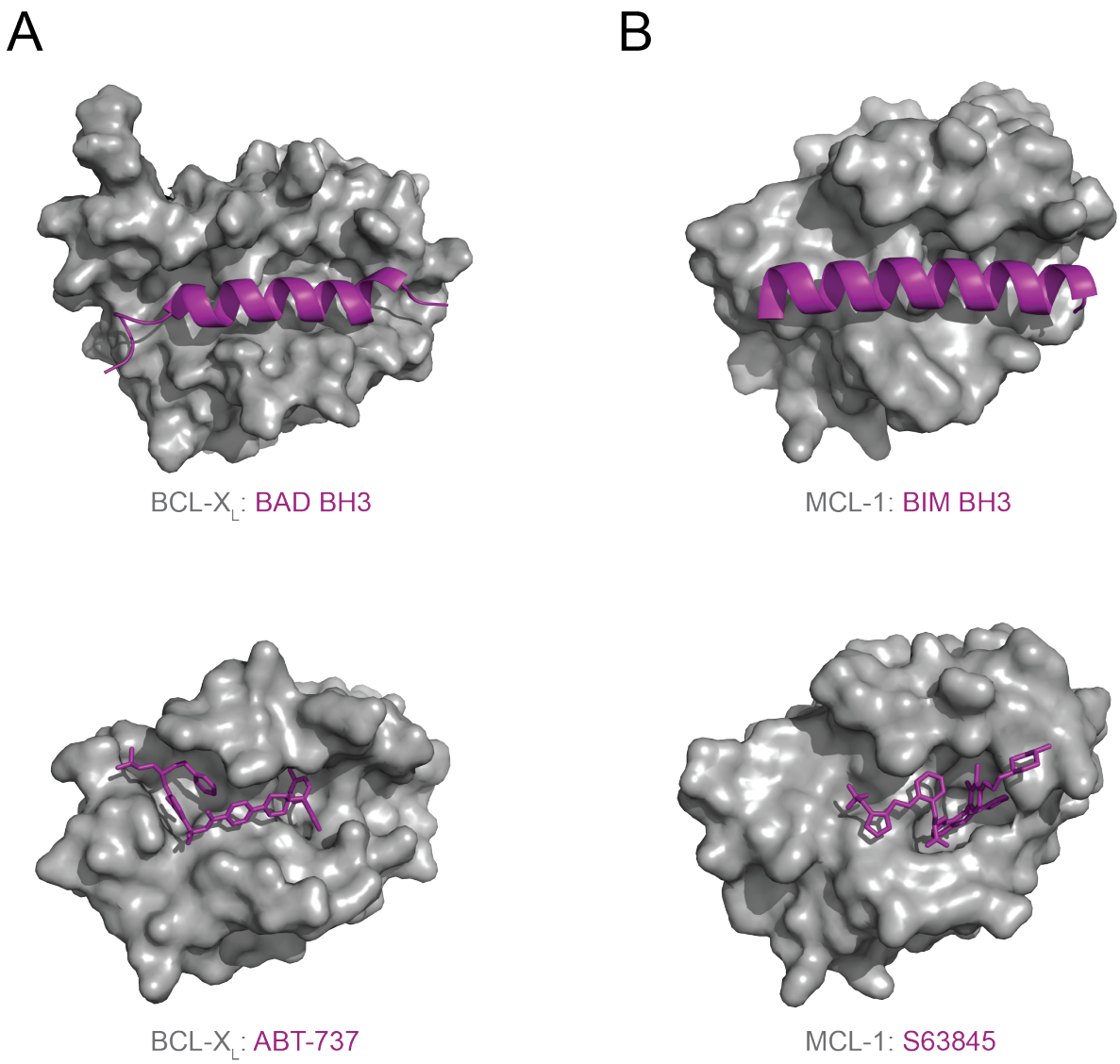

Figure 1.3 *Structural mimicry of compounds designed to inhibit the survival functionality of anti-apoptotic proteins in cancer.*

(**A**) Structure of BCL-X_L bound to a BAD BH3 peptide (top, PDB: 1G5J) and ABT-737 (bottom, PDB: 2YXJ). ABT-737 was modeled after the BAD BH3 domain and represents the first selective small molecule inhibitor of anti-apoptotic BCL-2 family proteins. (**B**) Structure of MCL-1 bound to a BIM BH3 peptide (top, PDB: 2PQK) and small molecule inhibitor S63845 (bottom, PDB: 5LOF). S63845 mimics interactions between BIM BH3 and the MCL-1 hydrophobic groove.

This prototype BCL-2 protein inhibitor was soon followed by a second generation inhibitor, ABT-263 or navitoclax, which was optimized to achieve oral bioavailability for clinical translation[75]. Although navitoclax showed early efficacy in the treatment of hematological malignancies and small cell lung cancer, clinical trials were halted due to dose-limiting thrombocytopenia that derived from targeting BCL-X_L, which turned out to be an essential survival factor of platelets[76,77]. To overcome this limitation, the structure of ABT-263 bound to BCL-2 was used to tailor the interaction for BCL-2 over BCL-X_L, yielding the potent and selective BH3-mimetic ABT-199 or venetoclax[78]. Venetoclax potently and specifically induced apoptosis of BCL-2-dependent cancers while avoiding dose-limiting thrombocytopenia. Over thirty years of BCL-2 family research led to FDA approval of venetoclax in 2016 for the treatment of patients with 17p-deleted CLL. Venetoclax is currently being tested in AML, non-Hodgkin's lymphoma, multiple myeloma, and breast cancer, both as a single agent and in combination with a host of other chemotherapeutic agents.

Invigorated by the clinical success of venetoclax, scientists in academia and pharma alike have expanded their screening efforts to target the canonical binding grooves of other anti-apoptotic targets, including the especially pervasive and malicious anti-apoptotic protein MCL-1[79-81] (**Figure 1.3B**). Most recently, the small molecule S63845 was shown to potently and selectively target MCL-1, inducing apoptosis of various MCL-1-dependent cancers in culture and *in vivo*[81]. Phase 1 testing of S63845 in AML and MDS is currently underway. Since cancer cells can express a variety of anti-apoptotic proteins to ensure their survival, developing a spectrum of inhibitors that target individual, subsets, and even all anti-apoptotic targets remains a pressing goal.

The Anti-Apoptotic Protein BFL-1/A1

Physiological Role and Expression Pattern of BFL-1

The anti-apoptotic BCL-2 family member *Bfl-1* is located on human chromosome 15q24.3 and encodes a 175-amino acid protein comprised of nine conserved α-helices[82]. BFL-1, also known as BCL2A1 or mouse A1, was first discovered in mice as an early-response gene in hematopoietic cells upon treatment with granulocyte-macrophage colony stimulating growth factor (GM-CSF), and was noted to have sequence similarity to the murine *Bcl-2* and *Mcl-1* genes[83]. The human homologue was subsequently cloned by two groups, and was found to be abundant in fetal liver tissue[84] and endothelial cells[85], and shares 72% sequence homology with the mouse gene. Early experiments in mice revealed four gene copies of murine *A1* and, like BCL-2, A1 was required for myeloid precursor cell survival upon growth-factor withdrawal[86] and primarily expressed in hematopoietic cells, including B and T cells, neutrophils, macrophages, and dendritic cells[87]. BFL-1/A1 contained the hallmark BH1, BH2, and BH3 domains and its overexpression was shown to be sufficient to suppress p53-induced apoptosis[88]. Mutational analysis of BFL-1 demonstrated that the BH1, BH2, and C-terminal domains were critical for this anti-apoptotic function[89].

Numerous genetic and biochemical studies have demonstrated the pro-survival functionality of BFL-1 within the mitochondrial pathway of apoptosis. Yeast two-hybrid experiments revealed that BFL-1 heterodimerizes with BAX and blocks its pro-apoptotic activity in a manner analogous to BCL-2, and that this interaction is dependent on the presence of the conserved hydrophobic surface groove on BFL-1[90]. Additionally, BFL-1 localizes to the mitochondria, where it is able to sequester tBID and inhibit tBID-induced

BAX activation and apoptosis[91]. Among anti-apoptotic targets, BFL-1's BH3-binding spectrum is most similar to that of MCL-1, engaging tBID, BIM, NOXA, and PUMA; in a cellular context, some studies suggest that BFL-1 displays a binding preference for BH3-only proteins over the BH3-exposed forms of BAX and BAK[82].

With respect to its physiologic function, there are conflicting reports regarding the specific role of BFL-1 in regulating the immune system. Although BFL-1 expression is more widespread in human tissues, including lung, small intestine, and smooth muscle, murine expression is confined to hematopoietic tissues[82]. Murine A1 expression is induced during myeloid differentiation[83], lymphocyte development[92], and lymphocyte activation[83,93], suggesting a role for A1 in immune cell regulation. RNAi and conditional knockdown of A1 in murine hematopoietic lineages revealed defective T cell development, impaired B cell proliferation[94], and reduced survival of activated B cells[95]. Recently, a more comprehensive genetic mouse model has been developed in which the three functional A1 isoforms were knocked out. This BFL-1/A1 knockout model lacks any overt phenotype, with mice displaying only minor defects in the hematopoietic system, including a slight reduction in *γδ*TCR T cell, memory $CD4^+$ T cell, and dendritic cell counts[96]. In examining the role of BFL-1 in T cell activation, the *A1* triple knockout mice displayed a normal T cell response upon acute infection, suggesting a non-essential role for BFL-1 in T cell-mediated immunity[97]. Current efforts are underway to elucidate the precise roles of BFL-1 in regulating murine hematopoiesis and thereby resolve the discrepancies between mouse models.

BFL-1 Regulation and Structure

BFL-1 expression and function are under tight transcriptional and post-translational control. BFL-1 is induced by GM-CSF and TNF-α, and is a direct transcriptional pro-survival target of NF-κB[98,99]. Though initial studies were focused on transcriptional regulation of BFL-1 in the immune system, NF-κB signaling has been found to induce BFL-1 expression to maintain cell survival in other cellular contexts, such as in response to etoposide[100]. These early studies suggested that BFL-1 induction by NF-κB could be a key factor in tumor resistance to chemotherapy. Induced BFL-1 expression has also been linked to reactive oxygen species (ROS). For example, low doses of H_2O_2 can prompt BFL-1 expression through NF-κB to protect against oxidative stress in T cells[101]. BFL-1 is a transcriptional target of PU.1, which is required for the normal function of granulocytes and macrophages and is transcriptionally active during neutrophil differentiation[102]. BFL-1 upregulation by PU.1 may be necessary for cell survival in this context to protect against the high levels of ROS that occur in these immune cells.

BFL-1 is also controlled at the post-translational level by proteasomal degradation. BFL-1 is constitutively ubiquitinated and subjected to proteasome-mediated turnover, resulting in a relatively short half-life in cells of ~2-3 hours[103]. Ubiquitination is believed to occur on lysine residues of the C-terminal tail of BFL-1, since deletion or mutation of these residues renders BFL-1 resistant to degradation[104]. Further regulation is mediated by phosphorylation of serine and threonine residues in this same region, which contributes to the ubiquitination and degradation of BFL-1[103]. However, the E3 ubiquitin ligases, kinases, and phosphatases involved in these post-translational modifications have not yet been identified.

X-ray crystallography has demonstrated that BFL-1 exhibits structural homology to other members of the BCL-2 family. A BFL-1 construct lacking the C-terminal helix was first crystallized in complex with a BIM BH3 peptide, and this structure confirmed that truncated BFL-1 is composed of 8 α-helices and shares similar three dimensional architecture to other anti-apoptotic proteins[105]. BFL-1 contains BH1, BH2, and BH3 domains that form the canonical surface groove, which is lined with hydrophobic patches critical for interaction with the highly conserved residues of amphipathic BH3 domains. The structure of BFL-1 has now been solved in complex with various BH3 domains from BID, NOXA, BAK, and PUMA. Most recently, we have reported the unliganded structure of BFL-1ΔC and, interestingly, the protein demonstrates a unique, solvent-exposed cysteine within the BH3-binding groove that can potentially be exploited for covalent targeting[106]. Of note, existing crystallography efforts have focused on the truncated form of BFL-1, given the hydrophobic nature of the C-terminal helix and its contribution to protein instability and insolubility. Though the structure of the C-terminal tail of BFL-1 has not been formally defined, it contains amphipathic character like most transmembrane helices and contributes to BFL-1 localization to the mitochondria. Molecular modeling studies suggest that, like its pro-apoptotic counterpart BAX, BFL-1 can exist in two distinct conformations: one with the C-terminal helix bound to its own BH3-binding groove, and another with the C-terminal helix inserted into the mitochondrial outer membrane[107]. The C-terminal helix-in-groove model suggests a possible auto-inhibitory mechanism, but the existence of this form and its mode of regulation have not been determined.

Role of BFL-1 in Cancer Development, Maintenance, and Chemoresistance

BFL-1 has been convincingly linked to the development and chemoresistance of numerous solid and hematological malignancies. For example, early studies documented BFL-1 as a molecular marker of T cell leukemia, with expression correlated with chemoresistance and associated with high levels of NF-κB signaling[99,108]. BFL-1 overexpression has been documented in numerous other cancers, including B-CLL[109,110], DLBCL[111,112], and melanoma[113-115] (**Figure 1.4**). In addition to driving cell survival in cancer, BFL-1 contributes to chemoresistance. BFL-1 upregulation has been shown to confer resistance to etoposide[100] and cisplatin[99] *in vitro*. High levels of BFL-1 also correlate with chemo-refractory disease in CLL[110], breast cancer[116], and bladder cancer[117]. In melanoma, BFL-1 is under direct transcriptional control of MITF and its overexpression confers resistance to small molecule BRAF inhibitors[114]. Importantly, BFL-1 overexpression can arise in numerous blood cancers as a resistance mechanism to selective BCL-2 inhibition[118,119]. In both solid and hematologic cancer settings, siRNA knockdown of BFL-1 can restore sensitivity to chemotherapy-induced apoptosis[110,112,114,118,120], thus establishing BFL-1 as a promising drug target for numerous malignancies.

Despite the clinical success of selective small molecule targeting of BCL-2 in cancer, BFL-1 targeting is relatively underdeveloped. Efforts to design peptide-binding aptamers that target BFL-1 by disrupting its interactions with pro-apoptotic partners have shown some success in sensitizing malignant B cells to apoptosis[121]. However, aptamers have not been deployed in a therapeutic context due to the challenges associated with the delivery of unmodified oligonucleotides. Although multiple groups

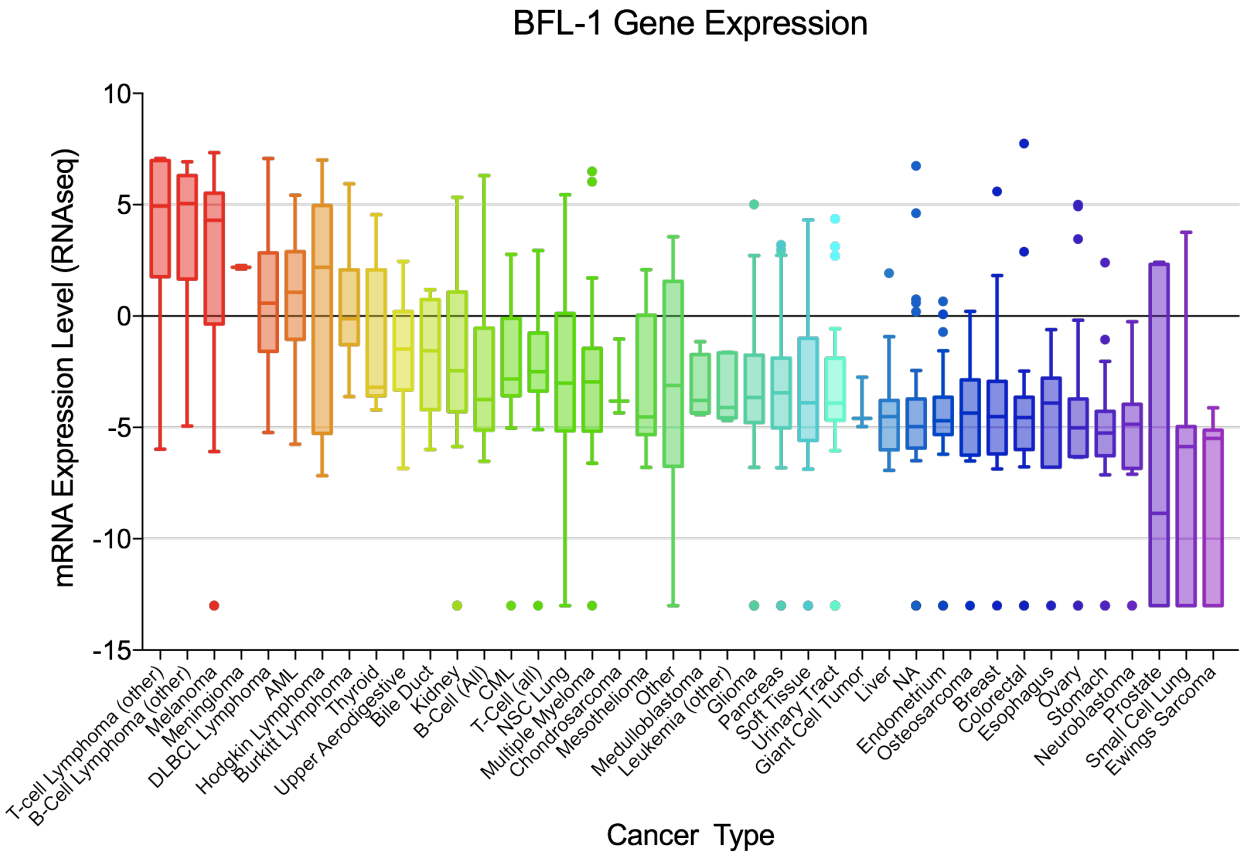

Figure 1.4 *BFL-1 gene expression levels across various cancer types.*

RNAseq data reflecting BFL-1 gene expression across human cancer revealed high level expression in lymphomas, melanoma, and leukemias (Cancer Cell Line Encyclopedia, Broad Institute).

have identified small molecules hits that disrupt the interaction between BFL-1 and BH3 peptides in competitive screening assays, none have been optimized for clinical development to date[122,123]. Given its roles in oncogenesis and chemoresistance, BFL-1 is a ripe target for therapeutic development.

Stapled Peptides: Unique Tools for Scientific Discovery and Therapeutic Development

Hydrocarbon Stapling Technology

Across all realms of biology, proteins interact with each other through complex molecular "handshakes", and these protein-protein interactions (PPIs) are responsible for controlling almost every cellular activity in health and disease. PPIs are defined by precise, complementary topographies and are composed of discrete protein substructures, such as α-helices, β-sheets, β-turns, random coils, and combinations thereof. The α-helix is one of the most ubiquitous and versatile shapes in the cell, with over 30% of protein secondary structure adopting helical conformations. Indeed, α-helical interactions regulate innumerable cellular processes, including infection, immune response, transcription, and apoptosis[124]. The human protein interactome is estimated to be composed of ~650,000 distinct pairwise interactions[125], and given the extent of their deregulation in human disease, many PPIs represent attractive targets for therapeutic intervention. However, drugging PPIs has proven particularly challenging.

A major component of the difficulty in targeting PPIs stems from the current landscape of drug classes, which are predominantly comprised of small molecules and biologics. Small molecules, which are typically composed of fewer than 100 atoms and

weigh less than 1000 Da, have long been a focus of the pharmaceutical industry owing to their rapid structure-activity based optimization by medicinal chemistry and the capacity to effectively scale-up production for the commercial marketplace. Following Lipinski's "rule of five" can allow for small molecules to be orally bioavailable[126]. Additional favorable qualities of small molecules include cell permeability and effectiveness at targeting small hydrophobic binding pockets[127]. However, since PPIs typically make contact over 800-1100 $Å^2$ of surface area[128], small molecules are typically incapable of blanketing such large and flat protein interfaces. Of the ~20,000 proteins encoded in the human genome, small molecules have been successfully developed against fewer than 300 proteins, with the majority targeting only ten classes of proteins[129]. The relatively narrow protein-targeting spectrum of small molecules has led to the classification of the remaining large reservoir of intracellular protein targets as "undruggable".

On the other end of the spectrum, numerous advances over the past several decades have yielded successful biologics. Biologics are protein-based bioactive molecules that are typically over 5000 Da, with prominent examples including antibodies and growth factors. One advantage of biologics is that technology exists to evolve proteins to engage almost any extracellular drug target with striking potency and selectivity[127]. Unlike small molecules, biologics are capable of binding large, flat surfaces, and are not limited to binding hydrophobic pockets. Biologics such as insulin have proved successful in the treatment of diabetes, and engineered antibodies such as anti-HER2 (trastuzumab) and anti-CD20 (rituximab) have been effective against breast cancer and non-Hodgkin's lymphoma, respectively[126]. The major drawback of biologics

is the lack of oral bioavailability and cell permeability, restricting them to intravenous administration for extracellular targets[127].

Many pathologic PPIs reside within the cell and cannot be accessed by small molecules or biologics. Whereas ~12% of proteins encoded by the human genome contain hydrophobic pockets amenable to small molecule binding, less than 10% of proteins are secreted or on the cell surface, leaving the majority of protein targets undruggable based on the two most common and successful drug classes[130]. Peptide therapeutics have the potential to bridge the gap between small molecules and biologics, given their ability to recognize larger protein surface areas and potentially mimic bioactive structures to disrupt PPIs. However, when taken out of context from the full length protein, short and otherwise structured peptide motifs can unfold, resulting in entropic penalties that can preclude refolding to engage a target[127]. Other major limitations of synthetic peptides include proteolytic instability and limited cell penetrance[124]. Despite these drawbacks, hundreds of peptide therapeutics have gained FDA approval for diverse indications, with the majority addressing extracellular targets[131].

Given the capacity of peptide therapeutics to effectively disrupt pathological PPIs, there have been significant efforts in recent years to chemically stabilize bioactive peptide conformations, with the goal of imparting drug-like properties and enhancing binding affinity. For example, a series of approaches have been taken to stabilize peptide α-helices based on crosslinking peptide side chains. A peptide in an α-helical configuration completes one turn every 3.6 residues[124], allowing for the installation of crosslinkable side chains at distances of *i*, *i+4* to span one turn of the helix and *i*, *i+7* to

span two turns. Early approaches to constrain peptides in α-helical conformation included the use of β-lactam bridges to structure hexapeptides[132] and the insertion of glutamine residues in *i*, *i+7* positions to stabilize α-helical structure by alkanediyl-chain tethering of the side chain nitrogen atoms[133]. Other strategies included formation of *i*, *i+4* amide bonds between lysine and glutamic acid residues[134], and generating disulfide bridges between cysteines at *i, i+3* positions[135]. While all of these approaches can impart α-helical character to synthetic peptides, the crosslinks are polar or pharmacologically labile, rendering the peptides susceptible to degradation and precluding cell penetrance.

A major breakthrough in ruthenium-catalyzed carbon-carbon bond formation was achieved by Dr. Robert Grubbs, earning him the Nobel Prize in Chemistry in 2005. Grubbs developed novel catalysts that crosslinked olefins by a ring-closing metathesis reaction. Blackwell and Grubbs applied this chemistry to successfully crosslink *i, i+4* positioned *O*-allyl serine residues, but the resulting peptides were not necessarily transformed into α-helices in solution[136]. Verdine and colleagues extended Grubbs' approach by instead substituting α,α-disubstituted amino acids bearing alkenyl tethers at *i*, *i+4* or *i*, *i+7* positions, and upon olefin metathesis, the all-hydrocarbon crosslinks yielded peptides with markedly enriched α-helical structure[137]. In addition to conferring helical structure, the crosslinks imparted substantial proteolytic resistance[137] (**Figure 1.5**). Walensky, Verdine, and Korsmeyer applied the peptide stapling technology to stabilize the BH3 domain of the BCL-2 family protein BID, resulting in helical induction, protease resistance, enhanced target binding affinity, and most notably, cellular uptake by an energy-dependent pinocytotic mechanism; this novel class of compounds,

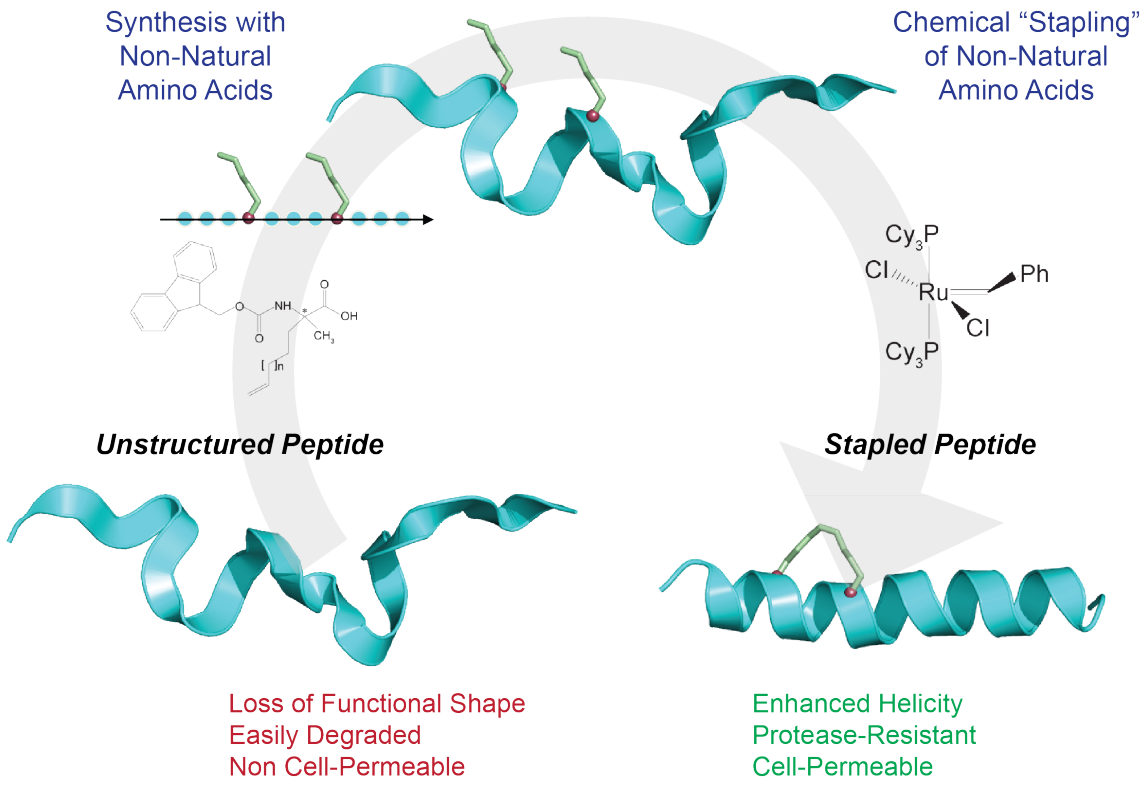

Figure 1.5 *Hydrocarbon staples restore α-helicity to synthetic peptides*.

Incorporation of α,α-disubstituted non-natural amino acids bearing olefinic side chains into synthetic peptides sequences enables peptide stapling by ruthenium-catalyzed olefin metathesis. The pictured all-hydrocarbon staple, spanning one helical turn of the peptide, reinforces helical structure and can confer a variety of beneficial properties including resistance to proteolysis and cell penetrance.

dubbed “stapled peptides,” was capable of activating apoptosis in cell culture and *in vivo*, providing proof-of-concept for an entirely new approach to studying and targeting intracellular PPIs[138].

Key hallmarks of stapled peptides included *in vivo* protease resistance and cell permeability. Because hydrocarbon stapling reinforces helical structure, the otherwise labile amide bonds are buried at the core of the helix, impairing proteolytic digestion *in vitro* and *in vivo*[137,138]. In the context of longer peptide constructs, insertion of a second hydrocarbon staple can further enhance structural stabilization and proteolytic resistance[139]. Cellular uptake of fluorescently-labeled stapled peptides has been documented by confocal imaging[138] and immunoelectron microscopy[140]. In a study of over 200 hundred stapled peptides with diverse staple positions, compositions, and overall charge, cell penetrance appeared to correlate with staple type and formal charge[141]. However, a systematic and unbiased statistical analysis of stapled peptide libraries pursued by Walensky and colleagues revealed that primarily hydrophobicity and secondarily α-helicity were the key drivers of stapled peptide penetrance[142]. This work provided validated design principles for generating stapled peptides with optimal cell penetrance, overcoming prior barriers to effectively targeting PPIs in cells and *in vivo*.

Use of Stapled Peptides to Dissect BCL-2 Family Interactions

With the majority of BCL-2 family PPIs mediated by α-helical BH3-in-groove interactions, stapled peptides have become a powerful tool for dissecting the BCL-2 family interaction network, and even manipulating it for therapeutic reactivation of

apoptosis in cancer. In 2004, Walensky developed the first Stabilized Alpha-Helix of BCL-2 domains (SAHB) modeled after the BH3 helix of BID and provided the first evidence that stapled peptides could modulate the function of physiological PPIs[138]. The insertion of an *i*, *i+4* staple in the native BID BH3 sequence rendered the peptide helical, resistant to proteolysis, and cell penetrant. ^{1}H-^{15}N heteronuclear single-quantum correlation (HSQC) NMR and fluorescence polarization assays (FPA) were used to demonstrate that BID SAHB specifically bound to the canonical BH3-binding groove of the anti-apoptotic protein BCL-X_L. From a functional standpoint, BID SAHB recapitulated the activity of native BID by inducing cytochrome *c* release from mouse liver mitochondria, activating apoptosis in a panel of human leukemia cells, and, notably, inducing activating apoptosis *in vivo* to suppress leukemic growth in mice. Based on this proof-of-concept for transforming a bioactive motif into a stable α-helix for therapeutic targeting of intracellular PPIs, the stage was set for broad application of this technology in both basic and translational research.

The original BID SAHB was further employed to interrogate the elusive interaction between select BH3-only proteins and the pro-apoptotic executioner proteins BAX and BAK, based on the hypothesis that these pore-forming proteins required direct activation to transform from inactive monomers into mitochondrial membrane-embedded oligomers[36]. The application of FITC-BID SAHB and recombinant BAX titration in FPA assays demonstrated for the first time a direct interaction between a BH3 helix and BAX, overcoming prior challenges in trying to capture this proposed “hit and run” interaction[36,143]. This binding interaction was then directly linked to functional BAX activation using correlative liposomal and mitochondrial membrane release

assays, and mutagenesis analyses. The *in vitro* liposomal assays not only quantified BH3-triggered and BAX-mediated poration, but also documented that no other component aside from the BID SAHB interaction was required for BAX activation. Through this study, stapled peptides demonstrated their utility as chemical tools to probe fundamental questions in the apoptosis field.

Applying peptide stapling technology to generate SAHBs modeled after the BH3 domain of BIM revealed a host of novel mechanistic insights into the mechanism of BH3-induced BAX activation. NMR analyses of BAX upon BIM SAHB titration revealed the site of BH3 interaction, which was distinct from the canonical BH3-binding groove[37]. Binding at this novel location, termed the “trigger site”, was then shown to drive a series of structural rearrangements that comprised the BAX activation process, which ultimately leads to apoptosis induction[37,144]. Multidisciplinary studies using BID SAHB to interrogate direct activation of BAK, the mitochondrial-membrane localized homolog of BAX, revealed that select SAHBs could also directly bind to and activate BAK, but in contrast to BAX, the site of interaction localized to the canonical C-terminal face of the protein, where anti-apoptotics engage BH3 domains[145]. Taken together, this work revealed that the unique binding site on BAX mediates its translocation from cytosol to mitochondria, a step not required for BAK, which is constitutively localized at the mitochondrial outer membrane. Owing to its capacity to potently activate both BAX and BAK (an “activate the activators” mechanism), and inhibit the canonical pockets of anti-apoptotic proteins (an “inhibit the inhibitors” mechanism), BIM SAHB was tested in mouse models of refractory AML and demonstrated anti-tumor activity as single agent

and in combination with the BCL-2/BCL-X_L inhibitor ABT-263[146], thus reinforcing the utility of stapled peptides as discovery tools and prototype therapeutics.

Given their ability to faithfully recapitulate native interaction domains and engage protein targets with high affinity, stapled peptides were also harnessed to create tools for proteomic discovery (**Figure 1.6**). Incorporating a non-natural amino acid bearing a benzophenone moiety into stapled peptide design yielded photoreactive SAHBs (pSAHBs) capable of covalent capture of interacting targets upon exposure to UV light[147]. The application of biotinylated pSAHBs enabled enrichment of covalently bound proteins by streptavidin pull-down, and then mass spectrometry analysis of cross-linked peptides identified both the protein targets and the sites of interaction. This platform was validated with established interaction partners, such as the BAD BH3/BCL-X_L helix-in-groove interaction[147], and then applied to uncover novel BH3 interactions. For example, PUMA pSAHBs were used to demonstrate that PUMA BH3 can directly engage BAX at both canonical and trigger sites, leading to BAX activation and apoptosis[148]. Coupled with HSQC NMR and hydrogen-deuterium exchange mass spectrometry (HXMS) analyses, pSAHBs modeled after the BH4 domain of BCL-2 were used to identify a novel inhibitory binding site on BAX, revealing an interaction mode distinct from the BH3-in-groove interaction that BCL-2 harnesses to block BAX[149]. Based on these and other examples[145,150,151], combining peptide stapling with covalent capture emerged as a powerful and versatile approach to proteomic discovery.

Structural reinforcement of the MCL-1 BH3 domain sparked numerous discoveries in basic biology and drug discovery. Screening a stapled peptide library of all natural BH3 domains, encompassing pro- and anti-apoptotic BCL-2 members,

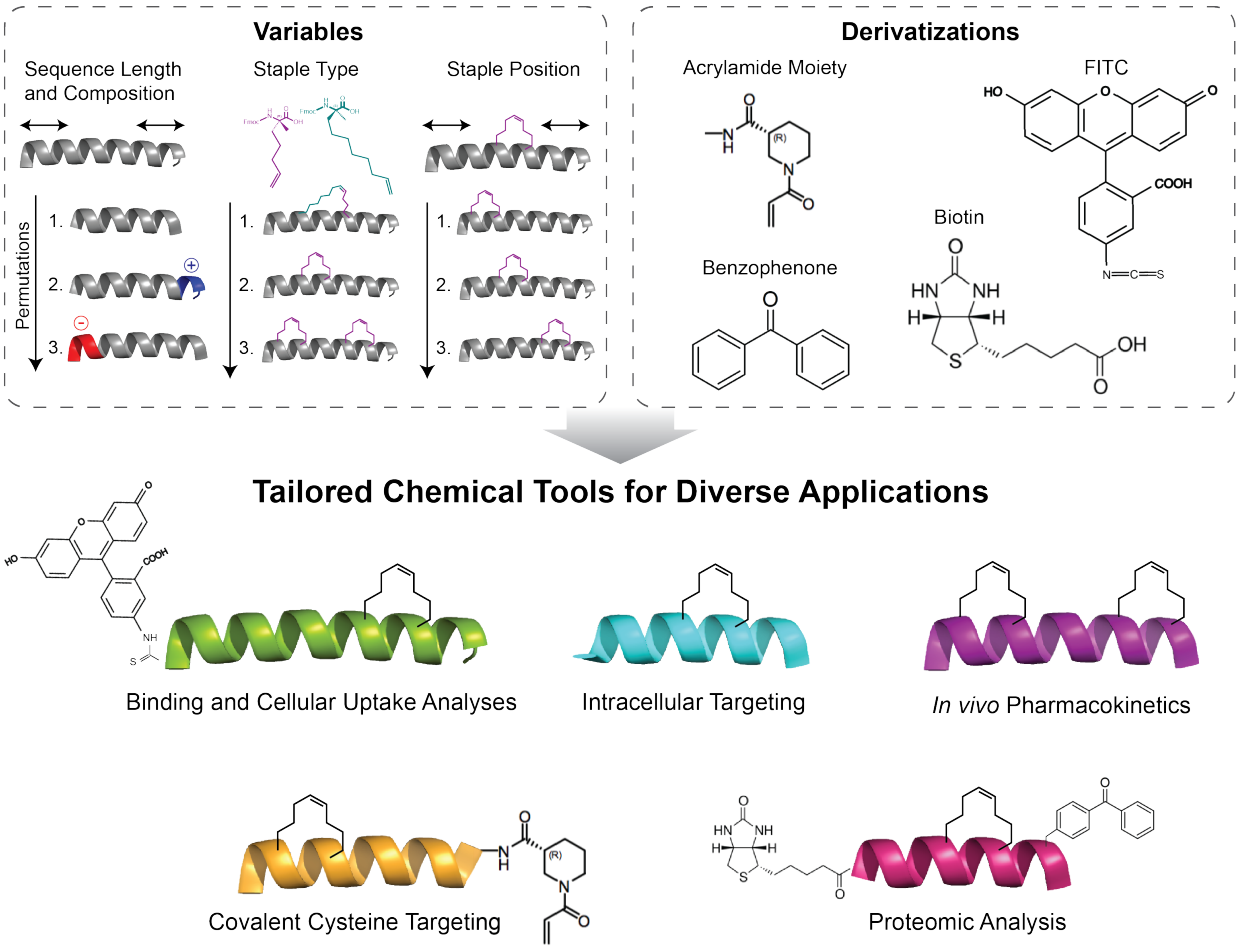

Figure 1.6 *Design and derivatization of stapled peptides for modulation of protein interactions and therapeutic targeting*.

Diverse libraries of stapled peptides can be generated through the iteration of peptide sequence composition, including peptide length and overall charge, staple type, and staple placement. Additionally, numerous derivatizations can be appended to tune the functionalities of such stapled peptides to suit a broad range of research and therapeutic applications.

identified the MCL-1 BH3 domain as the only exclusive inhibitor of MCL-1 in nature[152]. Solving the co-crystal structure of MCL-1 SAHB bound to MCL-1 revealed the molecular basis for its binding specificity and also led to the hypothesis that exposure of the MCL-1 BH3 domain could enable gain-of-function protein interactions, as is the case for BAX and BAK BH3 exposure. To test this hypothesis, MCL-1 SAHB was used as bait to identify novel interaction partners by mass spectrometry, which led to the identification of very long chain acyl CoA dehydrogenase (VLCAD) as a target of the MCL-1 BH3 helix; follow up mechanistic analyses *in vitro* and *in vivo* revealed that the mitochondrial matrix form of MCL-1 indeed regulates fatty acid β-oxidation through VLCAD interaction[151]. In addition to its use as a proteomic discovery tool, MCL-1 SAHB has been deployed in competitive small molecule screens to identify candidate selective inhibitors of the MCL-1 canonical groove[153], which in turn led to the discovery of small molecule inhibitors that indirectly blocked the BH3-pocket by targeting a novel allosteric binding site on MCL-1[154]. Taken together, these discoveries highlighted the versatility of stapled peptides in advancing both basic science inquiries and drug development efforts focused on BCL-2 family regulation.

Beyond the BCL-2 family, stapled peptides have proven to be valuable tools for targeting a broad range of pathologic PPIs mediated by α-helical domains. For example, aberrant activation of the Wnt signaling pathway contributes to the pathogenesis of multiple myeloma and colorectal cancer[155]. Stapled peptides modeled after an α-helix of BCL-9, a transcriptional cofactor in the Wnt pathway, effectively disrupted the interaction between BCL-9 and β-catenin, reducing Wnt transcriptional activity and suppressing multiple myeloma and colon cancer growth in culture and *in vivo*[156].

Stapled peptides have also been employed to modulate epigenetic programs in cancer. EZH2 and EED are two components of the polycomb repressive complex PRC2, which catalyzes histone H3K27 methylation to control gene expression; overexpression of the complex and deregulation of the pathway have been linked to the development and maintenance of such cancers as leukemia, DLBCL, and rhabdoid tumor[157,158]. Stapled peptides were modeled after an α-helical domain of EZH2 that engaged EED, and functioned to dissociate the PRC2, unexpectedly leading to both inhibition of H3K27 methylation enzymatic activity and proteosomal degradation of the dissociated PRC2 subunits; as a result, MLL-AF9 leukemia cells were observed to differentiate into monocytes/macrophages and proliferation arrest was observed in a variety of other PRC2-dependent cancers[159]. Stapled peptides modeled after an α-helical domain of the guanine-nucleotide exchange factor SOS1, which enhances KRAS activity through direct protein interaction, were capable of both disrupting the SOS1/KRAS interaction and also directly inhibiting wild-type KRAS and its mutant isoforms, presumably by altering the nucleotide exchange region[160]. These studies highlight the importance of α-helical domain interactions in cancer pathogenesis and the promise of stapled peptides to disrupt pathologic PPIs for therapeutic benefit.

Outside of the cancer field, stapled peptides have been used to target protein interactions that drive viral infection. Efforts to block HIV-1 infection led to the development of the FDA-approved drug Enfurvitide, a peptide inhibitor of viral fusion; however, the drug suffered from facile proteolytic degradation *in vivo* and lack of oral bioavailability so was quickly replaced by other agents[161]. Modeled after the HR2 domain of the HIV-1 gp41 envelope protein, Enfuvirtide serves as a helical decoy that

disrupts formation of the 6-helix bundle, which is critical to viral fusion with the host cell membrane[161]. Double-stapling of the gp41 HR2 domain reinforced its α-helical structure, conferred proteolytic resistance, and enhanced target engagement, resulting in an optimized peptide with improved pharmacologic properties and the capacity to overcome Enfuvirtide resistance[139]. Double-stapling the membrane-proximal region of gp41, a region of the protein that gave rise to neutralizing antibodies in long-term non-progressing patients infected with HIV-1, was also pursued as an HIV-1 vaccine development strategy[162]. Stapled peptides have also been deployed to develop fusion inhibitors of the respiratory syncytial virus (RSV), which shares the 6-helix bundle fusion mechanism with HIV-1. Double-stapled peptides of the RSV-F fusion protein potently inhibited RSV infectivity *in vitro* and both mitigated nasal RSV infection *in vivo* and blocked the spread of nasal infection to the lungs upon intranasal and intratracheal administration, respectively[163].

Stapled Peptides as Therapeutics

Given the prevalence of α-helices in mediating PPIs, and the urgent need to bridge the gap between therapeutic molecules and biologics, stapled peptides are actively being explored as a new drug modality. The most vetted example of stapled peptides as prototype therapeutics involves reactivation of the p53 tumor suppressor pathway by dual targeting of HDM2 and HDMX. The tumor suppressor protein p53, commonly referred to as the “guardian of the genome”, is the most frequently altered protein in human cancer, with aberrant expression or inactivating mutations found in approximately 50% of human cancers[164]. Though the activities of p53 are wide-ranging

and complex, its most basic function is to promote cell cycle arrest, leading to apoptosis or senescence, in response to cell stress such as DNA damage and oncogene-induced replicative stress[164]. p53 maintains the integrity of the genome by allowing for the repair or elimination of damaged cells, thereby preventing the propagation of deleterious mutations[164]. p53 is a sequence-specific DNA-binding protein, which exerts its tumor suppressor activity through the regulation of transcription[165]. p53 is composed of two N-terminal activation domains, followed by a proline-rich region, the critical DNA-binding domain, which is most frequently mutated in cancer, and a C-terminal domain responsible for its oligomerization and nuclear localization[164].

p53 function is further regulated by numerous post-translational modifications, many of which become deregulated in cancer[166]. A key mode of p53 regulation involves its ubiquitylation by the E3 ligase HDM2. p53 levels are typically maintained at a low level as a result of HDM2 activity and proteosomal degradation[167]. HDM2 is blocked in response to cell stress, resulting in p53 stabilization, which in turn upregulates HDM2 as a negative feedback loop[167]. HDM2 amplification and overexpression is found in ~7% of human tumors, eliminating the need for mutational inactivation of p53 in this context[168]. Thus, inhibiting the p53/HDM2 interaction to reactivate p53 is a potential route to cell cycle arrest and apoptosis induction in cancer cells that retain wild-type p53.

The crystal structure of the complex between the p53 transactivation domain and HDM2 revealed a single α-helix at the binding interface, with protein interaction primarily mediated by three hydrophobic residues[169]. In 2004, Vassilev and colleagues from Hoffman-La Roche advanced Nutlin-3a as a low nanomolar inhibitor of HDM2, and demonstrated potent reactivation of wild-type p53 in cancer cells resulting in

suppression of osteosarcoma growth in culture and *in vivo*[170]. Nutlin-3a was further optimized by medicinal chemistry, leading to RG7112, a clinical candidate with increased potency and more favorable pharmacologic properties[171]. Phase 1 testing of orally-administered RG7112 resulted in partial responses and stable disease in select liposarcoma patients[172]. However, all enrolled patients experienced at least one adverse event, which typically involved hematologic toxicity[172]. Despite the early promising results of small molecule HDM2 inhibitors developed by several groups, dose-limiting toxicity has been a persistent challenge and none of the compounds have achieved FDA approval to date.

Given the helix-in-groove nature of the p53/HDM2 interaction, stapled p53 peptides proved to be an alternative approach to reactivating p53 in cancer. In 2007, Bernal and colleagues designed *i*, *i*+*7* stapled peptides modeled after the α-helical transactivation domain of p53; the lead compound, SAH-p53-8, exhibited low nanomolar affinity for HDM2, reactivated p53 in cultured cells, and induced apoptosis[173]. Mechanistic studies employing SAH-p53-8 revealed HDMX expression as a key resistance factor for small molecule HDM2 inhibitors, and since the p53/HDMX interaction is mediated by the same p53 helix, dual targeting of HDM2/HDMX emerged as an especially valuable property to overcome p53 suppression *in vitro* and *in vivo*[174] (**Figure 1.7**). Whereas HDM2 binds and destroys p53, HDMX binds and sequesters p53. Thus, small molecule HDM2 inhibitors meet resistance when HDMX, which is not targeted by the small molecules, is present to capture and neutralize the drug-induced surge of p53.

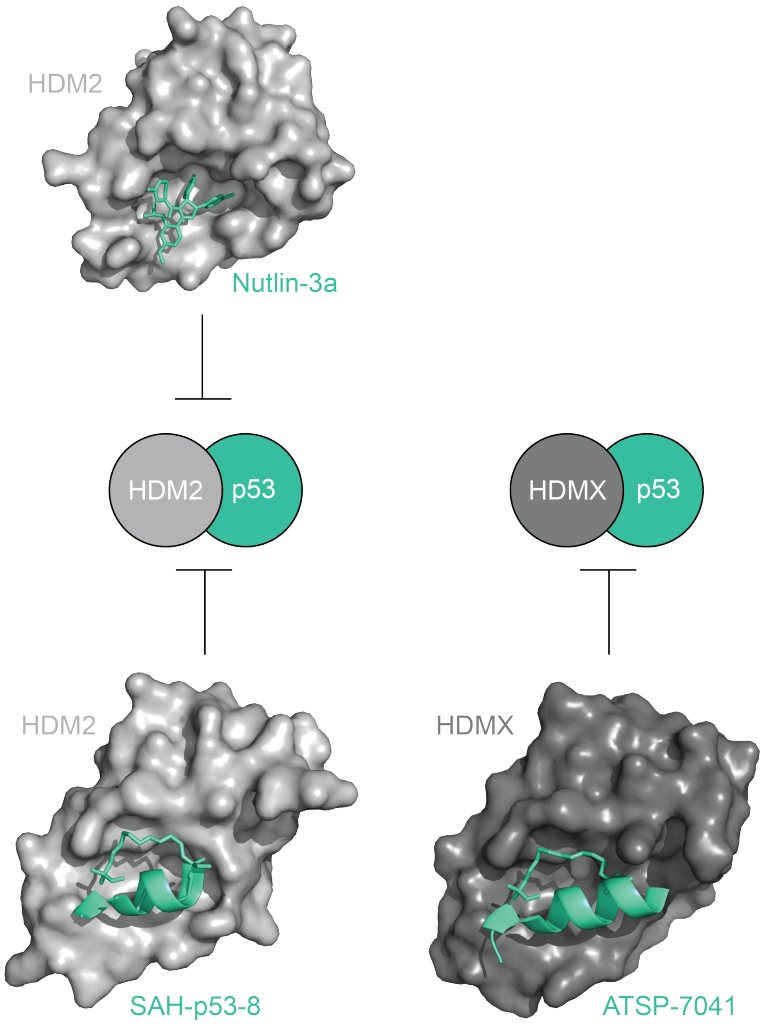

Figure 1.7 *Dual-targeting feature of stapled peptides to reactivate p53 as a therapeutic strategy in human cancers*.

In an effort to reactivate p53 in cancer, small molecule inhibitors, such as Nutlin-3a, have been designed to block the antagonistic interaction of HDM2 and p53 (top, PDB: 4HG7), however p53 is still susceptible to degradation by HDMX, which could potentially result in chemoresistance. In comparison, stapled peptides modeled after the transactivation domain of p53 display dual binding affinity for both HDM2 (left, PDB: 3V3B) and HDMX (right, PDB: 4N5T), thus demonstrating an advantage of stapled peptide therapeutics in overcoming specificity limitations of small molecule inhibitors.

Based on these mechanistic and *in vivo* findings, Aileron Therapeutics developed and optimized SAH-p53-8, preserving the original *i, i*+*7* staple position but incorporating several binding-enhancement mutations from peptide phage display[175]. The resultant lead peptide, ATSP-7041, demonstrated potent dual affinity for HDM2 and HDMX, reduced serum binding, efficient cellular uptake, and efficacy in a series of cancer xenograft models[176]. The crystal structure of the ATSP-7041/HDM2 complex demonstrated recapitulation of the three key hydrophobic contacts at the binding interface, in addition to adjunct interactions between the hydrophobic binding surface and the staple itself[176]. Aileron then advanced their lead stapled p53 peptide analog, ALRN-6924, to clinical testing, which has included a Phase 1 trial in advanced solid tumors (NCT02264613), a Phase 2A study in peripheral T-cell lymphoma (NCT02264613), and a Phase 1 trial in acute myeloid lymphoma and myelodysplastic syndrome (NCT02909972). Results from the first Phase 1 study demonstrated that ALRN-6924 was well tolerated from a safety standpoint; of the 41 study participants, there were 2 complete responses, 2 partial responses, and 20 patients with stable disease, and numerous patients continue to receive the treatment for well over a year[177]. These results represent the first example of the clinical translation of a stapled peptide for targeting an intracellular PPI. With over 3000 PPIs mediated by α-helices[178], stapled peptides could provide a new opportunity for addressing “undruggable” targets, transforming bioactive peptides into structurally-stabilized α-helices that penetrate intact cells and modulate their native protein targets.

REFERENCES

1. Vaux, D. L. & Korsmeyer, S. J. Cell death in development. *Cell* **96,** 245–254 (1999).

2. Lindsten, T. *et al.* The combined functions of proapoptotic Bcl-2 family members bak and bax are essential for normal development of multiple tissues. *Molecular Cell* **6,** 1389–1399 (2000).

3. Jacobson, M. D., Weil, M. & Raff, M. C. Programmed cell death in animal development. *Cell* **88,** 347–354 (1997).

4. Opferman, J. T. & Korsmeyer, S. J. Apoptosis in the development and maintenance of the immune system. *Nat. Immunol.* **4,** 410–415 (2003).

5. Vogt, C. *Untersuchungen über die Entwicklungsgeschichte der Geburtshelferkröte*. *Alytes obstetricians* **130** (1842).

6. Flemming, W. Uber die Bildung von Richtungsfiguren in Saugethiereiern beim Untergang Graaf'scher Follikel. *Arch Anat Entw Gesh* **221** (1885).

7. Kerr, J. F., Wyllie, A. H. & Currie, A. R. Apoptosis: a basic biological phenomenon with wide-ranging implications in tissue kinetics. *Br J Cancer* **26,** 239–257 (1972).

8. Ravichandran, K. S. & Lorenz, U. Engulfment of apoptotic cells: signals for a good meal. *Nat Rev Immunol* **7,** 964–974 (2007).

9. Lettre, G. & Hengartner, M. O. Developmental apoptosis in *C. elegans*: a complex CEDnario. *Nat Rev Mol Cell Biol* **7,** 97–108 (2006).

10. Sulston, J. E., Schierenberg, E., White, J. G. & Thomson, J. N. The embryonic cell lineage of the nematode *Caenorhabditis elegans*. *Dev. Biol.* **100,** 64–119 (1983).

11. Ellis, H. M. & Horvitz, H. R. Genetic control of programmed cell death in the nematode *C. elegans*. *Cell* **44,** 817–829 (1986).

12. Conradt, B. & Horvitz, H. R. The *C. elegans* protein EGL-1 is required for programmed cell death and interacts with the Bcl-2-like protein CED-9. *Cell* **93,** 519–529 (1998).

13. Hengartner, M. O., Ellis, R. E. & Horvitz, H. R. *Caenorhabditis elegans* gene ced-9 protects cells from programmed cell death. *Nature* **356,** 494–499 (1992).

14. del Peso, L., González, V. M. & Nunez, G. *Caenorhabditis elegans* EGL-1 disrupts the interaction of CED-9 with CED-4 and promotes CED-3 activation. *Journal of Biological Chemistry* **273,** 33495–33500 (1998).

15. Vaux, D., Weissman, I. & Kim, S. Prevention of programmed cell death in *Caenorhabditis elegans* by human bcl-2. *Science* **258,** 1955–1957 (1992).

16. Tait, S. W. G. & Green, D. R. Mitochondria and cell death: outer membrane permeabilization and beyond. *Nat Rev Mol Cell Biol* **11,** 621–632 (2010).

17. Fischer, U., Janicke, R. U. & Schulze-Osthoff, K. Many cuts to ruin: a comprehensive update of caspase substrates. *Cell Death and Differentiation* **10,** 76–100 (2003).

18. Lamkanfi, M., Festjens, N., Declercq, W., Berghe, T. V. & Vandenabeele, P. Caspases in cell survival, proliferation and differentiation. *Cell Death and Differentiation* **14,** 44–55 (2006).

19. Suda, T., Takahashi, T., Golstein, P. & Nagata, S. Molecular cloning and expression of the Fas ligand, a novel member of the tumor necrosis factor family. *Cell* **75,** 1169–1178 (1993).

20. Yin, X. M. *et al.* Bid-deficient mice are resistant to Fas-induced hepatocellular apoptosis. *Nature* **400,** 886–891 (1999).

21. Chipuk, J. E., Bouchier-Hayes, L. & Green, D. R. Mitochondrial outer membrane permeabilization during apoptosis: the innocent bystander scenario. *Cell Death and Differentiation* **13,** 1396–1402 (2006).

22. Hakem, R. *et al.* Differential requirement for caspase 9 in apoptotic pathways in vivo. *Cell* **94,** 339–352 (1998).

23. Shi, Y. Mechanical aspects of apoptosome assembly. *Current Opinion in Cell Biology* **18,** 677–684 (2006).

24. Harlin, H., Reffey, S. B., Duckett, C. S., Lindsten, T. & Thompson, C. B. Characterization of XIAP-deficient mice. *Molecular and Cellular Biology* **21,** 3604–3608 (2001).

25. Okada, H. *et al.* Generation and Characterization of Smac/DIABLO-Deficient Mice. *Molecular and Cellular Biology* **22,** 3509–3517 (2002).

26. Tsujimoto, Y., Cossman, J., Jaffe, E. & Croce, C. M. Involvement of the bcl-2 gene in human follicular lymphoma. *Science* **228,** 1440–1443 (1985).

27. Bakhshi, A. *et al.* Cloning the chromosomal breakpoint of t(14;18) human lymphomas: clustering around JH on chromosome 14 and near a transcriptional unit on 18. *Cell* **41,** 899–906 (1985).

28. Cleary, M. L. & Sklar, J. Nucleotide sequence of a t(14;18) chromosomal breakpoint in follicular lymphoma and demonstration of a breakpoint-cluster region near a transcriptionally active locus on chromosome 18. *Proc. Natl. Acad. Sci. U.S.A.* **82,** 7439–7443 (1985).

29. Vaux, D. L., Cory, S. & Adams, J. M. Bcl-2 gene promotes haemopoietic cell survival and cooperates with c-myc to immortalize pre-B cells. *Nature* **335,** 440–442 (1988).

30. McDonnell, T. J. *et al.* bcl-2-immunoglobulin transgenic mice demonstrate extended B cell survival and follicular lymphoproliferation. *Cell* **57,** 79–88 (1989).

31. Hockenbery, D., Nunez, G., Milliman, C., Schreiber, R. D. & Korsmeyer, S. J. Bcl-2 is an inner mitochondrial membrane protein that blocks programmed cell death. *Nature* **348,** 334–336 (1990).

32. Liu, X., Kim, C. N., Yang, J., Jemmerson, R. & Wang, X. Induction of apoptotic program in cell-free extracts: requirement for dATP and cytochrome c. *Cell* **86,** 147–157 (1996).

33. Yang, J. *et al.* Prevention of apoptosis by Bcl-2: release of cytochrome c from mitochondria blocked. *Science* **275,** 1129–1132 (1997).

34. Hsu, Y. T. & Youle, R. J. Bax in murine thymus is a soluble monomeric protein that displays differential detergent-induced conformations. *Journal of Biological Chemistry* **273,** 10777–10783 (1998).

35. Antonsson, B., Montessuit, S., Lauper, S., Eskes, R. & Martinou, J. C. Bax oligomerization is required for channel-forming activity in liposomes and to trigger cytochrome c release from mitochondria. *Biochem. J.* **345 Pt 2,** 271–278 (2000).

36. Walensky, L. D. *et al.* A stapled BID BH3 helix directly binds and activates BAX. *Molecular Cell* **24,** 199–210 (2006).

37. Gavathiotis, E. *et al.* BAX activation is initiated at a novel interaction site. *Nature* **455,** 1076–1081 (2008).

38. Rinkenberger, J. L., Horning, S., Klocke, B., Roth, K. & Korsmeyer, S. J. Mcl-1 deficiency results in peri-implantation embryonic lethality. *Genes Dev.* **14,** 23–27 (2000).

39. Motoyama, N. *et al.* Massive cell death of immature hematopoietic cells and neurons in Bcl-x-deficient mice. *Science* **267,** 1506–1510 (1995).

40. Veis, D. J., Sorenson, C. M., Shutter, J. R. & Korsmeyer, S. J. Bcl-2-deficient mice demonstrate fulminant lymphoid apoptosis, polycystic kidneys, and hypopigmented hair. *Cell* **75,** 229–240 (1993).

41. Print, C. G. *et al.* Apoptosis regulator bcl-w is essential for spermatogenesis but appears otherwise redundant. *Proc. Natl. Acad. Sci. U.S.A.* **95,** 12424–12431 (1998).

42. Oltvai, Z. N., Milliman, C. L. & Korsmeyer, S. J. Bcl-2 heterodimerizes in vivo with a conserved homolog, Bax, that accelerates programmed cell death. *Cell* **74,** 609–619 (1993).

43. Muchmore, S. W. *et al.* X-ray and NMR structure of human Bcl-xL, an inhibitor of programmed cell death. *Nature* **381,** 335–341 (1996).

44. Day, C. L. *et al.* Structure of the BH3 Domains from the p53-Inducible BH3-Only Proteins Noxa and Puma in Complex with Mcl-1. *Journal of Molecular Biology* **380,** 958–971 (2008).

45. Sattler, M. *et al.* Structure of Bcl-xL-Bak Peptide Complex: Recognition Between Regulators of Apoptosis. *Science* **275,** 983–986 (1997).

46. Danial, N. N. & Korsmeyer, S. J. Cell death: critical control points. *Cell* **116,** 205–219 (2004).

47. Chen, L. *et al.* Differential Targeting of Prosurvival Bcl-2 Proteins by Their BH3-Only Ligands Allows Complementary Apoptotic Function. *Molecular Cell* **17,** 393–403 (2005).

48. Letai, A. *et al.* Distinct BH3 domains either sensitize or activate mitochondrial apoptosis, serving as prototype cancer therapeutics. *Cancer Cell* **2,** 183–192 (2002).

49. Kuwana, T. *et al.* BH3 domains of BH3-only proteins differentially regulate Bax-mediated mitochondrial membrane permeabilization both directly and indirectly. *Molecular Cell* **17,** 525–535 (2005).

50. Oda, E. *et al.* Noxa, a BH3-only member of the Bcl-2 family and candidate mediator of p53-induced apoptosis. *Science* **288,** 1053–1058 (2000).

51. Nakano, K. & Vousden, K. H. PUMA, a novel proapoptotic gene, is induced by p53. *Molecular Cell* **7,** 683–694 (2001).

52. Dijkers, P. F., Medema, R. H., Lammers, J. W., Koenderman, L. & Coffer, P. J. Expression of the pro-apoptotic Bcl-2 family member Bim is regulated by the forkhead transcription factor FKHR-L1. *Curr. Biol.* **10,** 1201–1204 (2000).

53. Zha, J., Harada, H., Yang, E., Jockel, J. & Korsmeyer, S. J. Serine phosphorylation of death agonist BAD in response to survival factor results in binding to 14-3-3 not BCL-X(L). *Cell* **87,** 619–628 (1996).

54. Rinkenberger, J. L. & Korsmeyer, S. J. Errors of homeostasis and deregulated apoptosis. *Curr. Opin. Genet. Dev.* **7,** 589–596 (1997).

55. Friedlander, R. M. Apoptosis and caspases in neurodegenerative diseases. *N Engl J Med* **348,** 1365–1375 (2003).

56. Kang, P. M. & Izumo, S. Apoptosis in heart: basic mechanisms and implications in cardiovascular diseases. *Trends in Molecular Medicine* **9,** 177–182 (2003).

57. Aitken, R. J., Findlay, J. K., Hutt, K. J. & Kerr, J. B. Apoptosis in the germ line. *Reproduction* **141,** 139–150 (2011).

58. Hanahan, D. & Weinberg, R. A. Hallmarks of Cancer: The Next Generation. *Cell* **144,** 646–674 (2011).

59. Strasser, A., Harris, A. W., Bath, M. L. & Cory, S. Novel primitive lymphoid tumours induced in transgenic mice by cooperation between myc and bcl-2. *Nature* **348,** 331–333 (1990).

60. Beroukhim, R. *et al.* The landscape of somatic copy-number alteration across human cancers. *Nature* **463,** 899–905 (2010).

61. Hanada, M., Delia, D., Aiello, A., Stadtmauer, E. & Reed, J. C. bcl-2 gene hypomethylation and high-level expression in B-cell chronic lymphocytic leukemia. *Blood* **82,** 1820–1828 (1993).

62. Cimmino, A. *et al.* miR-15 and miR-16 induce apoptosis by targeting BCL2. *Proc. Natl. Acad. Sci. U.S.A.* **102,** 13944–13949 (2005).

63. Tagawa, H. *et al.* Genome-wide array-based CGH for mantle cell lymphoma: identification of homozygous deletions of the proapoptotic gene BIM. *Oncogene* **24,** 1348–1358 (2004).

64. Richter-Larrea, J. A. *et al.* Reversion of epigenetically mediated BIM silencing overcomes chemoresistance in Burkitt lymphoma. *Blood* **116,** 2531–2542 (2010).

65. Rampino, N. *et al.* Somatic frameshift mutations in the BAX gene in colon cancers of the microsatellite mutator phenotype. *Science* **275,** 967–969 (1997).

66. Miyashita, T. & Reed, J. C. Bcl-2 oncoprotein blocks chemotherapy-induced apoptosis in a human leukemia cell line. *Blood* **81,** 151–157 (1993).

67. Villunger, A. *et al.* p53- and drug-induced apoptotic responses mediated by BH3-only proteins puma and noxa. *Science* **302,** 1036–1038 (2003).

68. Certo, M. *et al.* Mitochondria primed by death signals determine cellular addiction to antiapoptotic BCL-2 family members. *Cancer Cell* **9,** 351–365 (2006).

69. Reed, J. C. *et al.* Antisense-mediated inhibition of BCL2 protooncogene expression and leukemic cell growth and survival: comparisons of phosphodiester and phosphorothioate oligodeoxynucleotides. *Cancer Research* **50,** 6565–6570 (1990).

70. Webb, A. *et al.* BCL-2 antisense therapy in patients with non-Hodgkin lymphoma. *The Lancet* **349,** 1137–1141 (1997).

71. Petros, A. M. *et al.* Discovery of a Potent Inhibitor of the Antiapoptotic Protein Bcl-x Lfrom NMR and Parallel Synthesis. *J. Med. Chem.* **49,** 656–663 (2006).

72. Hajduk, P. J. & Greer, J. A decade of fragment-based drug design: strategic advances and lessons learned. *Nat Rev Drug Discov* **6,** 211–219 (2007).

73. Oltersdorf, T. *et al.* An inhibitor of Bcl-2 family proteins induces regression of solid tumours. *Nature* **435,** 677–681 (2005).

74. Bruncko, M. *et al.* Studies Leading to Potent, Dual Inhibitors of Bcl-2 and Bcl-xL. *J. Med. Chem.* **50,** 641–662 (2007).

75. Tse, C. *et al.* ABT-263: A Potent and Orally Bioavailable Bcl-2 Family Inhibitor. *Cancer Research* **68,** 3421–3428 (2008).

76. Mason, K. D. *et al.* Programmed anuclear cell death delimits platelet life span. *Cell* **128,** 1173–1186 (2007).

77. Schoenwaelder, S. M. *et al.* Bcl-xL-inhibitory BH3 mimetics can induce a transient thrombocytopathy that undermines the hemostatic function of platelets. *Blood* **118,** 1663–1674 (2011).

78. Souers, A. J. *et al.* ABT-199, a potent and selective BCL-2 inhibitor, achieves antitumor activity while sparing platelets. *Nat Med* **19,** 202–208 (2013).

79. Leverson, J. D. *et al.* Potent and selective small-molecule MCL-1 inhibitors demonstrate on-target cancer cell killing activity as single agents and in combination with ABT-263 (navitoclax). *Cell Death and Disease* **6,** e1590 (2015).

80. Pelz, N. F. *et al.* Discovery of 2-Indole-acylsulfonamide Myeloid Cell Leukemia 1 (Mcl-1) Inhibitors Using Fragment-Based Methods. *J. Med. Chem.* **59,** 2054–2066 (2016).

81. Kotschy, A. *et al.* The MCL1 inhibitor S63845 is tolerable and effective in diverse cancer models. *Nature* **538,** 477–482 (2016).

82. Vogler, M. BCL2A1: the underdog in the BCL2 family. *Cell Death and Differentiation* **19,** 67–74 (2011).

83. Lin, E. Y., Orlofsky, A., Berger, M. S. & Prystowsky, M. B. Characterization of A1, a novel hemopoietic-specific early-response gene with sequence similarity to bcl-2. *J Immunol* **151,** 1979–1988 (1993).

84. Choi, S. S. *et al.* A novel Bcl-2 related gene, Bfl-1, is overexpressed in stomach cancer and preferentially expressed in bone marrow. *Oncogene* **11,** 1693–1698 (1995).

85. Karsan, A., Yee, E., Kaushansky, K. & Harlan, J. M. Cloning of human Bcl-2 homologue: inflammatory cytokines induce human A1 in cultured endothelial cells. *Blood* **87,** 3089–3096 (1996).

86. Lin, E. Y., Orlofsky, A., Wang, H. G., Reed, J. C. & Prystowsky, M. B. A1, a Bcl-2 family member, prolongs cell survival and permits myeloid differentiation. *Blood* **87,** 983–992 (1996).

87. Hatakeyama, S. *et al.* Multiple gene duplication and expression of mouse bcl-2-related genes, A1. *Int Immunol* **10,** 631–637 (1998).

88. D'Sa-Eipper, C., Subramanian, T. & Chinnadurai, G. bfl-1, a bcl-2 homologue, suppresses p53-induced apoptosis and exhibits potent cooperative transforming activity. *Cancer Research* **56,** 3879–3882 (1996).

89. D'Sa-Eipper, C. & Chinnadurai, G. Functional dissection of Bfl-1, a Bcl-2 homolog: anti-apoptosis, oncogene-cooperation and cell proliferation activities. *Oncogene* **16,** 3105–3114 (1998).

90. Zhang, H. *et al.* Structural basis of BFL-1 for its interaction with BAX and its anti-apoptotic action in mammalian and yeast cells. *Journal of Biological Chemistry* **275,** 11092–11099 (2000).

91. Werner, A. B., de Vries, E., Tait, S. W. G., Bontjer, I. & Borst, J. Bcl-2 Family Member Bfl-1/A1 Sequesters Truncated Bid to Inhibit Its Collaboration with Pro-apoptotic Bak or Bax. *Journal of Biological Chemistry* **277,** 22781–22788 (2002).

92. Tomayko, M. M. & Cancro, M. P. Long-lived B cells are distinguished by elevated expression of A1. *J Immunol* **160,** 107–111 (1998).

93. Verschelde, C. *et al.* A1/Bfl-1 expression is restricted to TCR engagement in T lymphocytes. *Cell Death and Differentiation* **10,** 1059–1067 (2003).

94. Ottina, E. *et al.* Targeting antiapoptotic A1/Bfl-1 by in vivo RNAi reveals multiple roles in leukocyte development in mice. *Blood* **119,** 6032–6042 (2012).

95. Sochalska, M. *et al.* Conditional knockdown of BCL2A1 reveals rate-limiting roles in BCR-dependent B-cell survival. *Cell Death and Differentiation* **23,** 628–639 (2016).

96. Mensink, M. *et al.* Anti-apoptotic A1 is not essential for lymphoma development in Eμ-Myc mice but helps sustain transplanted Eμ-Myc tumour cells. *Cell Death and Differentiation* **22,** 2755 (2018).

97. Tuzlak, S. *et al.* The BCL-2 pro-survival protein A1 is dispensable for T cell homeostasis on viral infection. *Cell Death and Differentiation* **24,** 523–533 (2017).

98. Zong, W. X., Edelstein, L. C., Chen, C., Bash, J. & Gelinas, C. The prosurvival Bcl-2 homolog Bfl-1/A1 is a direct transcriptional target of NF-kappaB that blocks TNFalpha-induced apoptosis. *Genes Dev.* **13,** 382–387 (1999).

99. Cheng, Q., Lee, H. H., Li, Y., Parks, T. P. & Cheng, G. Upregulation of Bcl-x and Bfl-1 as a potential mechanism of chemoresistance, which can be overcome by NF-kappaB inhibition. *Oncogene* **19,** 4936–4940 (2000).

100. Wang, C. Y., Guttridge, D. C., Mayo, M. W. & Baldwin, A. S. NF-kappaB induces expression of the Bcl-2 homologue A1/Bfl-1 to preferentially suppress chemotherapy-induced apoptosis. *Molecular and Cellular Biology* **19,** 5923–5929 (1999).

101. Kim, H., Kim, Y.-N., Kim, H. & Kim, C.-W. Oxidative stress attenuates Fas-mediated apoptosis in Jurkat T cell line through Bfl-1 induction. *Oncogene* **24,** 1252–1261 (2004).

102. Jenal, M. *et al.* The anti-apoptotic gene BCL2A1 is a novel transcriptional target of PU.1. *Leukemia* **24,** 1073–1076 (2010).

103. Kucharczak, J. F., Simmons, M. J., Duckett, C. S. & Gelinas, C. Constitutive proteasome-mediated turnover of Bfl-1/A1 and its processing in response to TNF receptor activation in FL5.12 pro-B cells convert it into a prodeath factor. *Cell Death and Differentiation* **12,** 1225–1239 (2005).

104. Fan, G. *et al.* Defective ubiquitin-mediated degradation of antiapoptotic Bfl-1 predisposes to lymphoma. *Blood* **115,** 3559–3569 (2010).

105. Herman, M. D. *et al.* Completing the family portrait of the anti-apoptotic Bcl-2 proteins: Crystal structure of human Bfl-1 in complex with Bim. *FEBS Letters* **582,** 3590–3594 (2008).

106. Harvey, E. P. *et al.* Crystal Structures of Anti-apoptotic BFL-1 and Its Complex with a Covalent Stapled Peptide Inhibitor. *Structure* **26,** 153–160.e4 (2018).

107. Brien, G. *et al.* C-terminal residues regulate localization and function of the antiapoptotic protein Bfl-1. *J. Biol. Chem.* **284,** 30257–30263 (2009).

108. Mandal, M. *et al.* The BCL2A1 gene as a pre–T cell receptor–induced regulator of thymocyte survival. *J Exp Med* **201,** 603–614 (2005).

109. Morales, A. A. *et al.* High expression of Bfl-1 contributes to the apoptosis resistant phenotype in B-cell chronic lymphocytic leukemia. *Int. J. Cancer* **113,** 730–737 (2004).

110. Olsson, A. *et al.* Upregulation of bfl-1 is a potential mechanism of chemoresistance in B-cell chronic lymphocytic leukaemia. *Br J Cancer* **97,** 769–777 (2007).

111. Mahadevan, D. *et al.* Transcript profiling in peripheral T-cell lymphoma, not otherwise specified, and diffuse large B-cell lymphoma identifies distinct tumor profile signatures. *Mol. Cancer Ther.* **4,** 1867–1879 (2005).

112. Brien, G., Trescol-Biemont, M.-C. & Bonnefoy-Bérard, N. Downregulation of Bfl-1 protein expression sensitizes malignant B cells to apoptosis. *Oncogene* **26,** 5828–5832 (2007).

113. Riker, A. I. *et al.* The gene expression profiles of primary and metastatic melanoma yields a transition point of tumor progression and metastasis. *BMC Med Genomics* **1,** 43–16 (2008).

114. Haq, R. *et al.* BCL2A1 is a lineage-specific antiapoptotic melanoma oncogene that confers resistance to BRAF inhibition. *Proc. Natl. Acad. Sci. U.S.A.* **110,** 4321–4326 (2013).

115. Hind, C. K. *et al.* Role of the pro-survival molecule Bfl-1 in melanoma. *Int. J. Biochem. Cell Biol.* **59,** 94–102 (2015).

116. Campone, M. *et al.* Prediction of metastatic relapse in node-positive breast cancer: establishment of a clinicogenomic model after FEC100 adjuvant regimen. *Breast Cancer Res Treat* **109,** 491–501 (2007).

117. Kim, J. K. *et al.* Up-regulation of Bfl-1/A1 via NF-κB activation in cisplatin-resistant human bladder cancer cell line. *Cancer Letters* **212,** 61–70 (2004).

118. Vogler, M. *et al.* Concurrent up-regulation of BCL-XL and BCL2A1 induces approximately 1000-fold resistance to ABT-737 in chronic lymphocytic leukemia. *Blood* **113,** 4403–4413 (2009).

119. Yecies, D., Carlson, N. E., Deng, J. & Letai, A. Acquired resistance to ABT-737 in lymphoma cells that up-regulate MCL-1 and BFL-1. *Blood* **115,** 3304–3313 (2010).

120. Lucas, K. M. *et al.* Modulation of NOXA and MCL-1 as a Strategy for Sensitizing Melanoma Cells to the BH3-Mimetic ABT-737. *Clinical Cancer Research* **18,** 783–795 (2012).

121. Brien, G. *et al.* Characterization of Peptide Aptamers Targeting Bfl-1 Anti-Apoptotic Protein. *Biochemistry* **50,** 5120–5129 (2011).

122. Zhai, D. *et al.* High-Throughput Fluorescence Polarization Assay for Chemical Library Screening against Anti-Apoptotic Bcl-2 Family Member Bfl-1. *J Biomol Screen* **17,** 350–360 (2012).

123. Mathieu, A.-L. *et al.* Identification of Small Inhibitory Molecules Targeting the Bfl-1 Anti-Apoptotic Protein That Alleviates Resistance to ABT-737. *J Biomol Screen* **19,** 1035–1046 (2014).

124. Azzarito, V., Long, K., Murphy, N. S. & Wilson, A. J. Inhibition of α-helix-mediated protein–protein interactions using designed molecules. *Nature Chem* **5,** 161–173 (2013).

125. Stumpf, M. P. H. *et al.* Estimating the size of the human interactome. *Proc. Natl. Acad. Sci. U.S.A.* **105,** 6959–6964 (2008).

126. Craik, D. J., Fairlie, D. P., Liras, S. & Price, D. The Future of Peptide-based Drugs. *Chemical Biology & Drug Design* **81,** 136–147 (2012).

127. Cromm, P. M., Spiegel, J. & Grossmann, T. N. Hydrocarbon Stapled Peptides as Modulators of Biological Function. *ACS Chem. Biol.* **10,** 1362–1375 (2015).

128. J Wilson, A. Inhibition of protein–protein interactions using designed molecules. *Chem. Soc. Rev.* **38,** 3289–13 (2009).

129. Laraia, L., McKenzie, G., Spring, D. R., Venkitaraman, A. R. & Huggins, D. J. Overcoming Chemical, Biological, and Computational Challenges in the Development of Inhibitors Targeting Protein-Protein Interactions. *Chemistry & Biology* **22,** 689–703 (2015).

130. Verdine, G. L. & Walensky, L. D. The Challenge of Drugging Undruggable Targets in Cancer: Lessons Learned from Targeting BCL-2 Family Members. *Clinical Cancer Research* **13,** 7264–7270 (2007).

131. Kaspar, A. A. & Reichert, J. M. Future directions for peptide therapeutics development. *Drug Discovery Today* **18,** 807–817 (2013).

132. Bracken, C., Gulyas, J., Taylor, J. W. & Baum, J. Synthesis and Nuclear Magnetic Resonance Structure Determination of an .alpha.-Helical, Bicyclic, Lactam-Bridged Hexapeptide. *J. Am. Chem. Soc.* **116,** 6431–6432 (1994).

133. Phelan, J. C., Skelton, N. J., Braisted, A. C. & McDowell, R. S. A General Method for Constraining Short Peptides to an α-Helical Conformation. *J. Am. Chem. Soc.* **119,** 455–460 (1997).

134. Bouvier, M. & Taylor, J. W. Probing the functional conformation of neuropeptide Y through the design and study of cyclic analogs. *J. Med. Chem.* **35,** 1145–1155 (1992).

135. Jackson, D. Y., King, D. S., Chmielewski, J., Singh, S. & Schultz, P. G. General approach to the synthesis of short alpha-helical peptides. *J. Am. Chem. Soc.* **113,** 9391–9392 (1991).

136. Blackwell, H. & Grubbs, R. Highly Efficient Synthesis of Covalently Cross-Linked Peptide Helices by Ring-Closing Metathesis. *Angew. Chem. Int. Ed.* **37,** 3281–3284 (1998).

137. Schafmeister, C. E., Po, J. & Verdine, G. L. An All-Hydrocarbon Cross-Linking System for Enhancing the Helicity and Metabolic Stability of Peptides. *J. Am. Chem. Soc.* **122,** 5891–5892 (2000).

138. Walensky, L. D. *et al.* Activation of apoptosis in vivo by a hydrocarbon-stapled BH3 helix. *Science* **305,** 1466–1470 (2004).

139. Bird, G. H. *et al.* Hydrocarbon double-stapling remedies the proteolytic instability of a lengthy peptide therapeutic. *Proc. Natl. Acad. Sci. U.S.A.* **107,** 14093–14098 (2010).

140. Edwards, A. L. *et al.* Cellular Uptake and Ultrastructural Localization Underlie the Pro-apoptotic Activity of a Hydrocarbon-stapled BIM BH3 Peptide. *ACS Chem. Biol.* **10,** 2149–2157 (2015).

141. Chu, Q. *et al.* Towards understanding cell penetration by stapled peptides. *MedChemComm* **6,** 111–119 (2014).

142. Bird, G. H. *et al.* Biophysical determinants for cellular uptake of hydrocarbon-stapled peptide helices. *Nature Chemical Biology* **12,** 845–852 (2016).

143. Eskes, R., Desagher, S., Antonsson, B. & Martinou, J. C. Bid induces the oligomerization and insertion of Bax into the outer mitochondrial membrane. *Molecular and Cellular Biology* **20,** 929–935 (2000).

144. Gavathiotis, E., Reyna, D. E., Davis, M. L., Bird, G. H. & Walensky, L. D. BH3-triggered structural reorganization drives the activation of proapoptotic BAX. *Molecular Cell* **40,** 481–492 (2010).

145. Leshchiner, E. S., Braun, C. R., Bird, G. H. & Walensky, L. D. Direct activation of full-length proapoptotic BAK. *Proc. Natl. Acad. Sci. U.S.A.* **110,** E986–95 (2013).

146. LaBelle, J. L. *et al.* A stapled BIM peptide overcomes apoptotic resistance in hematologic cancers. *J. Clin. Invest.* **122,** 2018–2031 (2012).

147. Braun, C. R. *et al.* Photoreactive Stapled BH3 Peptides to Dissect the BCL-2 Family Interactome. *Chemistry & Biology* **17,** 1325–1333 (2010).

148. Edwards, A. L. *et al.* Multimodal Interaction with BCL-2 Family Proteins Underlies the Proapoptotic Activity of PUMA BH3. *Chemistry & Biology* **20,** 888–902 (2013).

149. Barclay, L. A. *et al.* Inhibition of Pro-Apoptotic BAX by a Noncanonical Interaction Mechanism. *Molecular Cell* **57,** 873–886 (2015).

150. Szlyk, B. *et al.* A phospho-BAD BH3 helix activates glucokinase by a mechanism distinct from that of allosteric activators. *Nat Struct Mol Biol* **21,** 36–42 (2014).

151. Escudero, S. *et al.* Dynamic Regulation of Long-Chain Fatty Acid Oxidation by a Noncanonical Interaction between the MCL-1 BH3 Helix and VLCAD. *Molecular Cell* **69,** 729–743 (2018).

152. Stewart, M. L., Fire, E., Keating, A. E. & Walensky, L. D. The MCL-1 BH3 helix is an exclusive MCL-1 inhibitor and apoptosis sensitizer. *Nature Chemical Biology* **6,** 595–601 (2010).

153. Cohen, N. A. *et al.* A Competitive Stapled Peptide Screen Identifies a Selective Small Molecule that Overcomes MCL-1-Dependent Leukemia Cell Survival. *Chemistry & Biology* **19,** 1175–1186 (2012).

154. Lee, S. *et al.* Allosteric inhibition of antiapoptotic MCL-1. *Nat Struct Mol Biol* **23,** 600–607 (2016).

155. Zhan, T., Rindtorff, N. & Boutros, M. Wnt signaling in cancer. *Oncogene* **36,** 1461–1473 (2016).

156. Takada, K. *et al.* Targeted disruption of the BCL9/β-catenin complex inhibits oncogenic Wnt signaling. *Sci Transl Med* **4,** 148ra117 (2012).

157. Kim, K. H. & Roberts, C. W. M. Targeting EZH2 in cancer. *Nat Med* **22,** 128–134 (2016).

158. Kim, K. H. *et al.* SWI/SNF-mutant cancers depend on catalytic and non-catalytic activity of EZH2. *Nat Med* **21,** 1491–1496 (2015).

159. Kim, W. *et al.* Targeted disruption of the EZH2-EED complex inhibits EZH2-dependent cancer. *Nature Chemical Biology* **9,** 643–650 (2013).

160. Leshchiner, E. S. *et al.* Direct inhibition of oncogenic KRAS by hydrocarbon-stapled SOS1 helices. *Proc. Natl. Acad. Sci. U.S.A.* **112,** 1761–1766 (2015).

161. LaBonte, J., Lebbos, J. & Kirkpatrick, P. Enfuvirtide. *Nat Rev Drug Discov* **2,** 345–346 (2003).

162. Bird, G. H. *et al.* Stapled HIV-1 peptides recapitulate antigenic structures and engage broadly neutralizing antibodies. *Nat Struct Mol Biol* **21,** 1058–1067 (2014).

163. Bird, G. H. *et al.* Mucosal delivery of a double-stapled RSV peptide prevents nasopulmonary infection. *J. Clin. Invest.* **124,** 2113–2124 (2014).

164. Kastenhuber, E. R. & Lowe, S. W. Putting p53 in Context. *Cell* **170,** 1062–1078 (2017).

165. Laptenko, O. & Prives, C. Transcriptional regulation by p53: one protein, many possibilities. *Cell Death and Differentiation* **13,** 951–961 (2006).

166. Dai, C. & Gu, W. p53 post-translational modification: deregulated in tumorigenesis. *Trends in Molecular Medicine* **16,** 528–536 (2010).

167. Wang, S., Zhao, Y., Aguilar, A., Bernard, D. & Yang, C.-Y. Targeting the MDM2–p53 Protein–Protein Interaction for New Cancer Therapy: Progress and Challenges. *Cold Spring Harb Perspect Med* **7,** a026245–11 (2017).

168. Cheok, C. F. & Lane, D. P. Exploiting the p53 Pathway for Therapy. *Cold Spring Harb Perspect Med* **7,** a026310–15 (2017).

169. Kussie, P. H. *et al.* Structure of the MDM2 oncoprotein bound to the p53 tumor suppressor transactivation domain. *Science* **274,** 948–953 (1996).

170. Vassilev, L. T. *et al.* In vivo activation of the p53 pathway by small-molecule antagonists of MDM2. *Science* **303,** 844–848 (2004).

171. Vu, B. *et al.* Discovery of RG7112: A Small-Molecule MDM2 Inhibitor in Clinical Development. *ACS Med. Chem. Lett.* **4,** 466–469 (2013).

172. Ray-Coquard, I. *et al.* Effect of the MDM2 antagonist RG7112 on the P53 pathway in patients with MDM2-amplified, well-differentiated or dedifferentiated liposarcoma: an exploratory proof-of-mechanism study. *Lancet Oncol.* **13,** 1133–1140 (2012).

173. Bernal, F., Tyler, A. F., Korsmeyer, S. J., Walensky, L. D. & Verdine, G. L. Reactivation of the p53 Tumor Suppressor Pathway by a Stapled p53 Peptide. *J. Am. Chem. Soc.* **129,** 2456–2457 (2007).

174. Bernal, F. *et al.* A Stapled p53 Helix Overcomes HDMX-Mediated Suppression of p53. *Cancer Cell* **18,** 411–422 (2010).

175. Pazgier, M. *et al.* Structural basis for high-affinity peptide inhibition of p53 interactions with MDM2 and MDMX. *Proc. Natl. Acad. Sci. U.S.A.* **106,** 4665–4670 (2009).

176. Chang, Y. S. *et al.* Stapled α-helical peptide drug development: a potent dual inhibitor of MDM2 and MDMX for p53-dependent cancer therapy. *Proc. Natl. Acad. Sci. U.S.A.* **110,** E3445–54 (2013).

177. Meric-Bernstam, F. *et al.* Phase I trial of a novel stapled peptide ALRN-6924 disrupting MDMX- and MDM2-mediated inhibition of WT p53 in patients with solid tumors and lymphomas. *JCO* **35,** 2505–2505 (2017).

178. Jochim, A. L. & Arora, P. S. Systematic Analysis of Helical Protein Interfaces Reveals Targets for Synthetic Inhibitors. *ACS Chem. Biol.* **5,** 919–923 (2010).

Chapter II

Selective Covalent Targeting of Anti-Apoptotic BFL-1

by Cysteine-Reactive Stapled Peptide Inhibitors

ABSTRACT

Anti-apoptotic BCL-2 family proteins block cell death by trapping the critical α-helical BH3 domains of pro-apoptotic members in a surface groove. Cancer cells hijack this survival mechanism by overexpressing a spectrum of anti-apoptotic members, mounting formidable apoptotic blockades that resist chemotherapeutic treatment. Drugging the BH3-binding pockets of anti-apoptotic proteins has become a highest-priority goal, fueled by the clinical success of venetoclax, a selective BCL-2 inhibitor, in reactivating apoptosis in BCL-2-dependent cancers. BFL-1/A1 is a BCL-2 family protein implicated in the progression and chemoresistance of melanoma, lymphoma, and other cancers, yet it remains undrugged. A natural juxtaposition of two unique cysteines at the binding interface of the NOXA BH3 helix and BFL-1/A1 pocket informed the development of stapled BH3 peptides bearing acrylamide warheads to irreversibly inhibit BFL-1/A1 by covalent targeting. Here, we describe the development and application of cysteine-reactive stapled peptides that, compared to their non-covalent analogs, trigger more rapid mitochondrial cytochrome *c* release, caspase-3/7 activation, and apoptosis induction of BFL-1/A1-driven cancers such as melanoma. Mechanism of action studies demonstrated the exquisite BFL-1/A1 selectivity and mitochondrial localization of the *in situ* covalent reaction. Given the frequent proximity of native cysteines to regulatory binding surfaces, covalent stapled peptide inhibitors provide a new therapeutic strategy for targeting oncogenic protein interactions.

ATTRIBUTIONS

This chapter was published in the following manuscript: Huhn, A.J., Guerra, R.M., Harvey, E.P., Bird, G.H., and Walensky, L.D. Selective covalent targeting of anti-apoptotic BFL-1 by cysteine-reactive stapled peptide inhibitors. *Cell Chem Biol* **23**, 1123-1134 (2016).

Contributions to the work described in this chapter were made by Rachel M. Guerra, Annissa H. Huhn, Edward P. Harvey, Gregory H. Bird, and Loren D. Walensky.

G.H.B. and L.D.W. designed the study. G.H.B. generated stapled peptides and performed microscopy-based peptide-uptake studies. A.J.H. executed the biochemical experiments including *in vitro* binding and crosslinking analyses, with assistance from E.P.H. in generating peptide-protein conjugates for the liposomal assays. R.M.G. conducted all of the cellular work including immunoprecipitation, *in situ* crosslinking, viability, caspase-3/7, cytochrome *c* release, and cell-imaging studies. R.M.G., A.J.H., G.H.B., and L.D.W. analyzed the data. Additionally, we thank T. Oo for stapled peptide synthesis and E. Smith for graphics support.

INTRODUCTION

BCL-2 family proteins are key regulators of the apoptotic pathway and control the life-death decision made by cells in response to stress[1,2]. However, when left unchecked, deregulation of apoptosis can result in a host of human diseases[3]. Overexpression of the founding member of this family, BCL-2, promotes cell survival in follicular lymphoma[4-8]. The anti-apoptotic BCL-2 family members have emerged as ripe targets for therapeutic development as they are often overexpressed to enforce cellular immortality, representing a classic hallmark of cancer[9]. The canonical mechanism for apoptotic suppression involves sequestration of the BH3 killer domain helices of pro-apoptotic members in a binding pocket composed of the BH1, BH2, and BH3 domains of the anti-apoptotic BCL-2 family proteins[10]. Thus, structural mimicry of pro-apoptotic BH3 helices has been pursued to pharmacologically ‘‘inhibit the inhibitors’’ of apoptosis. For example, small-molecule BH3 mimetics, such as ABT-737[11] and ABT-263[12], were initially designed to target the BH3-binding pockets of both BCL-2 and BCL-X_L, and the next-generation clinical agent, ABT-199[13] was refined for selective BCL-2 inhibition at least in part to avoid the adverse effect of BCL-X_L inhibition on platelet survival[13,14]. Given the diversity of anti- apoptotic BCL-2 family proteins at the cancer cell’s disposal, developing inhibitors for each of these oncogenic proteins, including compounds active against subsets or all of the targets, is a priority. For example, because MCL-1 has emerged as one of the top ten most expressed pathologic proteins across all subtypes of human cancers[15], there has been significant interest in developing a selective small molecule inhibitor of MCL-1[16,17], with the first agents entering Phase 1 clinical testing in 2017[18].

The Walensky laboratory has taken an alternative approach to BCL-2 family targeting by transforming the spectrum of natural BH3 domain sequences into structurally reinforced α-helices that resist proteolysis *in vivo* and, when appropriately designed, achieve intracellular access through macropinosomal import[19,20]. The earliest classes of all-hydrocarbon-stapled peptides derived in the Walensky lab were modeled after the BH3 domains of BID[20,21] and BIM[22-24], two pro-apoptotic BCL-2 family members of the "BH3-only" subclass that can directly bind and activate the executioner proteins BAX and BAK, and also inhibit the entire spectrum of anti-apoptotic pockets. These stapled peptide helices, termed Stabilized Alpha-Helices of BCL-2 domains (SAHBs), have been used to dissect the molecular interactions of the BCL-2 family signaling network, discover novel interacting partners, and as prototype therapeutics themselves to reactivate apoptosis in cancer. Here, we sought to apply our stapling technology to develop a selective inhibitor of anti-apoptotic BFL-1, a relatively understudied anti-apoptotic BCL-2 family protein that has been implicated in the development, maintenance, and chemoresistance of select human cancers.

The pathologic expression of BFL-1 has been reported as an oncogenic driver of melanoma, lymphoma, and leukemia[25-29]. In melanoma, for example, BFL-1 overexpression correlates with chemoresistance and metastasis[30,31], and is directly regulated by the microphthalmia-associated transcription factor (MITF), which is essential to melanomagenesis[26]. In lymphoma, upregulation of BFL-1 accounts for resistance to selective inhibition of BCL-2 and BCL-X_L, underscoring the importance of developing BFL-1 inhibitors in the era of venetoclax[29]. Likewise, BFL-1 overexpression in the context of BRAF V600E mutation, which is found in 80% of BRAF-mutant

melanomas, blunts the pharmacologic benefit of small-molecule BRAF inhibitors, whereas small interfering RNA knockdown of BFL-1 sensitized the cells to apoptosis induction[26,32]. Taken together, there is a compelling rationale for developing a targeted inhibitor of anti-apoptotic BFL-1 for cancer treatment.

In planning a strategy for selective BFL-1 inhibition, we noted the unique juxtaposition of cysteines at the binding interface of BFL-1 and the BH3 domain of pro-apoptotic NOXA, as defined by X-ray crystallography of the complex (PDB: 3MQP). We reasoned that combining the high-affinity non-covalent interactions of a natural BH3 domain helix with the irreversible blockade afforded by covalent reaction could yield a high-fidelity BFL-1 inhibitor, a strategy that could also be applied to a broad spectrum of helix-in-groove interactions containing native cysteines within or near the protein-binding surface. Indeed, the development of small-molecule covalent inhibitors of more focal binding sites on kinases has seen remarkable success in recent years. For example, ibrutinib, which covalently targets C426 of Bruton's tyrosine kinase, is approved by the Food and Drug Administration (FDA) for the treatment of Waldenstrom's macroglobulinemia, chronic lymphocytic leukemias, and mantle cell lymphoma[33-35]. Afatinib is an irreversible covalent inhibitor that selectively targets the receptor tyrosine kinases epidermal growth factor receptor (EGFR) and HER2, and has been approved by the FDA for the treatment of metastatic, EGFR T790M-mutant non-small cell lung cancer[36-39]. Motivated by this resurgence of covalent inhibitor drugs and our identification of a uniquely positioned cysteine residue in the BH3-binding pocket of BFL-1, we designed, characterized, and validated a new class of stapled peptide inhibitors with highly selective covalent reactivity.

METHODS

Stapled Peptide Synthesis. Hydrocarbon-stapled peptides corresponding to the BH3 domains of BCL-2 family proteins, and either N-terminally derivatized with acetyl, FITC-βAla, biotin-PEG, or electrophilic warheads, or C-terminally derivatized with Lys-biotin, were synthesized, purified, and quantitated using our previously reported methods[40,41]. Acrylamide-bearing peptides were synthesized by either coupling acrylic acid or trans-crotonic acid to the peptide N-terminus, or by first coupling the Fmoc protected cyclic amino acids (Chem-Impex International) followed by Fmoc deprotection and acylation with acrylic acid, using standard Fmoc coupling and deprotection methods. Stapled peptide compositions, and their observed masses and use by figure, are listed in **Appendix: Table S1**.

FITC Derivatization of Acrylamide-Bearing Stapled Peptides. Cystamine dihydrochloride (1 eq) was dissolved in 10 mL DMSO, accompanied by 270 µL DIEA (3 eq), and then 400 mg (2 eq) of FITC was added. The reaction was monitored by LC/MS and, after overnight stirring and completion of the reaction, 2 eq TCEP in 1 mL of water was added. The reduced product was purified on an Isco CombiFlash purification system equipped with a 40 g C18 reversed phase column using a water-acetonitrile gradient. The fractions containing product were lyophilized to afford 385 mg of FITC-labeled cysteamine. The subsequent conjugation reaction with acrylamide-containing stapled peptide was found to be pH dependent as expected, with no reaction occurring at pH 6 or pH 8, whereas the reaction in pH 10 borate buffer went to completion after overnight incubation in a 1:1:3 solution of 1 mM DMSO peptide stock, 5 mM DMSO

stock of FITC-cysteamine, and 0.05 M borate buffer. The FITC-labeled peptide product, FITC-BIM SAHB$_A$-3, was then purified by HPLC.

Recombinant Protein Expression and Purification. The recombinant anti-apoptotic proteins were expressed in *Escherichia coli* BL21(DE3), and purified by sequential affinity and size-exclusion chromatography as described[42]. cDNA encoding BFL-1ΔC (aa 1-153) was cloned into the pET19b expression vector (Novagen) followed by DNA sequencing to verify the construct. Constructs bearing cysteine to serine mutations were created by PCR-based site-directed mutagenesis (QuikChange Mutagenesis Kit, Stratagene). Transformed *Escherichia coli* BL21(DE3) LOBSTR[43] (#EC1001, Kerafast) were cultured in ampicillin-containing Luria broth (LB) and protein expression induced with 0.5 mM isopropyl β-D-1-thiogalactopyranoside (IPTG) overnight at 16 °C. Bacterial pellets were resuspended in 20 mM Tris pH 7.5, 250 mM NaCl, and two complete protease inhibitor tablets (Roche), and then microfluidized (M-110L, Microfluidics) and centrifuged at 45,000 x g for 1 h. The supernatant was passed over a Ni-NTA (Qiagen) column equilibrated with 50 mM Tris pH 7.5, 250 mM NaCl. The column was sequentially washed with 25 mL of equilibration buffer containing 5 mM, 10 mM and 20 mM imidazole, and then His-BFL-1ΔC was eluted in equilibration buffer containing 300 mM imidazole. The fraction containing His-BFL-1ΔC was dialyzed against 50 mM Tris pH 8, 100 mM NaCl at 4 °C and then concentrated and loaded onto a Superdex S-75 (GE Healthcare) gel filtration column equilibrated with 50 mM Tris pH 8.0, 100 mM NaCl. The column was washed with 30 mL equilibration buffer and fractions containing His-BFL-1ΔC were pooled and analyzed both by SDS-PAGE

electrophoresis/Coomassie stain and anti-BFL-1 (Abcam, #125259) and anti-His (Abcam, #18184) western blotting. Purified protein was then concentrated, flash frozen using liquid nitrogen, and stored at -80 °C until use.

MCL-1ΔNΔC (aa 170-327) and BCL-X_LΔC (aa 1-212) constructs were cloned into pGEX-4T-1 (GE Healthcare) followed by DNA sequencing to verify the constructs. Transformed *Escherichia coli* BL21(DE3) (Sigma-Aldrich) were cultured in ampicillin-containing LB, and protein expression induced with 0.5 mM IPTG and grown for 4 h at 37°C. Bacterial pellets were resuspended in phosphate-buffered saline (PBS), 0.1% Triton X-100, and complete protease inhibitor tablet (Roche), and then microfluidized and centrifuged at 45,000 x g for 1 h. Supernatants were passed over a glutathione sepharose (GE Healthcare) column equilibrated with PBS containing 0.1% Triton X-100. The column was sequentially washed with 25 mL of PBS containing 0.1% Triton X-100 and PBS, and then GST cleaved on-resin with thrombin (Sigma) overnight at 25 °C. The GST-free protein was eluted with PBS, concentrated, and loaded onto a Superdex S-75 (GE Healthcare) gel filtration column equilibrated with 50 mM Tris pH 7.4, 150 mM NaCl. The column was washed with 30 mL equilibration buffer and fractions containing MCL-1ΔNΔC or BCL-X_LΔC were pooled and analyzed by SDS-PAGE electrophoresis and Coomassie staining. Purified protein was then concentrated, flash frozen using liquid nitrogen, and stored at -80 °C.

Biolayer Interferometry. Binding analyses of NOXA peptide interactions with BFL-1ΔC were performed on an Octet RED384 system (Fortebio, Menlo Park, CA) at 30 °C. Super streptavidin (SSA) tips were prewetted in 1x kinetics buffer (PBS, pH 7.4, 0.01%

BSA, 0.002% Tween-20) and then conjugated to NOXA SAHBs bearing an N-terminal biotin-PEG linker (10 μg/mL). Excess streptavidin was quenched by incubation with 2 μg/mL biocytin. The tips were then washed with kinetics buffer and soaked in a serial dilution of BFL-1ΔC for 10 min to measure association rate, followed by a 15 min incubation in kinetics buffer to measure dissociation rate. Dissociation constants were calculated using Octet Data Analysis version 9.0.

In Vitro Covalent Conjugation Assay. BFL-1ΔC constructs (40 μM) were combined with NOXA $SAHB_A$ or NOXA $SAHB_A$ C25S (120 μM) and 10 mM DTT in 50 mM Tris pH 8.0, 100 mM NaCl (final volume, 5 μL), and then incubated in the dark for 1 h at room temperature. After this incubation in a reducing environment, the mixture was diluted 5-fold into 50 mM Tris pH 8.0, 100 mM NaCl, 12 mM GSSG and incubated in the dark for an additional 30 min at room temperature. The samples were then boiled in 4x loading buffer lacking DTT and electrophoresed on 12% Bis-Tris gel. The gel was rinsed with water, subjected to FITC scan (Typhoon FLA 9500, GE Healthcare) and then Coomassie staining.

For warhead-bearing SAHBs, His-BFL-1ΔC C4S/C19S protein was pretreated with 10 mM DTT in 50 mM Tris pH 8.0, 100 mM NaCl for 30 min at room temperature (final volume, 9.5 μL), and then combined with a 10:1 molar ratio of NOXA $SAHB_A$ or BIM $SAHB_A$ peptides bearing warheads **1**-**8** (final volume, 10 μL) for an additional 2 h incubation at room temperature. Processing for gel electrophoresis and Coomassie staining was performed as above.

Streptavidin Pull-Down. Recombinant His-BFL-1ΔC, BCL-X_LΔC (tagless), and GST-MCL-1ΔNΔC (1 μM each) were combined and reduced with 3 mM DTT in PBS for 30 min at room temperature, and incubated with 1 μM biotinylated $SAHB_A$, $SAHB_A$-3, or vehicle for 4 hr at room temperature. The mixtures were then combined with PBS-washed high-capacity SA agarose (Thermo Fisher Pierce) and incubated with rotation for 2 hr at room temperature. The beads were centrifuged at 3,000 rpm, washed twice with NP-40 lysis buffer (1% NP-40, 50 mM Tris [pH 8.0], 100 mM NaCl, 2.5 mM $MgCl_2$), once with PBS, and the bound protein was eluted by boiling in 10% SDS containing 10 mg/mL biotin. Inputs (10%) and eluates were electrophoresed on a 12% Bis-Tris gel and then subjected to silver staining and imaging.

Liposomal Release Assay. Large unilamellar vesicles (LUVs) with encapsulated ANTS and DPX were generated and purified as described[44,45]. The indicated combinations of BAX (400 nM), tBID (40 nM), and BFL-1ΔC or $SAHB_A$-3/BFL-1ΔC conjugates (1.5 μM), were added to liposomes (5 μL) in 384 well plates (final volume, 30 μL), and released fluorophore was measured over 120 min using an M1000 Infinite plate reader (Tecan) with excitation and emission wavelengths of 355 nm and 520 nm, respectively. $SAHB_A$-3/BFL-1ΔC conjugates were prepared by treating BFL-1ΔC (10 μM) with DTT (20 mM) for 30 min at 4 °C, followed by sequential incubation with NOXA $SAHB_A$-3 or BIM $SAHB_A$-3 peptides at peptide:protein molar ratios of 1.2x, 0.75x, and 0.5x for 1 hr each at 4 °C. Conjugation efficiency was confirmed by 12% Bis-Tris gel electrophoresis and Coomassie staining. The protein conjugate was then concentrated to 75 μM, loaded onto a Superdex S-75 (GE Healthcare) gel filtration column equilibrated with 20 mM

HEPES pH 7.5, 300 mM NaCl, 1 mM DTT, washed with 30 mL equilibration buffer, and fractions collected, analyzed by SDS-PAGE electrophoresis, and used fresh in liposomal assays. Percent ANTS/DPX release was calculated as [(F-F0)/(F100-F0)] x 100, where F0 is baseline fluorescence at time 0, F is the fluorescence recorded for each time point, and F100 is the maximum amount of ANTS/DPX release based on liposomal treatment with 1% Triton X-100.

BFL-1 Targeting in Lysates and Cells. 293T cells were maintained in DMEM containing 10% FBS and penicillin/streptomycin, and transfections performed with 2 μg pCMV plasmid containing HA-BFL-1ΔC C4S/C19S using X-tremeGENE 9 (Roche). For lysate experiments, cells were trypsinized 24 hr post-transfection, washed with PBS, and lysed by incubation with 1% CHAPS lysis buffer (150 mM NaCl, 50 mM Tris pH 7.4, 100 mM DTT). Protein concentration of the soluble fraction was measured using a BCA kit according to manufacturer's instructions (Thermo Scientific). Biotinylated NOXA $SAHB_A$-3 or BIM $SAHB_A$-3 (10 μM) was added to 100 μg of lysate and incubated at RT for 2 hr. Samples were then boiled in LDS buffer and subjected to western analysis using 1:1000 dilutions of HA (Sigma-Aldrich, #12CA5) and biotin (Abcam, #53494) antibodies. To evaluate the capacity of biotinylated SAHBs to compete with tBID for interactions with BFL-1 and MCL-1, 293T cells were transfected with either HA-BFL-1ΔC C4S/C19S or FLAG-MCL-1 in the p3XFLAG-CMV-10 vector (Sigma) as above. After 24 hr, cells were trypsinized, washed with PBS, lysed in 1% CHAPS buffer, and the supernatant collected for protein concentration determination by BCA kit. Lysate samples (0.5 mg) were incubated with 0.25 μM recombinant tBID (R&D Systems) and 5

μM biotinylated BIM SAHB$_A$ or BIM SAHB$_A$-3 for 6 h at RT. The mixtures were then subjected to HA or FLAG (Sigma-Aldrich, F7425) immunoprecipitation, followed by western analysis using 1:1000 dilutions of HA, FLAG, and BID (Santa Cruz sc-11423) antibodies. For HA-immunoprecipitation from 293T cells treated with biotinylated peptides, cells were transfected with HA-BFL-1ΔC C4S/C19S as above and, after 24 hr, incubated with 20 μM biotinylated BIM SAHB$_A$ or BIM SAHB$_A$-3 in DMEM containing 5% FBS for 6 hr. Cells were harvested and lysed as above, and incubated overnight with anti-HA agarose beads (Pierce). The beads were washed 3 times with lysis buffer, eluted by boiling in LDS buffer, and subjected to western analysis with HA and biotin antibodies. For 293T treatment with non-biotinylated SAHBs, cells were transfected with HA-BFL-1ΔC C4S/C19S as above, incubated with 20 μM BIM SAHB$_A$ or BIM SAHB$_A$-3 in DMEM containing 5% FBS, and lysates harvested as above at the indicated time points for western analysis using the HA and actin antibodies. For A375P melanoma studies, cells were maintained in DMEM containing 10% FBS and penicillin/streptomycin, and biotinylated NOXA SAHB$_A$-3 or BIM SAHB$_A$-3 (30 μM) was added to 1 mg of lysate, followed by overnight incubation in CHAPS lysis buffer at 4 °C. Biotin capture was accomplished by incubating the mixture with high-capacity SA agarose (Thermo Scientific) for 2 hr at 4 °C, followed by centrifugation and washing the pelleted beads with 3 x 1 mL lysis buffer. Bead-bound proteins were eluted by boiling in 10% SDS containing 10 mg/mL biotin for 10 min and then subjected to electrophoresis and western blotting using BFL-1 (Abcam, #125259) and MCL-1 (Rockland, #600-401-394S) antibodies.

Cellular Uptake of Stapled Peptides. To evaluate cellular uptake of biotinylated SAHBs by biotin western analysis of electrophoresed lysates from treated cells, 293T cells were plated in 6-well Corning plates (2 x 10^5 cells/well) in DMEM containing 10% FBS and penicillin/streptomycin. After 24 h, biotinylated NOXA $SAHB_A$-3 or BIM $SAHB_A$-3 peptides (20 μM) were added to the cells in DMEM containing 5% FBS for an additional 24 h incubation. The cells were then trypsinized to remove any surface-bound peptide, washed with PBS, lysed as above in 1% CHAPS lysis buffer, and the supernatant collected for protein concentration determination by BCA kit according to manufacturer's instructions (Thermo Scientific). Cellular lysate samples (50 μg) were boiled in LDS buffer and subjected to western analysis using a 1:1000 dilution of anti-biotin (Abcam, #53494) and 1:2000 dilution of anti-actin (Sigma-Aldrich, #A1978) antibodies. To evaluate the potential effect of transfection conditions on stapled peptide uptake, 293T cells were plated in 6-well Corning plates (2 x 10^5 cells/well) and cultured as above. After 24 h, a mock transfection was performed with X-tremeGENE 9 (Roche) and no plasmid alongside control cells that were not transfected. After an additional 24 hour incubation, 20 μM biotinylated BIM $SAHB_A$-3 peptide was added to the cells in DMEM containing 5% FBS and incubated for 4 h. Cells were then washed, trypsinized, and lysed as above, and lysates subjected to biotin and actin western analyses.

For cellular uptake analysis by ImageXpress high-content epifluorescence microscopy, the indicated cell lines were plated in black, clear bottom 96-well plates overnight at a density of 1.5 x 10^4 cells per well for MEFs or 1 x 10^4 cells per well for A375P cells in DMEM supplemented with 10% FBS, 1% penicillin/streptomycin, and 1% glutamine. The following day, cells were treated with the FITC-labeled peptides or the

equivalent amount of vehicle (0.1% DMSO) for 4 hr in DMEM supplemented with 5% FBS, and then stained with Hoechst 33342 and CellMask Deep Red (CMDR, Invitrogen) for 10 min. The media was then aspirated and cells fixed with 4% (wt/vol) paraformaldehyde for 10 min, followed by washing three times with PBS and imaging by ImageXpress Microscopy (Molecular Devices). Data were collected for five sites per well at 20x magnification, with each treatment performed in triplicate, and then analyzed and quantified using MetaXpress software. The CMDR stain was used to visualize the boundaries of the cell and to create a mask for measuring FITC-peptide inside the cell, thereby excluding fluorescent debris from the analysis. A custom module in MetaXpress was applied to incrementally recede the CMDR image mask from the cellular border, further restricting the analyzed FITC signal to internalized peptide. The measurement of Total Internalized Fluorescence Intensity (TIFI) represents the level of absolute fluorescence detected per cell, per peptide construct. Maximum and minimum thresholding was utilized to exclude FITC and Cy5 outliers that were much larger and brighter than average, and total intensity and average intensity per cell thresholds were set such that vehicle-treated cells scored negative by the analysis.

Cell Viability, LDH Release, and Caspase-3/7 Activation Assays. Cancer cells were cultured using their standard culture medium containing 10% fetal bovine serum (FBS) and penicillin-streptomycin (A375P: DMEM; SK-MEL-2, SK-MEL-28, and MCF-7: EMEM; A549 and H929: RPMI). Cells were plated in 96-well plates (5 x 10^3 cells per well) and, after overnight incubation, treated with the indicated concentrations of BIM $SAHB_{A1}$ or BIM $SAHB_A$-3 in the corresponding medium supplemented with 5% FBS for

the indicated durations. Cell viability and caspase-3/7 activation was measured using CellTiter-Glo and Caspase-Glo 3/7 chemiluminescence reagents (Promega), respectively, and luminescence was detected by a microplate reader (Spectramax M5, Molecular Devices). LDH release was quantified after 30 min of peptide incubation by plate centrifugation at 1,500 rpm for 5 min at 4 °C, transfer of 100 mL of cell-culture medium to a clear plate (Corning), incubation with 100 mL of LDH reagent (Roche) for 30 min while shaking, and measurement of absorbance at 490 nm on a Spectramax M5 microplate reader.

Mitochondrial Cytochrome *c* Release and Biotinylation Assays. A375P cells were plated in 6-well Corning plates (3 x 10^5 cells/well) and cultured as described above. After 24 hr, the cells were treated with BIM $SAHB_{A1}$ or BIM $SAHB_A$-3 (40 μM) in DMEM containing 5% FBS for the indicated durations and then trypsinized and washed with PBS. The cytosol (supernatant) and mitochondrial (pellet) fractions were then isolated as described[46]. In brief, pelleted cells were resuspended at 1 x 10^7 cells/mL in permeabilization buffer (20 mM HEPES/KOH [pH 7.5], 250 mM sucrose, 50 mM KCl, 2.5 mM $MgCl_2$) supplemented with 0.025% digitonin and protease inhibitors, followed by incubation on ice for 10 min and centrifugation at 13,000 x *g*. The resultant supernatant and pellet fractions were boiled in LDS buffer and subjected to western analysis using a 1:1,000 dilution of cytochrome *c* antibody (BD Pharmingen #556433). For biotinylation studies, A375P mitochondria were isolated as described above, resuspended in permeabilization buffer, and treated with biotinylated BIM $SAHB_A$ or BIM $SAHB_A$-3 (50 μM) for 4 hr at room temperature. Samples were then boiled in LDS buffer and

subjected to western analysis using 1:1,000 dilutions of BFL-1 (Abcam #125259), biotin (Abcam, #53494), and VDAC1 (Abcam #14734) antibodies.

Confocal Microscopy. A375P cells were plated in chambered coverglass (1.5 x 10^4 cells/well) and cultured as described above. After 24 hr, cells were treated with FITC-BIM $SAHB_{A1}$ or BIM $SAHB_A$-3 (1 μM) for 4 hr in phenol red-free DMEM containing 5% FBS. Cells were washed, stained with MitoTracker Red (Thermo) and Hoechst 33342, and imaged live. Confocal images were collected with a Yokogawa CSU-X1 spinning-disk confocal (Andor Technology) mounted on a Nikon Ti-E inverted microscope (Nikon Instruments). Images were acquired using a 1003 1.4 NA Plan Apo objective lens with an Orca ER CCD camera (Hamamatsu Photonics) and 488-nm laser. Acquisition parameters, shutters, filter positions, and focus were controlled by Andor iQ software (Andor Technology).

RESULTS

Covalent Reaction between Cysteines at the Binding Interface of NOXA BH3 and BFL-1

The BH3-only protein NOXA exhibits natural, dual selectivity for interaction with anti-apoptotic MCL-1 and BFL-1[47,48], and therefore its BH3 sequence was selected as a starting point for developing a BFL-1 inhibitor. In examining the crystal structure of human BFL-1ΔC in complex with NOXA BH3 (PDB: 3MQP), we observed the proximity of NOXA C25 to BFL-1ΔC C55 at a distance of 3.9 Å, compatible with disulfide bond formation (**Figure 2.1**). As no other anti-apoptotic BCL-2 family member contains a cysteine in its BH3-binding pocket, we reasoned that C55 targeting by a stapled BH3 peptide could yield a BFL-1 inhibitor with selective covalent reactivity. To test our hypothesis, we first generated stapled NOXA BH3 peptides and recombinant BFL-1ΔC constructs bearing their native cysteines (NOXA: C25; BFL-1: C4, C19, C55) and a series of serine mutants (NOXA: C25S; BFL-1: C4S/C19S, C4S/C19S/C55S) for binding studies. For the stabilized α helices of BCL-2 domains (SAHBs) modeled after NOXA BH3 (amino acids [aa] 19–43), we positioned the *i, i + 4* all-hydrocarbon staple at our classic ‘‘A’’ position[20] (substitution of R31 and K35) and derivatized the N-termini with polyethylene glycol (PEG)-biotin for biolayer interferometry analyses. We found that the peptide/protein pairs all demonstrated dissociation constants within a range of 46–165 nM (**Figure 2.2**). Thus, serine mutagenesis, in and of itself, appeared to have no detrimental effect on binding affinity and, if anything, somewhat enhanced BFL-1 interaction by up to 3.5-fold.

We then sought to determine whether disulfide bond formation between NOXA C25 and BFL-1ΔC C55 was biochemically feasible. Indeed, upon DTT (10 mM)

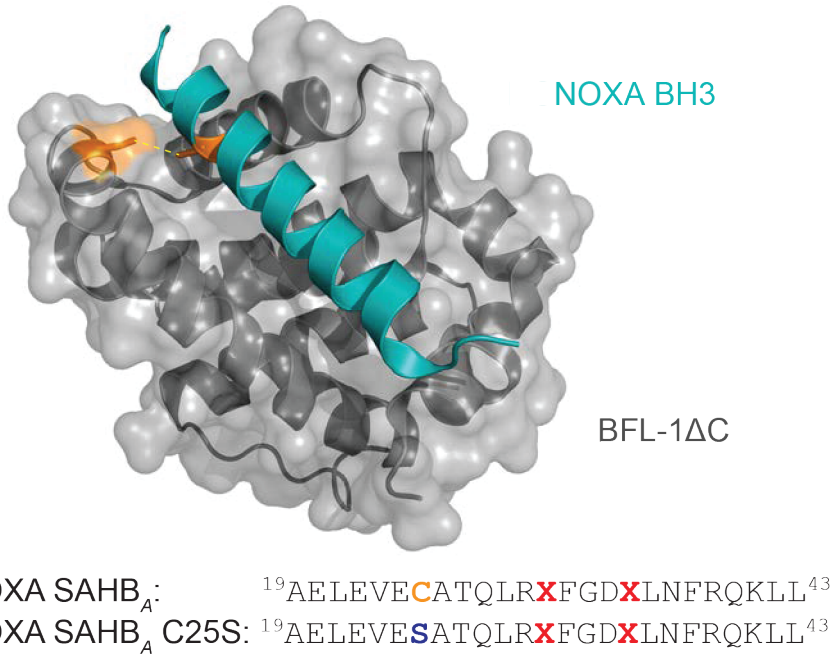

Figure 2.1 *BFL-1 contains a unique cysteine in its BH3-binding surface groove*.

Structure of the NOXA BH3 (cyan) and BFL-1ΔC (gray) complex, highlighting the juxtaposition between NOXA C25 and BFL-1 C55 (orange). PDB: 3MQP

Figure 2.2 *Biolayer interferometry analysis of NOXA SAHB binding interactions with BFL-1ΔC*.

The association and dissociation binding interactions between BFL-1ΔC constructs and biotin-PEG-NOXA $SAHB_A$ peptides bearing the indicated native cysteines and cysteine-to-serine mutations were measured by biolayer interferometry. Experiments were performed in technical and biological duplicate, with exemplary associations and dissociation profiles shown.

Figure 2.2 (Continued)

Protein	SAHB	K_d (nM)
BFL-1 WT	NOXA WT	122
BFL-1 C4S/C19S	NOXA WT	165
BFL-1 C4S/C19S/C55S	NOXA WT	118
BFL-1 WT	NOXA C25S	46.6
BFL-1 C4S/C19S	NOXA C25S	47.2
BFL-1 C4S/C19S/C55S	NOXA C25S	58.2

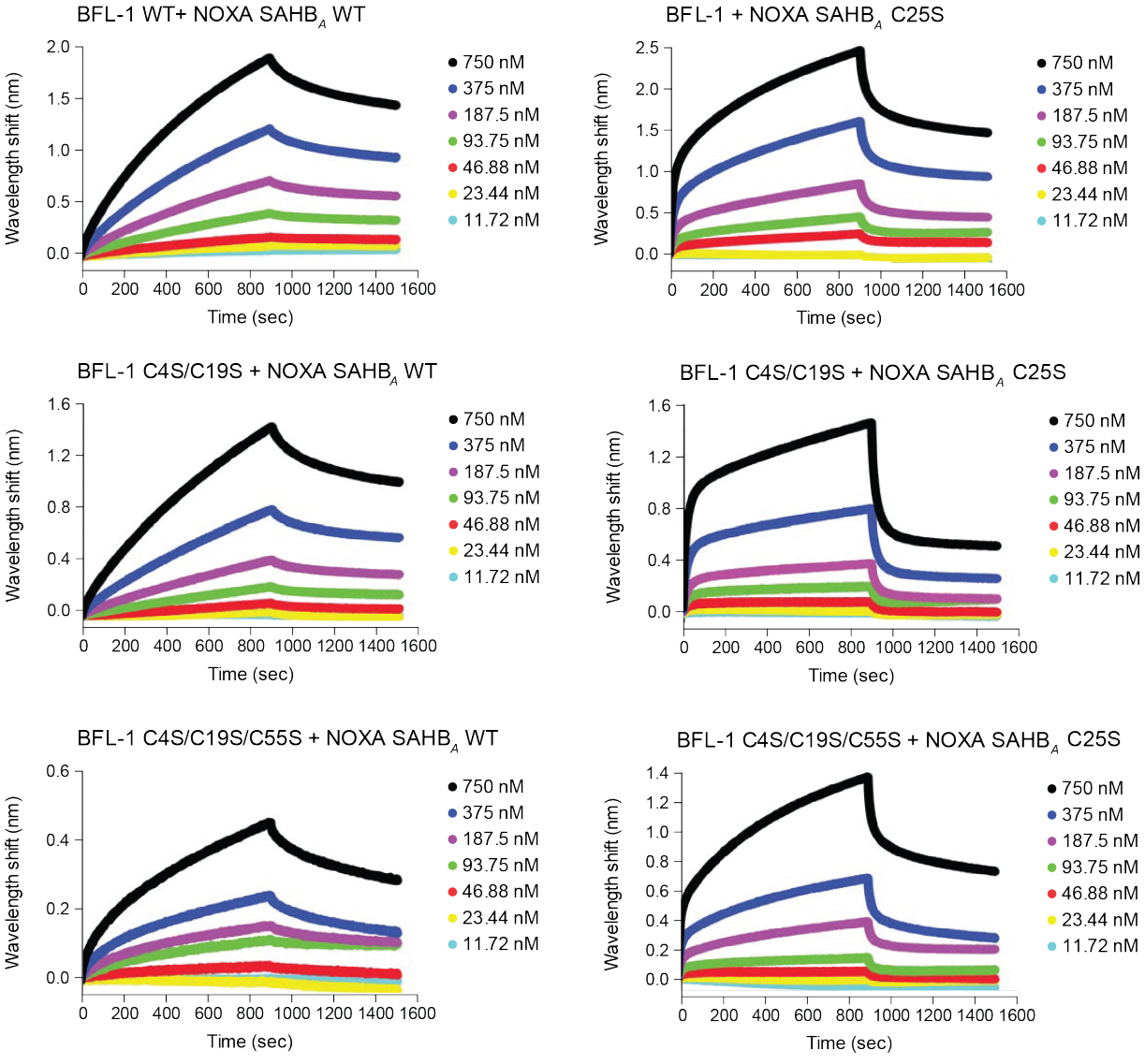

reduction followed by glutathione disulfide (GSSG) oxidation (12 mM), we observed a shift in the molecular weight of wild-type BFL-1ΔC when incubated with NOXA $SAHB_A$ but not its C25S mutant, as assessed by gel electrophoresis under denaturing and non-reducing conditions and Coomassie staining (**Figure 2.3A, top**). Our use of fluorescein isothiocyanate (FITC)-NOXA $SAHB_A$ peptides provided confirmation that the BFL-1 protein was labeled by the wild-type but not C25S mutant peptide, as detected by FITC scan (**Figure 2.3A, bottom**). We likewise determined that NOXA C25 formed a disulfide bond with BFL-1ΔC C55, as demonstrated both by the molecular weight shift (Coomassie stain) and FITC labeling of the BFL-1ΔC C4S/C19S construct (in which only C55 is present), but no adduct with the BFL-1ΔC C4S/C19S/C55S construct that lacks C55 **(Figure 2.3A**). As a measure of cysteine specificity, we repeated the experiment using MCL-1ΔNΔC and BCL-X_LΔC, both of which contain cysteines (MCL-1 C286, BCL-X_L C151), and observed no molecular weight shift or FITC labeling upon incubation with NOXA $SAHB_A$ under oxidizing conditions (**Figure 2.3B**). These data confirm that the juxtaposed cysteines at the NOXA BH3/BFL-1 interface can indeed form a disulfide bond and, moreover, in a selective fashion.

Selective BFL-1 Reactivity of Stapled BH3 Peptides Bearing Electrophilic Warheads

The capacity of NOXA $SAHB_A$ and BFL-1ΔC to engage through disulfide bond formation suggested a novel opportunity to develop stapled peptides for covalent targeting of cysteines localized to key regulatory surfaces, such as the BH3-binding pocket of BFL-1. Because relying on intracellular disulfide bond formation as a basis for protein target inhibition is not a tractable pharmacologic strategy, we instead examined possible sites

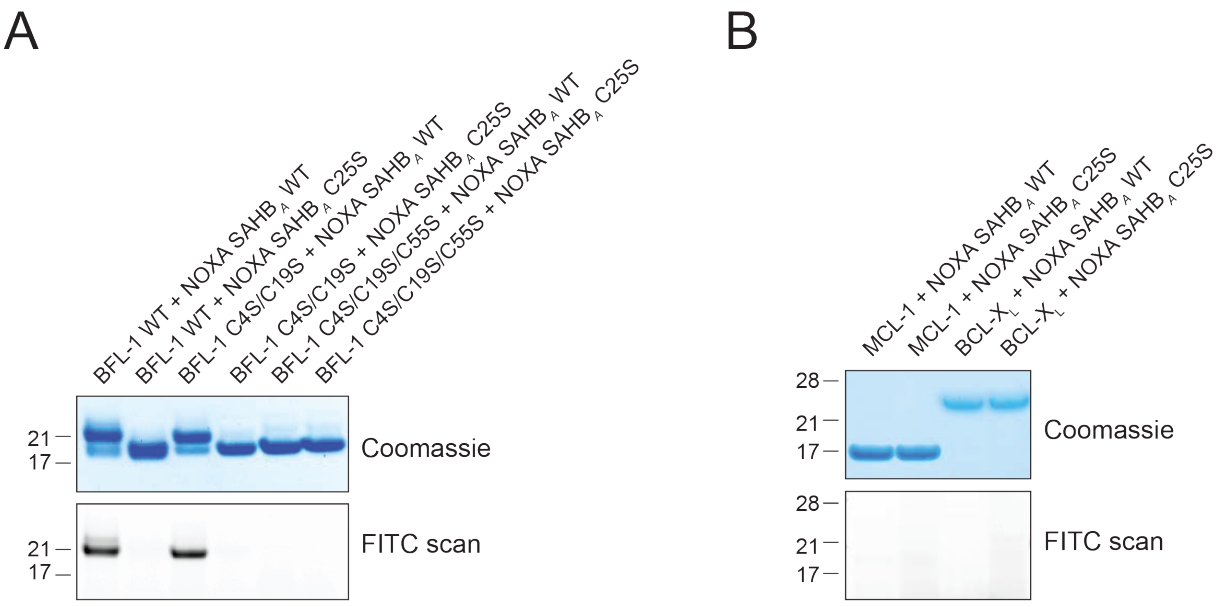

Figure 2.3 *Disulfide bond formation between NOXA BH3 and BFL-1.*

(**A**) Exposure of BFL-1ΔC and FITC-NOXA SAHB$_A$ constructs to oxidizing conditions yielded a molecular weight shift only for peptide/protein pairs that retained native NOXA C25 and BFL-1 C55, as detected by Coomassie staining (top). Disulfide bond formation between BFL-1ΔC bearing C55 and wild-type NOXA SAHBA was confirmed by FITC scan (bottom). (**B**) Incubation of FITC-NOXA SAHB$_A$ peptides with alternative anti-apoptotic BCL-2 family proteins, such as MCL-1ΔNΔC or BCL-X$_L$ΔC, under oxidizing conditions caused no molecular weight shift, as evaluated by Coomassie staining (top), or FITC-peptide labeling of protein, as assessed by FITC scan (bottom).

for insertion of non-natural amino acids bearing reactive acrylamide moieties, and identified NOXA L21 as having even closer proximity to BFL-1 C55 than NOXA C25 (3.3 versus 3.9 Å, respectively) based on the crystal structure of the NOXA BH3/BFL-1ΔC complex (PDB: 3MQP) (**Figure 2.4A, top**). In the case of the more promiscuous BIM BH3 sequence, W147 manifests optimal adjacency to BFL-1 C55 (3.6 Å) based on the crystal structure of the BIM BH3/BFL-1ΔC complex (PDB: 2VM6) (**Figure 2.4A, bottom**). Thus, we capped NOXA $SAHB_A$[48] and BIM $SAHB_A$[21] at positions L21 and W147, respectively, with a series of non-natural amino acids bearing distinct acrylamide species (**Figure 2.4B**). In comparing the reactivity of the electrophilic ‘‘warhead’’-bearing NOXA (aa 21–43) and BIM $SAHB_A$ (aa 147–166) panels, we observed efficient conversion of BFL-1ΔC to the heavier, conjugated adduct for SAHBs bearing warheads **1**, **3**, **5**, and **8**, as assessed by reducing and denaturing gel electrophoresis and Coomassie staining (**Figure 2.4C**). We advanced NOXA and BIM SAHBs bearing one of the most effective warheads, D-nipecotic acid acrylamide (**3**), to specificity testing. First, we tested the selectivity of NOXA $SAHB_A$-3 and BIM $SAHB_A$-3 for BFL-1 C55. Upon incubation of $SAHB_A$-3 compounds with BFL-1ΔC constructs bearing all native cysteines (BFL-1 wild-type), C55 only (BFL-1 C4S/C19S), C4 and C19 only (BFL-1 C55S), or no cysteines (BFL-1 C4S/C19S/C55S), we observed exclusive reactivity with the wild-type and BFL-1 C4S/C19S constructs, underscoring the cysteine selectivity of NOXA $SAHB_A$-3 and BIM $SAHB_A$-3 for C55 of the BH3-binding pocket (**Figure 2.4D**). As a further measure of compound specificity, we repeated the experiment using MCL-1ΔNΔC and BCL-X_LΔC and observed no non-specific reactivity, despite the presence of cysteines in these anti-apoptotic BCL-2 family proteins (**Figure 2.4E**). Thus, we found

Figure 2.4 *Incorporation of electrophilic warheads into stapled NOXA and BIM BH3 helices for covalent targeting of BFL-1 C55.*

(**A**) The structures of the NOXA BH3/BFL-1ΔC (top, PDB: 3MQP) and BIM BH3/BFL-1ΔC (bottom, PDB: 2VM6) complexes demonstrate the proximity of discrete BH3 residues to C55 for replacement with electrophilic warheads. (**B**) Chemical structures of the reactive acrylamide moieties installed at the N termini of NOXA and BIM SAHB peptides. (**C**) Reactivity of BIM and NOXA SAHBs bearing warheads 1–8 with BFL-1ΔC C4S/C19S, which only retains the native C55. (**D**) BIM and NOXA $SAHB_A$-3 peptides selectively reacted with BFL-1ΔC protein bearing C55. (**E**) BIM and NOXA $SAHB_A$-3 peptides did not react with MCL-1ΔNΔC or BCL-X_LΔC, despite the presence of cysteines in these anti-apoptotic targets.

Figure 2.4 (Continued)

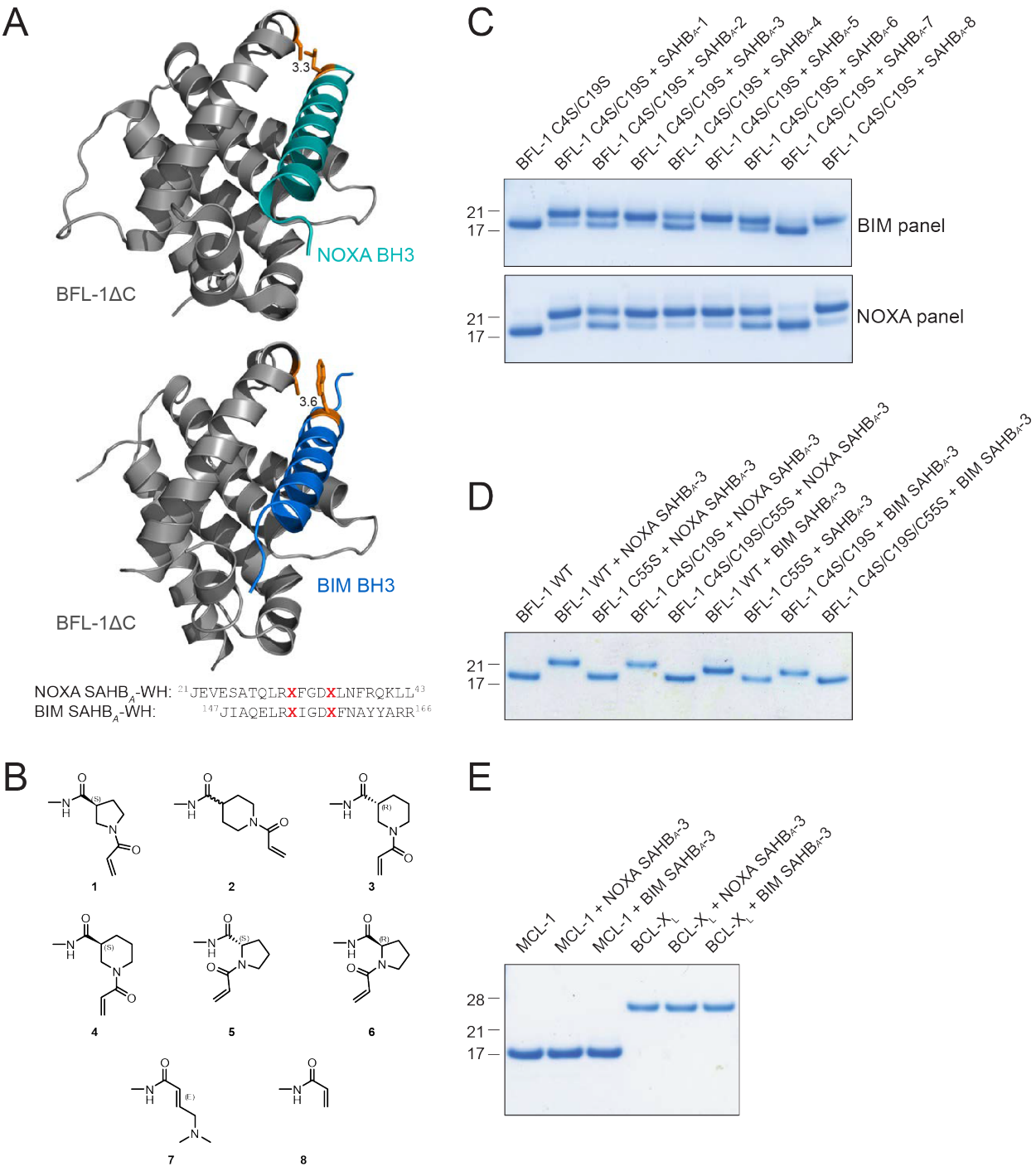

that installing a cysteine-reactive warhead in stapled NOXA and BIM BH3 peptides results in efficient and selective covalent targeting of the BFL-1 BH3-binding groove.

We next explored how conversion of NOXA and BIM SAHBs to BFL-1 C55-reactive agents influenced the balance between non-covalent and covalent SAHB interactions in the context of an anti-apoptotic protein mixture. First, we generated recombinant MCL-1ΔNΔC, BCL-X_LΔC, and BFL-1ΔC proteins with differential N-terminal tags (glutathione S-transferase [GST], tagless, and His, respectively) so that each could be readily identified upon gel electrophoresis and silver staining (**Figures 2.5A and 2.5B**). Upon incubation of the anti-apoptotic mixture with biotinylated NOXA $SAHB_A$ or NOXA $SAHB_A$-3 (1:1:1:1 for each component), we only see a shift in the molecular weight of BFL-1ΔC, corresponding to the selective covalent reaction (**Figure 2.5A, left**). Streptavidin (SA) pull-down revealed prominent non-covalent capture of MCL-1ΔNΔC by NOXA $SAHB_A$ but a notable shift in the interaction propensity of NOXA $SAHB_A$-3, with relatively less MCL-1ΔNΔC and notably more BFL-1ΔC engagement as a result of covalent BFL-1ΔC conjugation (**Figure 2.5A, right**). Consistent with the broader anti-apoptotic binding spectrum of BIM BH3, the corresponding BIM SAHBs engaged BCL-X_LΔC in addition to MCL-1ΔNΔC and BFL-1ΔC, but an increased BFL-1ΔC targeting propensity was again observed for BIM $SAHB_A$-3 relative to BIM $SAHB_A$ as a consequence of covalent conjugation (**Figure 2.5B**). Thus, the capacity for selective covalent reaction with BFL-1ΔC shifted the competitive balance of SAHB interactions toward BFL-1.

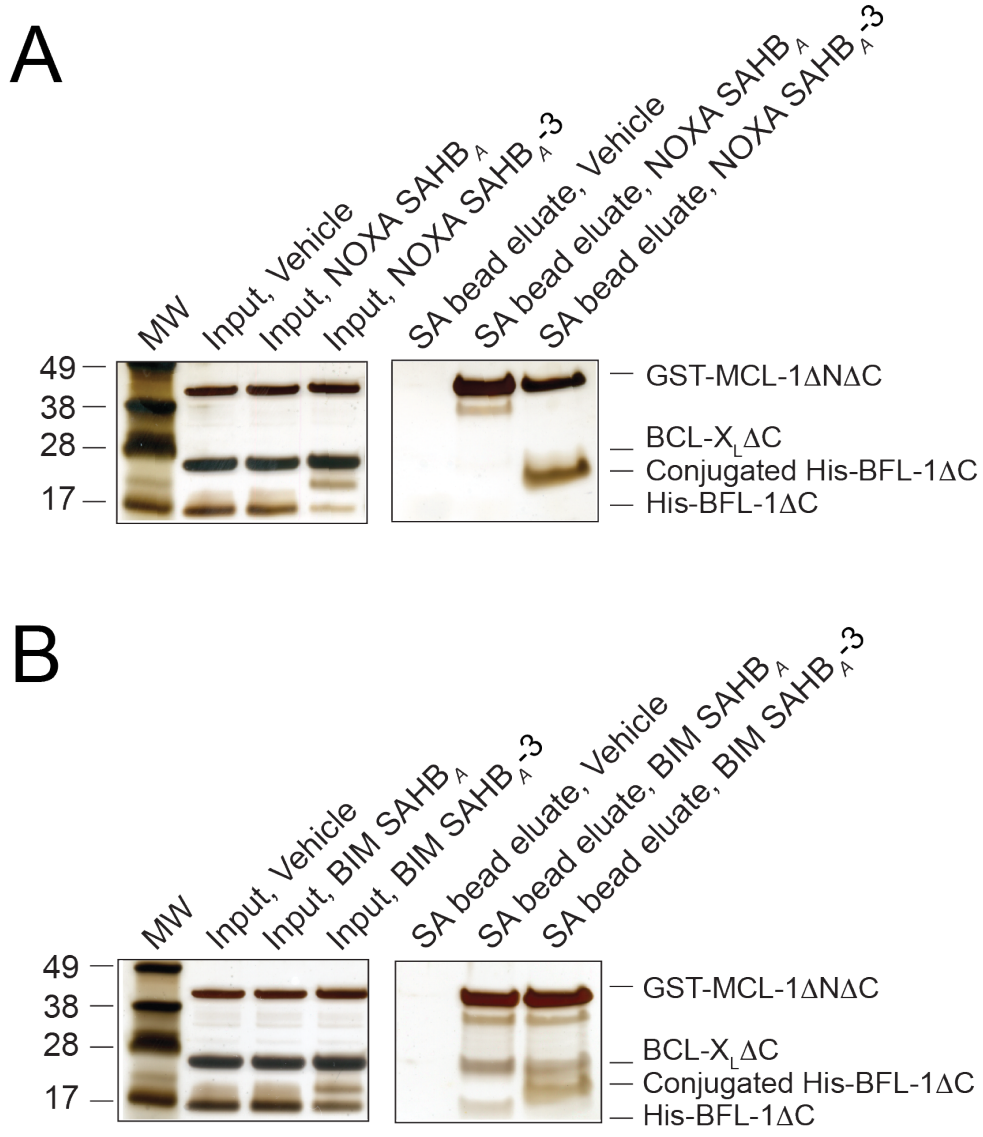

Figure 2.5 *Covalent conjugation to the BH3-binding pocket enhances BFL-1 targeting.* (**A** and **B**) Incorporation of an acrylamide moiety into NOXA and BIM SAHBs provided a competitive advantage for BFL-1 targeting, as demonstrated by streptavidin pulldown of a 1:1:1:1 mixture (1 μM each) of biotinylated NOXA (**A**) or BIM (**B**) SAHBs with recombinant His-BFL-1ΔC, BCL-X_LΔC (tagless), and GST-MCL-1ΔNΔC.

Targeted Blockade of BFL-1 in Liposomes, Lysates, and Cells

To determine the functional consequences of covalent targeting of the BFL-1 BH3-binding pocket, we performed liposomal release assays designed to monitor the influence of BFL-1 on direct BAX activation. We generated ANTS/DPX-encapsulated large unilamellar vesicles and monitored liposomal release of fluorophore upon BAX-mediated membrane poration. Whereas BAX alone had no effect on the liposomes, the addition of the direct activator BH3-only protein tBID triggered time-responsive, BAX-mediated release, a process that was suppressed by BFL-1ΔC (**Figures 2.6B and 2.6C**). However, upon addition of either NOXA SAHB$_A$-3 or BIM SAHB$_A$-3 conjugated BFL-1ΔC (**Figure 2.6A**), the inhibitory function of BFL-1 was lost (**Figures 2.6B and 2.6C**). These data highlight that covalently ‘‘plugging’’ the BH3-binding pocket of BFL-1 with NOXA SAHB$_A$-3 or BIM SAHB$_A$-3 irreversibly neutralized its anti-apoptotic function.

We next sought to test whether our covalent stapled peptide inhibitors could selectively react with BFL-1 in more complex protein mixtures. To specifically track C55 derivatization, we transiently expressed HA-BFL-1ΔC C4S/C19S in 293T cells and, after 24 hr, harvested cell lysates for crosslinking analyses with C-terminal Lys-biotin derivatized SAHB constructs that either did or did not contain the electrophilic warhead. Anti-HA western analyses revealed prominent molecular weight shifts only for warhead-bearing SAHBs, consistent with covalent incorporation of both NOXA SAHB$_A$-3 and BIM SAHB$_A$-3 into the BFL-1 protein at C55 (**Figure 2.7A, top**). To confirm that the observed molecular weight shifts reflected NOXA SAHB$_A$-3 and BIM SAHB$_A$-3 incorporation, we performed biotin western analyses. We found that the shifted HA-BFL-1ΔC bands were indeed biotin immunoreactive and, importantly, there was little to no non-specific

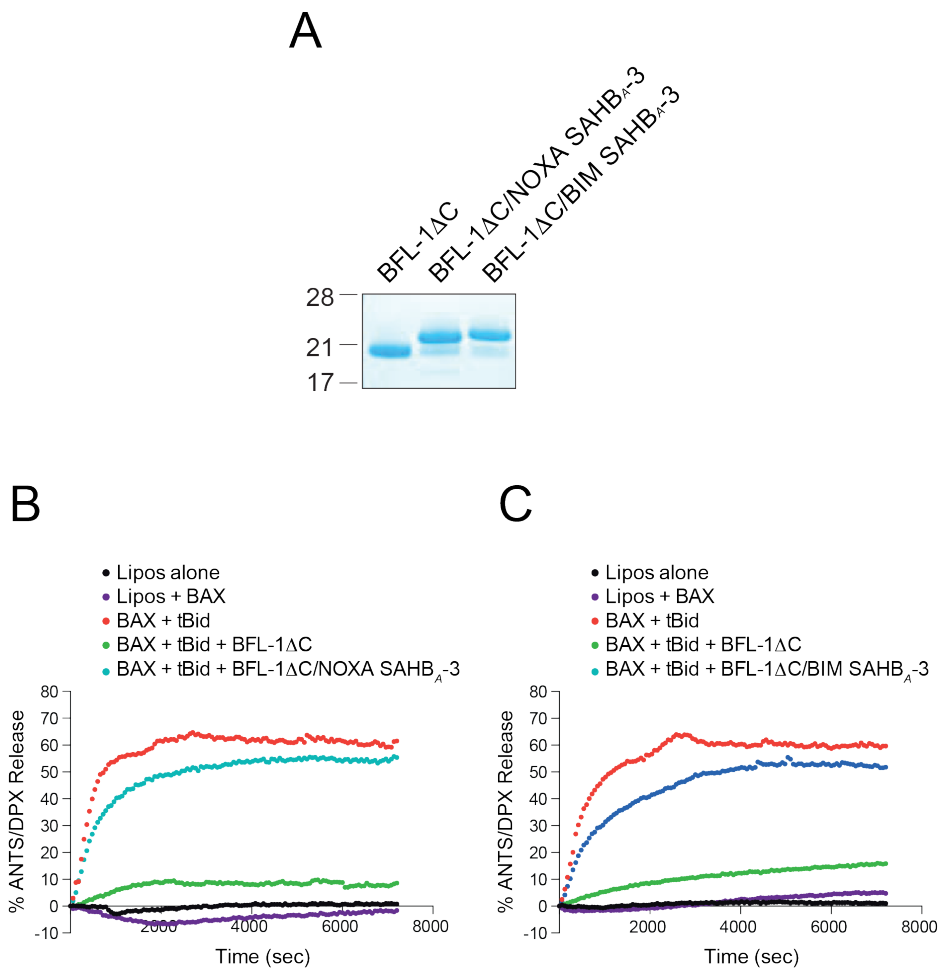

Figure 2.6 *Covalent targeting of the BFL-1 BH3-binding pocket neutralizes anti-apoptotic activity.*

(**A**) Coomassie stain of recombinant BFL-1ΔC and its NOXA SAHB$_A$-3 and BIM SAHB$_A$-3 conjugates employed in liposomal release assays. (**B** and **C**) BH3-only protein tBID directly activated BAX-mediated liposomal poration, as monitored by ANTS/DPX release. Whereas BFL-1ΔC completely blocked tBID-triggered BAX poration, covalent engagement of BFL-1ΔC by either NOXA SAHB$_A$-3 (**B**) or BIM SAHB$_A$-3 (**C**) effectively inhibited the functional activity of BFL-1ΔC. Liposomal experiments were performed in triplicate with exemplary release profiles shown. BAX, 400 nM; tBID, 40 nM, BFL-1ΔC or SAHB$_A$-3/BFL-1ΔC conjugates, 1.5 μM.

Figure 2.7 *Covalent targeting of BFL-1 C55 in lysates and cells.*

(**A**) Biotinylated NOXA and BIM SAHB$_A$-3 peptides crosslinked to HA-BFL-1ΔC C4S/C19S in lysates from transfected 293T cells, as evidenced by the shift in molecular weight of BFL-1ΔC observed upon anti-HA western analysis. Anti-biotin blotting confirmed the selective incorporation of biotin into the HA-BFL-1ΔC band, with little to no cross-reactivity with other proteins in the cellular lysate. (**B**) Treatment of transfected 293T cells with biotinylated BIM SAHB$_A$-3 followed by cellular lysis, HA immunoprecipitation (IP), and biotin western analysis demonstrated the capacity of a warhead-bearing BIM SAHB to gain intracellular access and covalently target expressed HA-BFL-1ΔC C4S/C19S containing the native C55. (**C**) Covalent modification of HA-BFL-1ΔC C4S/C19S by cellular treatment with BIM SAHB$_A$-3, but not the corresponding construct lacking the acrylamide-based warhead. Crosslinked BFL-1ΔC was observed by 2 hr and levels continued to increase in a time-dependent fashion throughout the 12-hr treatment period, as monitored by HA western analysis.

Figure 2.7 (Continued)

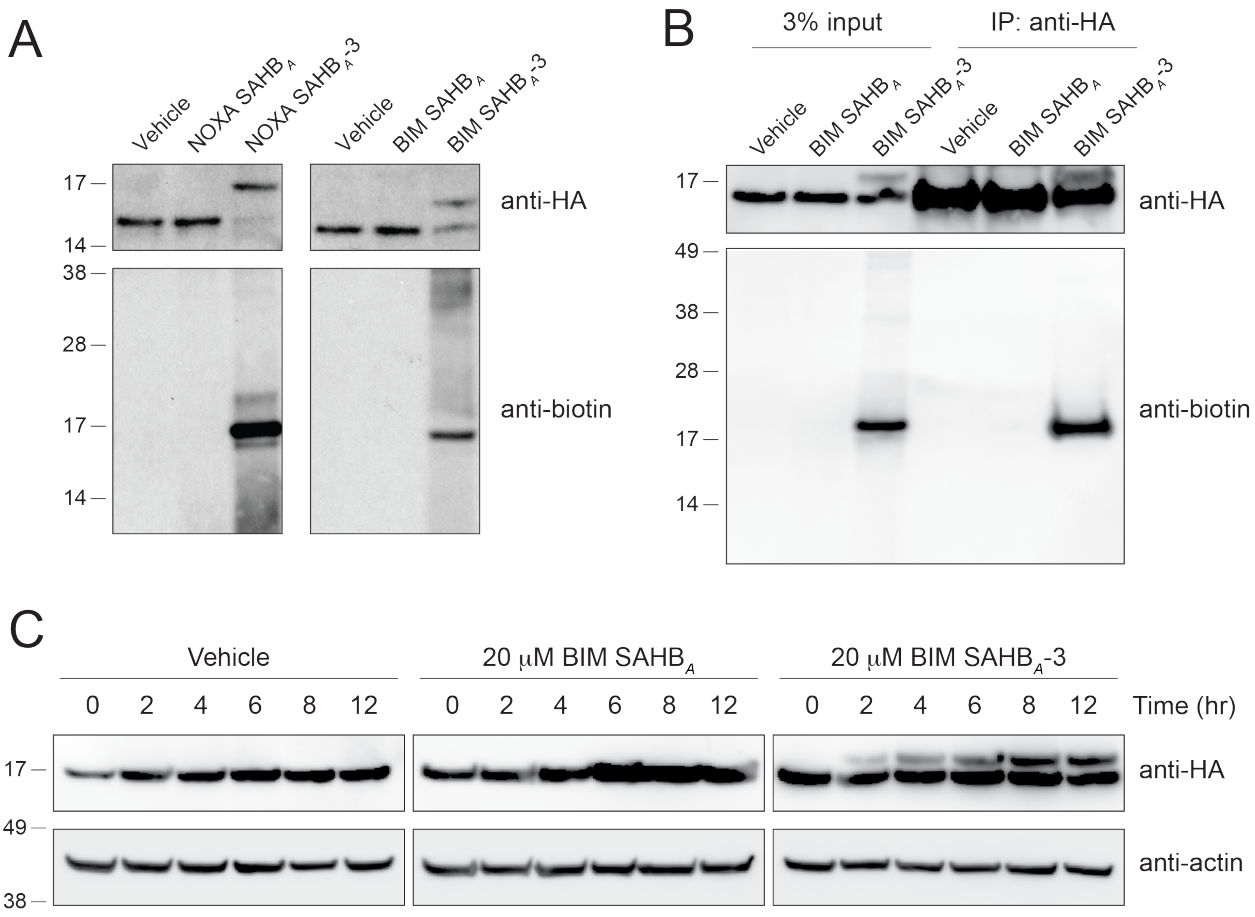

reactivity with other electrophoresed proteins from the 293T lysates (**Figure 2.7A, bottom**).

To advance our strategy to cellular testing, we first evaluated the cellular uptake potential of our biotinylated NOXA SAHB$_A$-3 and BIM SAHB$_A$-3 constructs. We incubated 293T cells with the compounds at 20 μM dosing for 24 hr, trypsinized and washed the cells to remove any adherent peptide, and generated lysates for anti-biotin western analyses. We found that cellular uptake of NOXA SAHB$_A$-3 was relatively limited, and therefore proceeded with BIM SAHB$_A$-3 for cellular testing (**Figure 2.8A**). We further confirmed that the transfection conditions themselves did not independently influence the cellular uptake of BIM SAHB$_A$-3 (**Figure 2.8B**). 293T cells transiently overexpressing HA-BFL-1ΔC C4S/C19S were treated with biotinylated BIM SAHB$_A$ (aa 148–166) or BIM SAHB$_A$-3 (20 μM, 6 hr) and then lysates, generated as above, were subjected to anti-HA immunoprecipitation. Biotin western analysis of the input revealed a single, prominent protein band only in the denatured and reduced electrophoresed lysate of cells treated with BIM SAHB$_A$-3 (**Figure 2.7B, left**). Subjecting the immunoprecipitate to anti-HA western analysis revealed the BFL-1 doublet, and biotin western analysis confirmed that the upper band indeed corresponded to biotinylated HA-BFL-1ΔC (**Figure 2.7B, right**). In anticipation of cancer cell treatment studies, we turned to the corresponding non-biotinylated BIM SAHB$_A$ constructs to probe the kinetics and efficiency of covalent targeting of BFL-1 in cells. Comparing BIM SAHB$_A$- and BIM SAHB$_A$-3-treated 293T cells transiently overexpressing HA-BFL-1ΔC C4S/C19S, we observed a discrete molecular weight shift in BFL-1 by anti-HA western analysis within 2 hr of BIM SAHB$_A$-3 exposure, with a progressive increase in the

Figure 2.8 *Cellular uptake of NOXA and BIM SAHB$_A$-3 peptides.*

(**A**) 293T cells were treated with biotinylated NOXA SAHB$_A$-3 or BIM SAHB$_A$-3 (20 μM) for 24 hr followed by washing, trypsinizing, rewashing and lysing the cells. Comparative stapled peptide uptake was assessed by electrophoresis of the cellular lysates and biotin western analysis. (**B**) 293T cells were either mock transfected or not, and then 24 hr later treated with biotinylated BIM SAHB$_A$-3 (20 μM) for an additional 4 hr, and then processed as above for comparative biotin blotting of cellular lysates. (**C** and **D**) TIFI values for A375P (1 x 10^4 cells/well) and MEF (1.5 x 10^4 cells/well) cells treated with the indicated doses of BIM SAHB peptides and measured by IXM (20x) after 4 hr. Data are mean ± SD for experiments performed in triplicate wells with 5 image acquisitions per well. Two biological replicates (independent cell cultures and platings) were performed with similar results. (**E** and **F**) Representative IXM images of A375P (**E**) and MEF (**F**) cells treated with the indicated BIM SAHBs at 1 μM dosing. Blue, DAPI; red, CellMask; green, FITC-peptide.

Figure 2.8 (Continued)

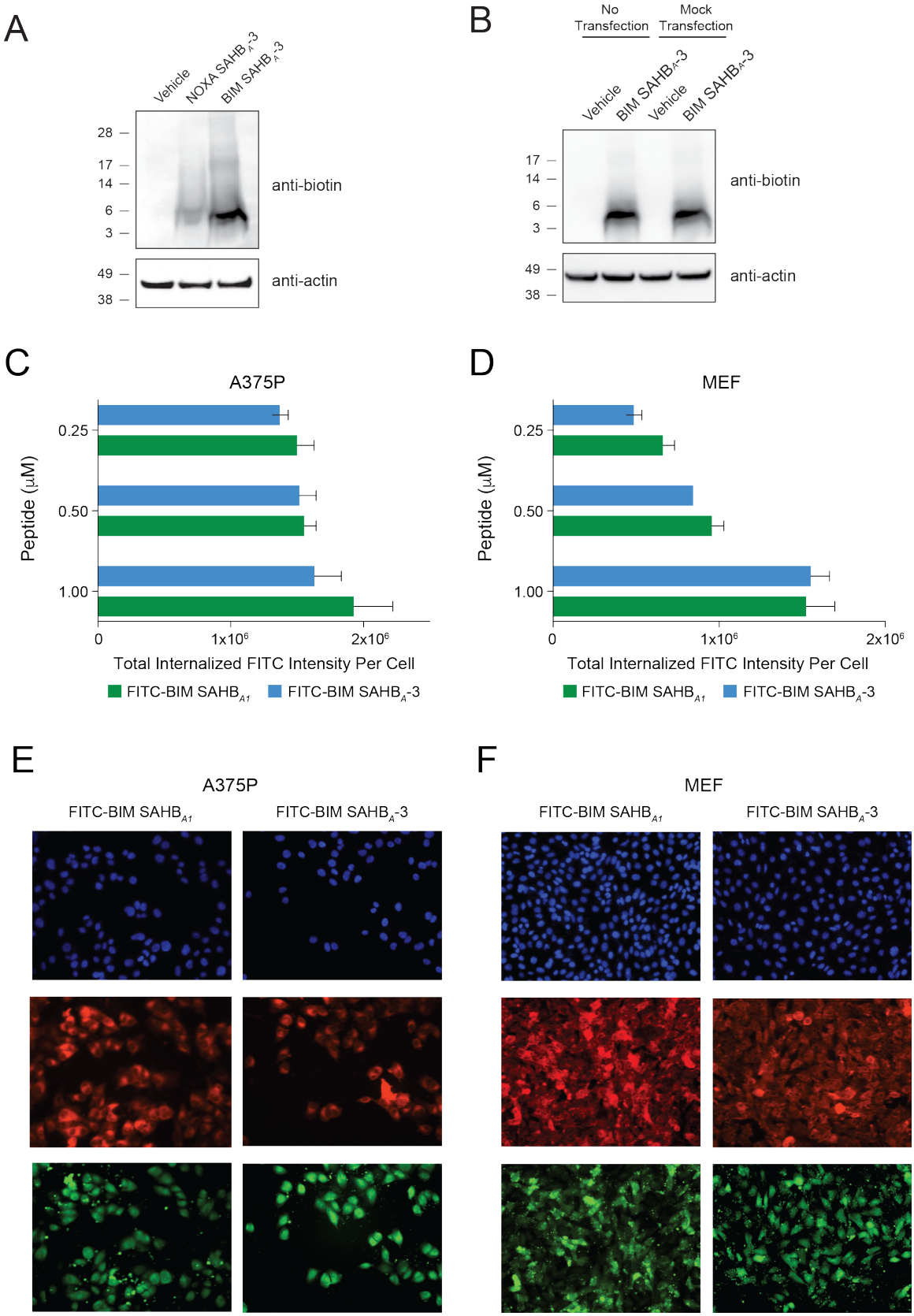

crosslinked species over the 12-hr evaluation period (**Figure 2.7C**). Taken together, these data highlight the capacity of a stapled peptide bearing an electrophilic warhead to covalently target BFL-1 in treated lysates and cells.

Having documented the feasibility of specific labeling of intracellular BFL-1 upon treating cells with biotinylated BIM SAHB$_A$-3, we then examined the relative influence of covalent versus non-covalent engagement on the capacity of BIM SAHBs to disrupt BFL-1 complexes. For this experiment, we added tBID to the lysates from 293T cells transiently transfected with HA-BFL-1ΔC C4S/C19S, incubated the mixture with biotinylated BIM SAHB$_A$ or BIM SAHB$_A$-3, performed anti-HA immunoprecipitation, and blotted for HA and tBID. Strikingly, BIM SAHB$_A$ was incapable of competing with tBID for HA-BFL-1 binding, whereas the warhead-bearing BIM SAHB$_A$-3 construct covalently trapped HA-BFL-1, as exemplified by complete protein conversion to the higher molecular weight species and near total inhibition of tBID co-immunoprecipitation (**Figure 2.9A**). When the experiment was repeated using lysates from 293T cells transiently expressing FLAG-MCL-1, which bears no cysteine in its BH3-binding pocket, both BIM SAHB$_A$ peptides were equally effective as non-covalent disruptors of tBID/FLAG-MCL-1 co-immunoprecipitation (**Figure 2.9B**). Thus, by installing the warhead and enabling stapled peptide covalent reaction, we can selectively enhance the BFL-1 targeting efficacy of BIM SAHB$_A$.

Preferential Activation of Apoptosis by a Cysteine-Reactive BIM SAHB$_A$ in BFL-1-Expressing Melanoma

BFL-1 has recently been implicated as a lineage-specific driver of human melanoma,

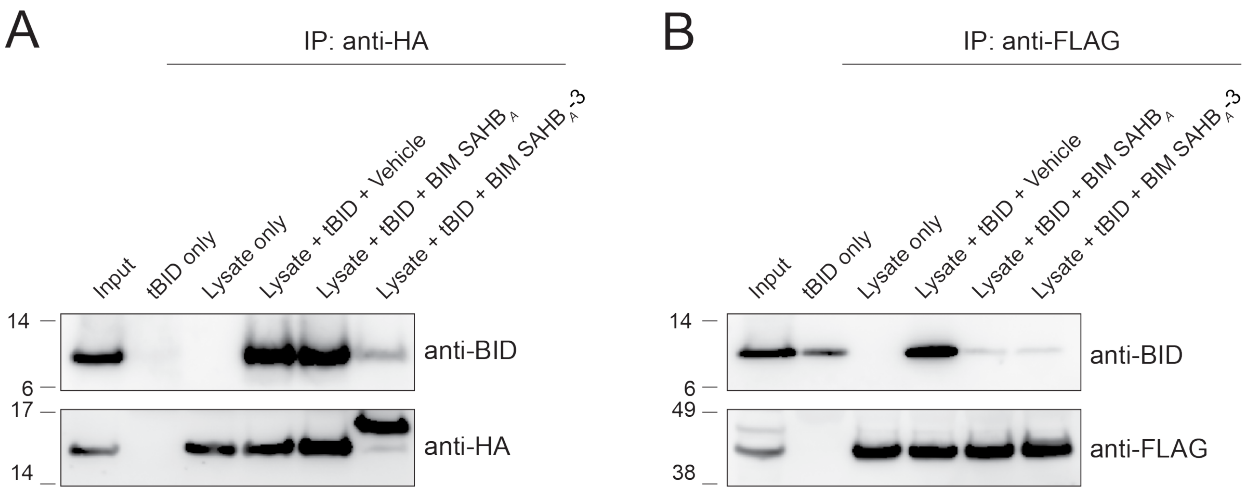

Figure 2.9 *Covalent binding of BIM SAHB$_A$-3 to BFL-1 blocks the inhibitory interaction with BH3-only protein tBID.*

(**A** and **B**) BIM SAHB$_A$-3, but not BIM SAHB$_A$, effectively competed with tBID for HA-BFL-1ΔC C4S/C19S interaction in 293T lysates, achieving robust covalent conjugation (**A**), whereas in the context of exclusive non-covalent FLAG-MCL-1 interaction, the compounds were equally effective at competing with tBID (**B**), as measured by the indicated immunoprecipitation and western analyses.

with gene amplification observed in 30% of cases and BFL-1 overexpression mediated by the MITF transcription factor, a melanoma oncogene[26]. Thus, to explore the functional impact of covalent BFL-1 targeting in cancer cells driven by BFL-1 expression, we tested the comparative effect of BIM SAHB$_A$-3 with our lead non-covalent stapled peptide modulator of BCL-2 family proteins, BIM SAHB$_{A1}$[24] in A375P melanoma cells[26]. We first confirmed that BIM SAHB$_{A1}$ and BIM SAHB$_A$-3 have equivalent cellular uptake, as quantified by ImageXpress Micro high-content epifluorescence microscopy of treated A375P cells and mouse embryonic fibroblasts (MEFs), which we have used previously to benchmark the comparative cell penetrance of FITC-labeled stapled peptides[49] (**Figures 2.8C and 2.8D**). The mechanism of uptake for BIM SAHBs is consistent with macropinocytosis, as previously reported[20,50], and evidenced here by the epifluorescence microscopy pattern of treated A375P and MEF cells at 4 hr (**Figures 2.8E and 2.8F**).

Upon exposure of A375P cells to BIM SAHBs, we observed significant enhancement in cytotoxicity over time for the warhead-bearing BIM SAHB$_A$-3 compared with BIM SAHB$_{A1}$ (**Figure 2.10A**). We confirmed by lactate dehydrogenase (LDH)-release assay that BIM SAHBs had no membranolytic effect on the cells (**Figure 2.10B**). The observed cytotoxicity was instead consistent with mitochondrial apoptosis induction, as reflected by time-responsive caspase-3/7 activation (**Figure 2.10C**) and mitochondrial cytochrome *c* release (**Figure 2.10D**). In accordance with its more pronounced impairment of cell viability, BIM SAHB$_A$-3 treatment induced higher levels of caspase-3/7 activation and cytochrome *c* release compared with that observed for BIM SAHB$_{A1}$ (**Figures 2.10C and 2.10D**). Importantly, we observed comparative

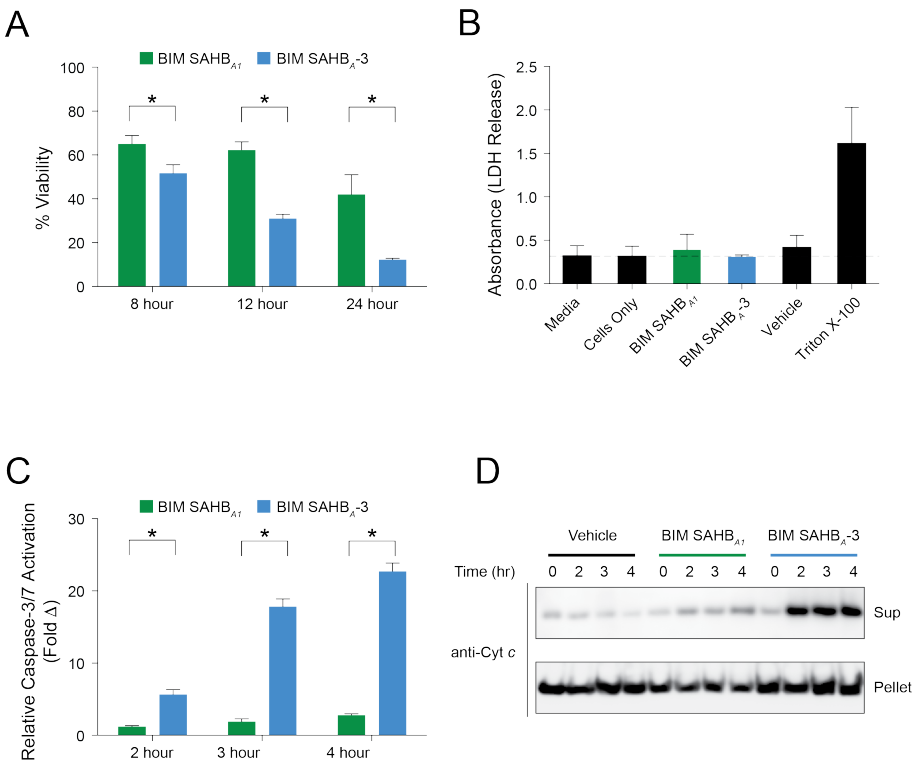

Figure 2.10 *Enhanced apoptotic response of BFL-1-driven melanoma cells upon treatment with a cysteine-reactive BIM SAHB.*

(**A**) A375P cells were treated with BIM SAHB$_{A1}$ or BIM SAHB$_A$-3 (40 μM) and viability measured by CellTiter-Glo assay at the indicated time points. Data are mean ± SD for experiments performed in technical sextuplicate. (**B**) Quantitation of LDH release upon treatment of A375P cells with BIM SAHB$_{A1}$ or BIM SAHB$_A$-3 (40 μM) for 30 min. Data are mean ± SD for experiments performed in technical triplicate. (**C**) A375P cells were treated with BIM SAHB$_{A1}$ or BIM SAHB$_A$-3 (40 μM) and caspase-3/7 activation measured by CaspaseGlo assay at the indicated time points. Data are mean ± SD for experiments performed in technical sextuplicate. (**D**) Mitochondrial cytochrome *c* release in A375P cells treated with BIM SAHB$_{A1}$ or BIM SAHB$_A$-3 (40 μM), as detected by cytochrome *c* western analysis of cytosolic and mitochondrial fractions. *$p < 0.001$ by two-tailed Student's *t* test.

enhancement in cytotoxicity and caspase-3/7 activation for BIM SAHB$_A$-3 in two additional BFL-1-expressing melanoma cell lines (SK-MEL-2 and SK-MEL-28)[26,30] (**Figure 2.11**), but no evidence of this phenomenon in non-melanoma lines that either lack BFL-1 or maintain BFL-1 expression but are driven by alternative oncogenic mechanisms (e.g., A549, MCF7, H929)[16,26,51] (**Figure 2.12**).

To mechanistically link the enhanced susceptibility of A375P cells to preferential BIM SAHB$_A$-3 engagement of BFL-1, we incubated A375P lysates with the corresponding biotinylated BIM SAHBs, followed by SA pull-down and anti-BFL-1 and MCL-1 western analyses. Whereas BIM SAHB$_A$ and BIM SAHB$_A$-3 demonstrated equivalent binding to anti-apoptotic MCL-1, as previously observed in the context of competitive interaction with recombinant anti-apoptotic proteins (**Figure 2.5**), the warhead-bearing construct again showed markedly increased engagement of BFL-1 (**Figure 2.13A**). To verify that BIM SAHB$_A$-3 can indeed label native mitochondrial BFL-1[30], we incubated mitochondria purified from A375P cells with biotinylated BIM SAHBs and observed BIM SAHB$_A$-3-selective biotinylation of mitochondrial protein at the identical molecular weight as immunoreactive BFL-1 (**Figure 2.13B**). Live confocal microscopy imaging of A375P cells treated with FITC-BIM SAHB$_A$-3 further revealed the stapled peptide's striking intracellular localization at the mitochondria, the physiologic site of BFL-1 activity, in both morphologically normal A375P cells (**Figure 2.13C**) and those undergoing apoptosis induction, as reflected by cell shrinkage, nuclear condensation, and membrane blebbing (**Figure 2.13D**). Taken together, these data highlight the mechanistic advantage of the warhead-bearing BIM SAHB$_A$-3 in the context of BFL-1-dependent cancer, as reflected by more effective engagement of

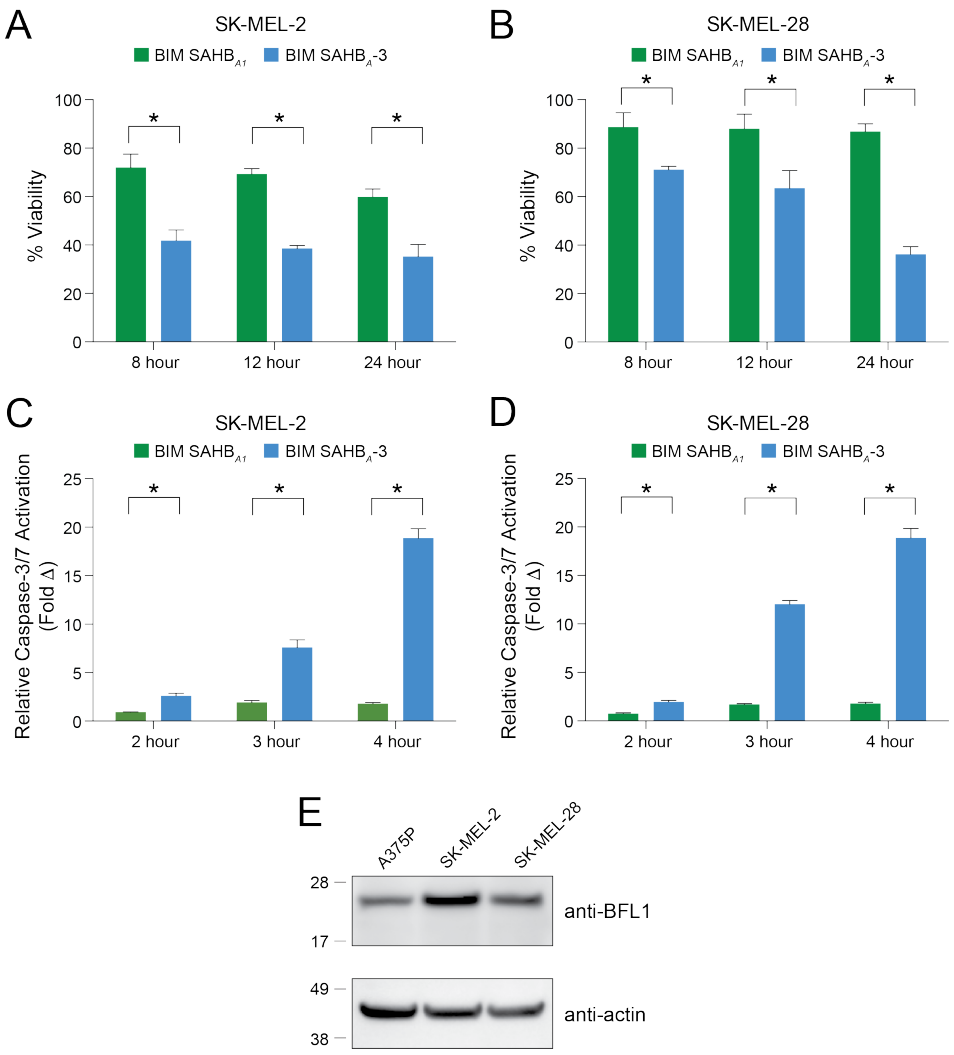

Figure 2.11 *Cell viability and caspase-3/7 activation of BFL-1-expressing melanoma cells treated with BIM SAHBs.*

(**A** and **B**) Cell viability of SK-MEL-2 and SK-MEL-28 cells treated with BIM SAHB$_{A1}$ or BIM SAHB$_A$-3 (40 μM), as measured by CellTiter-Glo assay at the indicated time points. (**C** and **D**) Caspase-3/7 activation in SK-MEL-2 and SK-MEL-28 cells treated with BIM SAHB$_{A1}$ or BIM SAHB$_A$-3 (40 μM), as monitored by CaspaseGlo at the indicated time points. Data are mean ± SD for experiments performed in technical sextuplicate. (**E**) BFL-1 western analysis of electrophoresed lysates from A375P, SK-MEL-2, and SK-MEL-28 cells. *, $p < 0.001$ by two-tailed Student's *t* test.

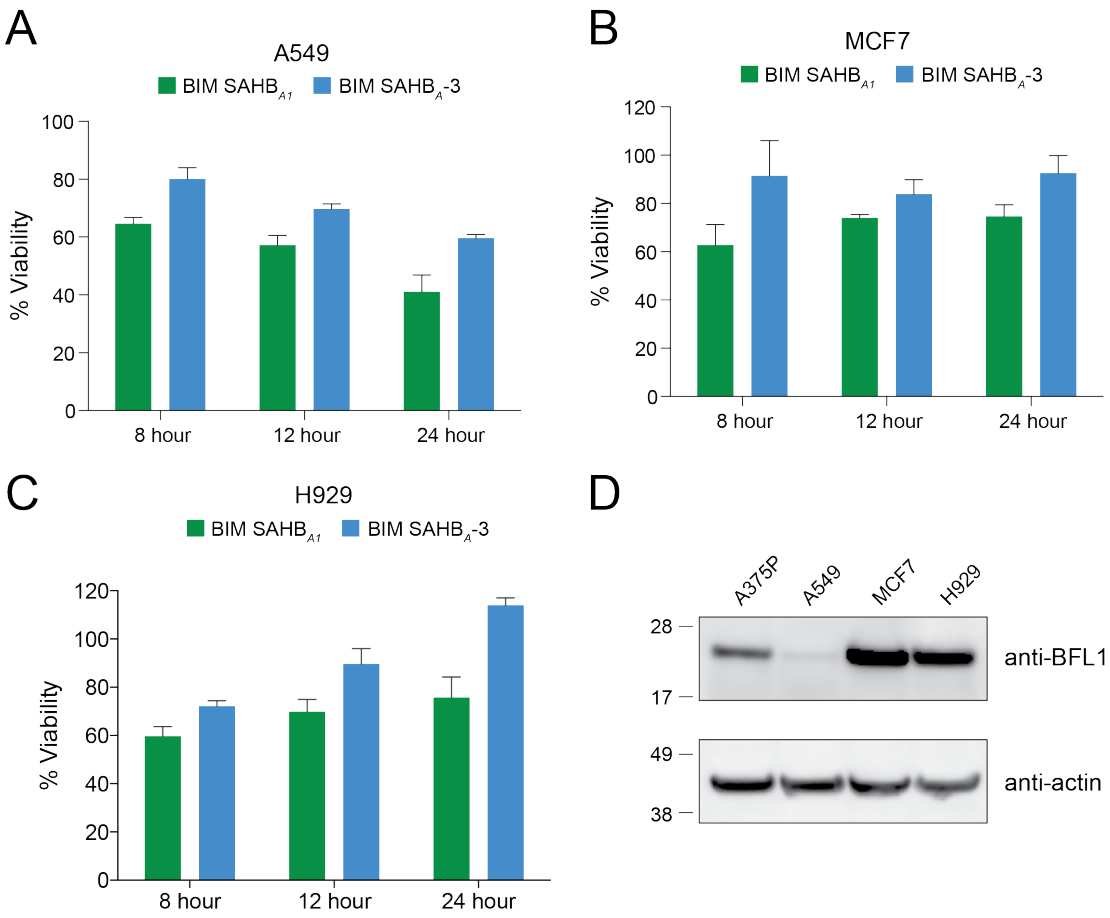

Figure 2.12 *Cell viability of BIM SAHB-treated non-melanoma cancer cells that either lack BFL-1 expression or are driven by alternate oncogenic mechanisms.*

(**A**-**C**) Cell viability of A549 (**A**), MCF7 (**B**), and H929 (**C**) cells treated with BIM SAHB$_{A1}$ or BIM SAHB$_A$-3 (40 μM for A549 and MCF7, 10 μM for H929), as measured by CellTiter-Glo assay at the indicated time points. Data are mean ± SD for experiments performed in technical sextuplet for A549 and MCF7 cells, and technical triplicate for H929 cells. (**D**) BFL-1 western analysis of electrophoresed lysates from A375P, A549, MCF7, and H929 cells.

Figure 2.13 *Endogenous BFL-1 targeting and mitochondrial localization of a warhead-bearing BIM SAHB in A375P melanoma cells.*

(**A**) Enhanced targeting of native BFL-1 by biotinylated BIM $SAHB_A$-3, compared with BIM $SAHB_A$, in A375P lysates, as monitored by SA pull-down and BFL-1 western analysis (top). In contrast, both compounds are equally effective at engaging MCL-1, which bears no cysteine in its BH3-binding groove and thus provides no competitive advantage for BIM $SAHB_A$-3 (bottom). (**B**) BIM $SAHB_A$-3, but not BIM $SAHB_A$, biotinylates mitochondrial protein that migrates at the same molecular weight as immunoreactive BFL-1. (**C**) Live confocal microscopy of A375P cells treated with FITC-BIM $SAHB_A$-3 reveals its localization at the mitochondria, the intracellular site of native BFL-1. Blue, Hoechst; green, FITC-BIM $SAHB_A$-3; red, MitoTracker; yellow, co-localization of FITC-BIM $SAHB_A$-3 and MitoTracker. Scale bar, 10 μm. (**D**) A FITC-BIM $SAHB_A$-3-treated A375P cell is observed to undergo apoptosis induction, as manifested by cell shrinkage, nuclear condensation, and membrane blebbing. The co-localization of FITC-BIM $SAHB_A$-3 and MitoTracker is also evident, as described in (**C**). Scale bar, 10 μm.

Figure 2.13 (Continued)

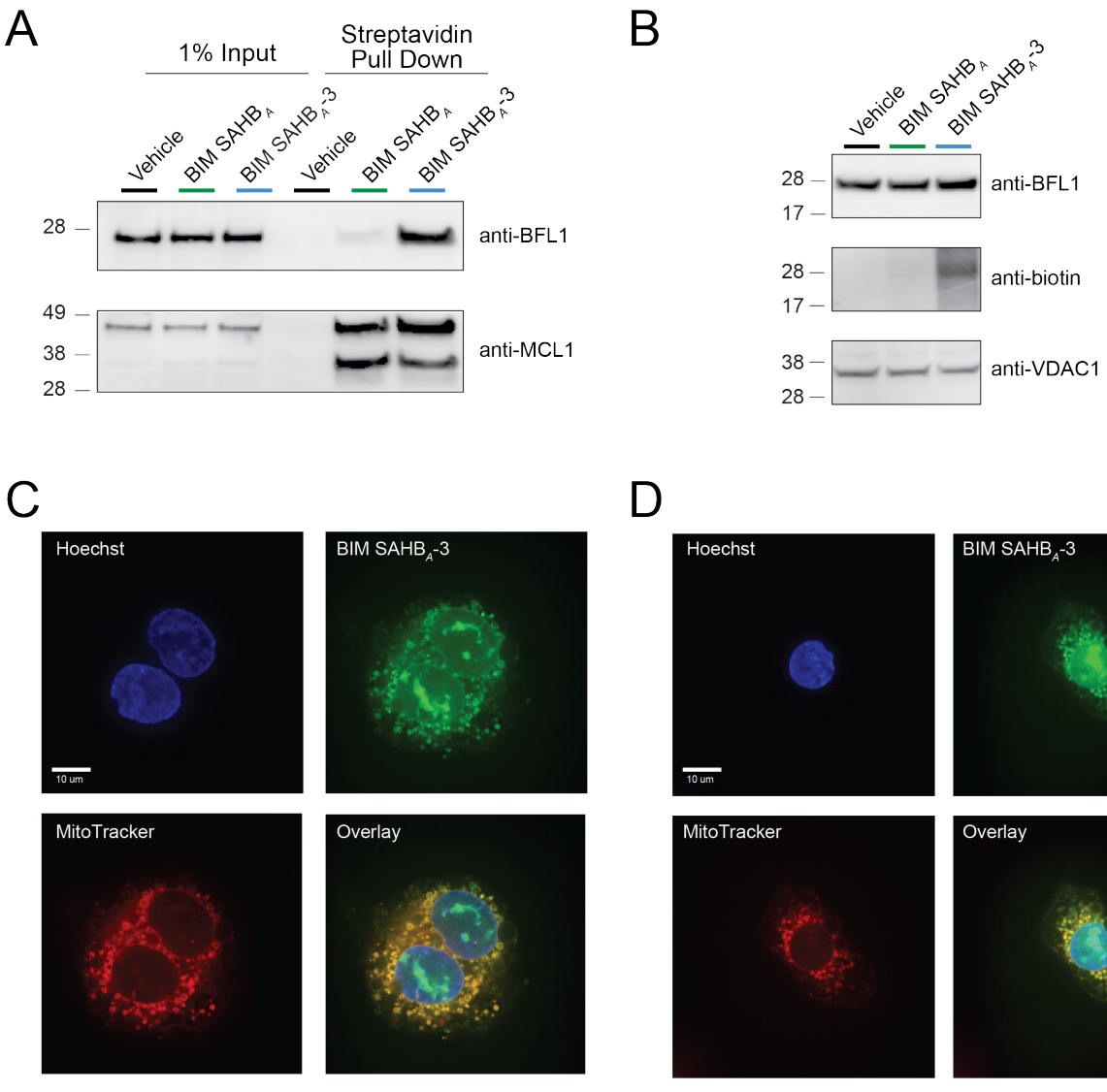

native BFL-1 and greater efficacy in triggering apoptosis. Thus, in addition to harnessing a cysteine-reactive targeting strategy to selectively trap BFL-1, heightened susceptibility to covalent BFL-1 inhibitors such as BIM SAHB$_A$-3 may provide a diagnostic approach for identifying BFL-1 dependency in human cancers.

DISCUSSION

BFL-1, like its homologs BCL-2, BCL-X_L, and MCL-1, has emerged as an oncogenic protein that drives discrete subtypes of human cancer and promotes chemoresistance and metastasis[25-31]. Whereas selective small-molecule targeting of BCL-2 with venetoclax has shown remarkable success in BCL-2-dependent cancers, including relapsed chronic lymphocytic leukemia[52], recapitulating this achievement for the diversity of anti-apoptotic targets remains a formidable challenge. The capacity to harness the natural selectivity of BH3 domain sequences for targeting individual, subsets, and all anti-apoptotic targets is an attractive feature of hydrocarbon-stapled BH3 peptides[24,48,53]. Here, we identified the first example of a BH3-only and anti-apoptotic protein pair that juxtapose cysteines at their binding interface in a manner that could support disulfide bond formation. We translated this insight into the first proof of concept for generating covalent stapled peptide inhibitors that can selectively derivatize an intracellular protein target to obstruct its key regulatory binding surface.

The development of covalent inhibitors for intracellular protein targets has seen a recent resurgence, owing to the breakthrough success of such agents as ibrutinib and afitinib[33,35,37,39]. An important hurdle for covalent drugs is balancing reactivity with selectivity, since non-specific protein derivatization can lead to off-target activities and unwanted toxicities[54]. Combining the natural selectivity and relatively large non-covalent binding interface of bioactive α helices with embedded, focally-reactive electrophilic warheads could provide a new opportunity to engage otherwise intractable protein targets. Given the presence of native cysteines either within or immediately adjacent to the regulatory ‘‘helix-in-groove’’ binding surfaces of a host of therapeutic targets[55-59], we

envision that our covalent stapled peptide inhibitor approach could be broadly applied.

Tuning the specificity of α-helical domains by installing electrophilic warheads provides a new dimension to stapled peptide design. In the case of BFL-1, we demonstrate that a semi-selective NOXA BH3 peptide and an otherwise pan-interacting BIM BH3 sequence can be fashioned to react with C55 at the critical BH3-binding groove, yet not form analogous covalent bonds with alternative cysteines within BFL-1, its homologs MCL-1 or BCL-X_L, or other cellular proteins. The enhanced BFL-1 targeting capacity of warhead-bearing stapled BH3 peptides, when compared with the corresponding constructs capable of non-covalent interaction alone, translated into enhanced apoptosis induction of BFL-1-dependent melanoma cells. This selective reactivity feature, coupled with the general proteolytic resistance of stapled peptides, their capacity for cellular uptake, and recent advancement to Phase 2 testing in human cancer, suggests that incorporation of electrophilic warheads could yield a new class of chimeric molecules that combine the advantages of stapled peptides and covalent inhibitors for preclinical and clinical development.

REFERENCES

1. Danial, N. N. BCL-2 Family Proteins: Critical Checkpoints of Apoptotic Cell Death. *Clinical Cancer Research* **13,** 7254–7263 (2007).

2. Youle, R. J. & Strasser, A. The BCL-2 protein family: opposing activities that mediate cell death. *Nat Rev Mol Cell Biol* **9,** 47–59 (2008).

3. Danial, N. N. & Korsmeyer, S. J. Cell Death: Critical Control Points. *Cell* **116,** 205–219 (2004).

4. Pegoraro, L. *et al.* A 14;18 and an 8;14 chromosome translocation in a cell line derived from an acute B-cell leukemia. *Proc. Natl. Acad. Sci. U.S.A.* **81,** 7166–7170 (1984).

5. Cleary, M. & Sklar, J. Nucleotide sequence of a t(14;18) chromosomal breakpoint in follicular lymphoma and demonstration of a breakpoint-cluster region near a transcriptionally active locus on chromosome 18. *Proc. Natl. Acad. Sci. U.S.A.* **82,** 7439–7443 (1985).

6. Bakhshi, A. *et al.* Cloning the chromosomal breakpoint of t(14;18) human lymphomas: clustering around JH on chromosome 14 and near a transcriptional unit on 18. *Cell* **41,** 899–906 (1985).

7. McDonnell, T. J. *et al.* bcl-2-Immunoglobulin transgenic mice demonstrate extended B cell survival and follicular lymphoproliferation. *Cell* **57,** 79–88 (1989).

8. Tsujimoto, Y., Finger, L. R., Yunis, J., Nowell, P. C. & Croce, C. M. Cloning of the chromosome breakpoint of neoplastic B cells with the t(14;18) chromosome translocation. *Science* **226,** 1097–1099 (1984).

9. Hanahan, D. & Weinberg, R. A. Hallmarks of Cancer: The Next Generation. *Cell* **144,** 646–674 (2011).

10. Sattler, M. *et al.* Structure of Bcl-xL-Bak Peptide Complex: Recognition Between Regulators of Apoptosis. *Science* **275,** 983–986 (1997).

11. Oltersdorf, T. *et al.* An inhibitor of Bcl-2 family proteins induces regression of solid tumours. *Nature* **435,** 677–681 (2005).

12. Tse, C. *et al.* ABT-263: A Potent and Orally Bioavailable Bcl-2 Family Inhibitor. *Cancer Research* **68,** 3421–3428 (2008).

13. Souers, A. J. *et al.* ABT-199, a potent and selective BCL-2 inhibitor, achieves antitumor activity while sparing platelets. *Nat Med* **19,** 202–208 (2013).

14. Mason, K. D. *et al.* Programmed anuclear cell death delimits platelet life span. *Cell* **128,** 1173–1186 (2007).

15. Beroukhim, R. *et al.* The landscape of somatic copy-number alteration across human cancers. *Nature* **463,** 899–905 (2010).

16. Leverson, J. D. *et al.* Potent and selective small-molecule MCL-1 inhibitors demonstrate on-target cancer cell killing activity as single agents and in combination with ABT-263 (navitoclax). *Cell Death and Disease* **6,** e1590 (2015).

17. Pelz, N. F. *et al.* Discovery of 2-Indole-acylsulfonamide Myeloid Cell Leukemia 1 (Mcl-1) Inhibitors Using Fragment-Based Methods. *J. Med. Chem.* **59,** 2054–2066 (2016).

18. Kotschy, A. *et al.* The MCL1 inhibitor S63845 is tolerable and effective in diverse cancer models. *Nature* 1–20 (2016).

19. Walensky, L. D. & Bird, G. H. Hydrocarbon-Stapled Peptides: Principles, Practice, and Progress. *J. Med. Chem.* **57,** 6275–6288 (2014).

20. Walensky, L. D. *et al.* Activation of apoptosis in vivo by a hydrocarbon-stapled BH3 helix. *Science* **305,** 1466–1470 (2004).

21. Walensky, L. D. *et al.* A stapled BID BH3 helix directly binds and activates BAX. *Molecular Cell* **24,** 199–210 (2006).

22. Gavathiotis, E. *et al.* BAX activation is initiated at a novel interaction site. *Nature* **455,** 1076–1081 (2008).

23. Gavathiotis, E., Reyna, D. E., Davis, M. L., Bird, G. H. & Walensky, L. D. BH3-Triggered Structural Reorganization Drives the Activation of Proapoptotic BAX. *Molecular Cell* **40,** 481–492 (2010).

24. LaBelle, J. L. *et al.* A stapled BIM peptide overcomes apoptotic resistance in hematologic cancers. *J. Clin. Invest.* **122,** 2018–2031 (2012).

25. Fan, G. *et al.* Defective ubiquitin-mediated degradation of antiapoptotic Bfl-1 predisposes to lymphoma. *Blood* **115,** 3559–3569 (2010).

26. Haq, R., Yokoyama, S. & Hawryluk, E. B. BCL2A1 is a lineage-specific antiapoptotic melanoma oncogene that confers resistance to BRAF inhibition. *Proc. Natl. Acad. Sci. U.S.A.* **110,** 4321-4326 (2013).

27. Mahadevan, D. *et al.* Transcript profiling in peripheral T-cell lymphoma, not otherwise specified, and diffuse large B-cell lymphoma identifies distinct tumor profile signatures. *Mol. Cancer Ther.* **4,** 1867–1879 (2005).

28. Placzek, W. J. *et al.* A survey of the anti-apoptotic Bcl-2 subfamily expression in cancer types provides a platform to predict the efficacy of Bcl-2 antagonists in cancer therapy. *Cell Death and Disease* **1,** e40–9 (2010).

29. Yecies, D., Carlson, N. E., Deng, J. & Letai, A. Acquired resistance to ABT-737 in lymphoma cells that up-regulate MCL-1 and BFL-1. *Blood* **115,** 3304–3313 (2010).

30. Hind, C. K. *et al.* Role of the pro-survival molecule Bfl-1 in melanoma. *Int. J. Biochem. Cell Biol.* **59,** 94–102 (2015).

31. Riker, A. I. *et al.* The gene expression profiles of primary and metastatic melanoma yields a transition point of tumor progression and metastasis. *BMC Med Genomics* **1,** 43–16 (2008).

32. Davies, H. *et al.* Mutations of the BRAF gene in human cancer. *Nature* **417,** 949–954 (2002).

33. Burger, J. A. *et al.* Ibrutinib as Initial Therapy for Patients with Chronic Lymphocytic Leukemia. *N Engl J Med* **373,** 2425–2437 (2015).

34. Dreyling, M. *et al.* Ibrutinib versus temsirolimus in patients with relapsed or refractory mantle-cell lymphoma: an international, randomised, open-label, phase 3 study. *Lancet* **387,** 770–778 (2016).

35. Treon, S. P. *et al.* Ibrutinib in Previously Treated Waldenström's Macroglobulinemia. *N Engl J Med* **372,** 1430–1440 (2015).

36. Li, D. *et al.* BIBW2992, an irreversible EGFR/HER2 inhibitor highly effective in preclinical lung cancer models. *Oncogene* **27,** 4702–4711 (2008).

37. Miller, V. A. *et al.* Afatinib versus placebo for patients with advanced, metastatic non-small-cell lung cancer after failure of erlotinib, gefitinib, or both, and one or two lines of chemotherapy (LUX-Lung 1): a phase 2b/3 randomised trial. *Lancet Oncol.* **13,** 528–538 (2012).

38. Solca, F. *et al.* Target binding properties and cellular activity of afatinib (BIBW 2992), an irreversible ErbB family blocker. *Journal of Pharmacology and Experimental Therapeutics* **343,** 342–350 (2012).

39. Wu, Y.-L. *et al.* Afatinib versus cisplatin plus gemcitabine for first-line treatment of Asian patients with advanced non-small-cell lung cancer harbouring EGFR mutations (LUX-Lung 6): an open-label, randomised phase 3 trial. *Lancet Oncol.* **15,** 213–222 (2014).

40. Bird, G. H., Bernal, F., Pitter, K. & Walensky, L. D. Synthesis and biophysical characterization of stabilized alpha-helices of BCL-2 domains. *Meth. Enzymol.* **446,** 369–386 (2008).

41. Bird, G. H., Crannell, W. C. & Walensky, L. D. Chemical synthesis of hydrocarbon-stapled peptides for protein interaction research and therapeutic targeting. *Curr Protoc Chem Biol* **3,** 99–117 (2011).

42. Pitter, K., Bernal, F., LaBelle, J. & Walensky, L. D. Dissection of the BCL-2 family signaling network with stabilized alpha-helices of BCL-2 domains. *Meth. Enzymol.* **446,** 387–408 (2008).

43. Andersen, K. R., Leksa, N. C. & Schwartz, T. U. Optimized E. coli expression strain LOBSTR eliminates common contaminants from His-tag purification. *Proteins* **81,** 1857–1861 (2013).

44. Leshchiner, E. S., Braun, C. R., Bird, G. H. & Walensky, L. D. Direct activation of full-length proapoptotic BAK. *Proc. Natl. Acad. Sci. U.S.A.* **110,** E986–95 (2013).

45. Lovell, J. F. *et al.* Membrane Binding by tBid Initiates an Ordered Series of Events Culminating in Membrane Permeabilization by Bax. *Cell* **135,** 1074–1084 (2008).

46. Dewson, G. Investigating Bax subcellular localization and membrane integration. *Cold Spring Harb Protoc* **2015,** 467–471 (2015).

47. Rooswinkel, R. W., van de Kooij, B., Verheij, M. & Borst, J. Bcl-2 is a better ABT-737 target than Bcl-xL or Bcl-w and only Noxa overcomes resistance mediated by Mcl-1, Bfl-1, or Bcl-B. *Cell Death and Disease* **3,** e366 (2012).

48. Stewart, M. L., Fire, E., Keating, A. E. & Walensky, L. D. The MCL-1 BH3 helix is an exclusive MCL-1 inhibitor and apoptosis sensitizer. *Nature Chemical Biology* **6,** 595–601 (2010).

49. Bird, G. H. *et al.* Biophysical determinants for cellular uptake of hydrocarbon-stapled peptide helices. *Nature Chemical Biology* **12,** 845–852 (2016).

50. Edwards, A. L. *et al.* Cellular Uptake and Ultrastructural Localization Underlie the Pro-apoptotic Activity of a Hydrocarbon-stapled BIM BH3 Peptide. *ACS Chem. Biol.* **10,** 2149–2157 (2015).

51. Acquaviva, J. *et al.* Targeting KRAS-mutant non-small cell lung cancer with the Hsp90 inhibitor ganetespib. *Mol. Cancer Ther.* **11,** 2633–2643 (2012).

52. Roberts, A. W. *et al.* Targeting BCL2 with Venetoclax in Relapsed Chronic Lymphocytic Leukemia. *N Engl J Med* **374,** 311–322 (2016).

53. Edwards, A. L. *et al.* Multimodal Interaction with BCL-2 Family Proteins Underlies the Proapoptotic Activity of PUMA BH3. *Chemistry & Biology* **20,** 888–902 (2013).

54. Singh, J., Petter, R. C., Baillie, T. A. & Whitty, A. The resurgence of covalent drugs. *Nat Rev Drug Discov* **10,** 307–317 (2011).

55. Allen, B. L. & Taatjes, D. J. The Mediator complex: a central integrator of transcription. *Nat Rev Mol Cell Biol* **16,** 155–166 (2015).

56. Kise, Y. *et al.* A short peptide insertion crucial for angiostatic activity of human tryptophanyl-tRNA synthetase. *Nat Struct Mol Biol* **11,** 149–156 (2004).

57. Kitagawa, D. *et al.* Release of RASSF1C from the nucleus by Daxx degradation links DNA damage and SAPK/JNK activation. *The EMBO Journal* **25,** 3286–3297 (2006).

58. Margarit, S. M., Sondermann, H., Hall, B. E. & Nagar, B. Structural evidence for feedback activation by Ras· GTP of the Ras-specific nucleotide exchange factor SOS. *Cell* **112,** 685–695 (2003).

59. Scott, F. L. *et al.* The Fas-FADD death domain complex structure unravels signalling by receptor clustering. *Nature* **457,** 1019–1022 (2009).

Chapter III

Precision Targeting of BFL-1/A1 and an ATM Co-Dependency

to Reactivate Apoptosis in Human Cancer

ABSTRACT

BCL-2 family proteins are critical regulators of mitochondrial apoptosis during health and disease. Anti-apoptotic members, such as BCL-2, MCL-1 and BFL-1/A1, suppress apoptosis by trapping the critical BCL-2 homology 3 (BH3) domain helix of pro-apoptotic members in a surface groove, preventing the activation and mitochondrial poration of the executioner proteins, BAX and BAK. Cancer cells can overexpress anti-apoptotic BCL-2 family proteins to enforce cellular immortality and cause treatment resistance, prompting drug development efforts to target these oncogenic proteins. Whereas a selective BCL-2 inhibitor molecule has now been FDA-approved and several small molecule inhibitors of MCL-1 have recently entered Phase 1 clinical testing, BFL-1/A1 remains undrugged. We have developed and applied hydrocarbon-stapled BH3 peptide α-helices as an alternative strategy for targeting individual, subsets, and all BCL-2 family proteins, to reactivate apoptosis in cancer. Here, we experimented with a series of stapled peptide design principles to engineer a functionally-selective and cell-permeable BFL-1/A1 inhibitor that was specifically cytotoxic to BFL-1/A1-dependent human cancer cells. Because cancers harbor a diversity of resistance mechanisms, and thus typically require multi-agent treatment in the clinic, we further investigated BFL-1/A1 co-dependencies based on genome-scale CRISPR-Cas9 screening. We identified an oncogenic co-dependency of BFL-1/A1 and ataxia-telangiectasia mutated (ATM) kinase in acute myeloid leukemia (AML), and achieved synergistic killing by combining our selective BFL-1/A1 inhibitor with a clinical-grade ATM kinase inhibitor. Thus, we discovered new stapled peptide compositions with precise BFL-1/A1 targeting capability for development as next-generation drug prototypes for BFL-1/A1-dependent cancers.

ATTRIBUTIONS

Contributions to the work described in this chapter were made by Rachel M. Guerra, Gregory H. Bird, Edward P. Harvey, Neekesh V. Dharia, Kimberly Stegmaier, and Loren D. Walensky.

R.M.G., G.H.B. and L.D.W. conceived of and designed the study. R.M.G., G.H.B., and L.D.W. designed SAHB peptides, R.M.G. performed the biochemical and cellular experiments, E.P.H. generated BFL-1 plasmids and methodology for the *in vitro* anti-apoptotic pulldown assay, and N.V.D. conducted the gene dependency analyses under the supervision of K.S. Additionally, we thank T. Oo for technical assistance with peptide production.

INTRODUCTION

BCL-2 family proteins are essential regulators of apoptosis, and the protein interactions among pro-survival and pro-death members dictate cellular life-and-death decisions during homeostasis and disease. Anti-apoptotic members, such as BCL-2, BCL-X_L, MCL-1, and BFL-1/A1, suppress apoptosis by trapping the BCL-2 homology 3 (BH3) helix of pro-apoptotic proteins in a surface groove[1]. This "BH3 blockade" involves two distinct mechanisms of action[2]. First, entrapment of the exposed BH3-helices of activated BAX and BAK proteins can arrest the dynamic process of self-association and mitochondrial outer membrane poration that triggers apoptosis. Second, sequestering the BH3 motifs of "direct-activator" BH3-only proteins (e.g. BIM, BID, PUMA), which serve as upstream sensors of cell stress, can prevent their direct triggering of BAX/BAK; this binding mode can also block the indirect activation of BAX/BAK, which ensues upon "sensitizer" BH3-only protein (e.g. NOXA, BAD) dissociation of the inhibitory complexes between anti-apoptotic proteins and activated monomers of BAX and BAK[3]. Pathologic overexpression of anti-apoptotic proteins establishes formidable BH3 blockades that drive the development, maintenance, and chemoresistance of many human cancers. Thus, pharmacologic targeting of anti-apoptotic protein grooves has emerged as a validated therapeutic strategy for reactivating apoptosis in human cancer.

Decades of research into the structure and function of anti-apoptotic proteins, coupled with Herculean medicinal chemistry efforts to construct selective anti-apoptotic inhibitors, are now bearing fruit. Venetoclax is an FDA-approved BCL-2 inhibitor that is demonstrating clinical efficacy in triggering apoptosis in BCL-2 dependent cancers by harnessing the indirect mechanism for activating BAX/BAK[4,5]. Within the last year, a

series of selective small molecule MCL-1 inhibitors have entered Phase 1 clinical testing[6]. We have pursued an alternative structured-peptide based strategy in which the evolutionary-honed BH3 sequences themselves are chemically stabilized by insertion of an all-hydrocarbon "staple" to generate Stabilized Alpha-Helices of BCL-2 domains (SAHBs) for basic research and clinical translation[7]. Applying this approach to the transactivation α-helix of p53 has led to the advancement of stapled peptide dual inhibitors of HDM2/HDMX to Phase 1 and 2 clinical testing in human cancer[8-10]. Because cancer cells can harbor dependencies on individual and subsets of BCL-2 family anti-apoptotic proteins, developing both selective and multimodal inhibitors is a high priority goal, particular for those members that remain undrugged, such as BFL-1/A1.

The previous chapter describes our discovery of a selectivity factor for targeting BFL-1/A1 based on the presence of a unique cysteine in its BH3-binding groove[11,12]. By incorporating acrylamide moieties into stapled BH3 peptides, we demonstrated efficient and specific covalent targeting of BFL-1/A1 and its inhibitory complexes in lysates and cells, which resulted in selective apoptosis induction of BFL-1-driven melanoma cells. Whereas cysteine-reactive BIM and NOXA SAHBs covalently targeted BFL-1/A1 and retained non-covalent binding to MCL-1, yielding dual BFL-1/MCL-1 inhibitors, only the BIM constructs were found to be cell permeable and biologically-active in cells[11]. Here, we pursued a series of new design principles to transform cysteine-reactive NOXA SAHBs into cell permeable constructs with precision selectivity for BFL-1/A1, revealing a powerful and reliable workflow for optimizing stapled peptides. Given the importance of combination therapies in overcoming the apoptotic blockades of human cancer, we

further explored BFL-1/A1 co-dependencies based on CRISPR/Cas9 screening, and identified an unanticipated synergy between our selective BFL-1/A1 inhibitor and molecular targeting of the ATM kinase in BFL-1-driven AML.

METHODS

Stapled Peptide Synthesis. Hydrocarbon-stapled peptides corresponding to the BH3 domains of BCL-2 family proteins, and either N-terminally derivatized with acetyl, FITC-β-Ala, or electrophilic warheads, or C-terminally derivatized with Lys-biotin, were synthesized, purified, and quantitated using our previously reported methods[11,13,14]. Stapled peptide compositions, and their observed masses and use by figure, are listed in **Appendix: Table S2**.

Recombinant Protein Expression and Purification. Recombinant anti-apoptotic BFL-1ΔC (aa 1-151) and its cysteine to serine mutants were cloned into pET17b (Novagen, N-terminal hexahistidine tag), expressed in *Escherichia coli* LOBSTR BL21(DE3) (Kerafast), and purified by sequential Ni-affinity and size-exclusion chromatography as described[11,15]. Recombinant anti-apoptotic BCL-X_LΔC (aa 1-212) and MCL-1ΔNΔC (aa 172-329) were cloned into the pGEX-4T-1 (GE Healthcare, N-terminal GST tag) expression vector, expressed in BL21(DE3) *Escherichia coli* (Sigma Aldrich), and purified as described previously[11,15]. In purifying BCL-X_LΔC, the GST tag was cleaved using thrombin (12-15 units) to provide a size difference between BCL-X_LΔC and GST-MCL-1ΔNΔC for facile protein identification by silver stain in streptavidin pull-down experiments.

In Vitro Covalent Conjugation Assay. His-BFL-1ΔC C4S/C19S protein (5 μM) was pre-treated with 10 mM DTT in 50 mM Tris (pH 8.0) and 100 mM NaCl for 30 min at room temperature (final volume 9.5 μL) and then combined with a 10:1 molar ratio of

warhead-bearing NOXA SAHB for an additional 1 hr incubation at room temperature. The samples were then boiled in 3X loading buffer with DTT, electrophoresed on a 12% Bis-Tris gel, and subjected to Coomassie staining.

Covalent BFL-1 Targeting Assay. 293T cells were cultured in Dulbecco's Modified Eagle's Medium (DMEM) containing 10% fetal bovine serum (FBS) and penicillin-streptomycin, and transfected with 2 μg pCMV plasmid containing HA-BFL-1ΔC C4S/C19S using Lipofectamine LTX Plus (Thermo Scientific). After 24 hr, the transfected cells were treated with 20 μM of the indicated peptides in DMEM containing 5% FBS for 8 hr. Treated cells were washed with PBS, harvested, and then lysed by incubation with 1% CHAPS lysis buffer (150 mM NaCl, 50 mM Tris pH 7.4, 100 mM DTT). Protein concentration of the isolated supernatant fraction was measured using a BCA kit according to manufacturer's instructions (Thermo Scientific). Samples were then boiled in LDS buffer and subjected to western analysis using 1:1000 dilutions of HA (Sigma-Aldrich, #12CA5) and actin (Sigma-Aldrich, #A1978) antibodies.

LDH Release Assay. A375P melanoma cells were cultured in DMEM containing 10% fetal bovine serum (FBS) and penicillin-streptomycin, and plated in 96-well plates (5 x 10^3 cells per well). After overnight incubation, the cells were treated with the indicated concentrations of cysteine-reactive NOXA SAHBs in DMEM supplemented with 5% FBS for 30 min. After plate centrifugation at 1,500 rpm (Thermo Scientific Sorvall Four-Place Swinging Bucket Rotor [75006445]; 478 x g) for 5 min at 4 °C, LDH release was quantified by transferring 100 μL of cell-culture medium to a clear plate (Corning),

incubating with 100 μL of LDH reagent (Roche) for 30 min while shaking, and then measuring absorbance at 490 nm on a microplate reader (Spectramax M5, Molecular Devices).

Recombinant Anti-Apoptotic Protein Pulldown Assay. WT His-BFL-1ΔC, BCL-X_LΔC (tagless), and GST-MCL-1ΔNΔC (1 μM each) were combined and incubated with 3 mM DTT in PBS for 30 min at room temperature. Mixtures were treated with vehicle (0.1% DMSO) or the indicated C-terminally biotinylated NOXA SAHB (1 μM) for 4 hr, and then added to 30 μL PBS-washed high-capacity streptavidin agarose (Thermo Fisher Pierce) beads, followed by incubation with rotation at room temperature for 2 hr. The beads were washed 3 times with NP-40 lysis buffer (1% NP-40, 50 mM Tris pH 8, 100 mM NaCl, 2.5 mM $MgCl_2$) and then 3 times with PBS. To elute bound protein, the beads were boiled for 10 min in 10% SDS containing 10 mg/mL biotin. After elution, samples were boiled in 3x LDS and 2 M DTT for twenty minutes. Inputs (2%) and eluates (5 μL) were subjected to gel electrophoresis using a 12% Bis-Tris gel and proteins detected by silver staining (Pierce Silver Staining Kit, Thermo Fisher).

Native Anti-Apoptotic Protein Pulldown Assay. Cultured A375P cells were trypsinized, washing with PBS, and lysed by incubating with 1% CHAPS lysis buffer (150 mM NaCl, 50 mM Tris pH 7.4, 100 mM DTT). Protein concentration of the isolated supernatant was measured using a BCA kit according to the manufacturer's instructions (Thermo Scientific). Lysate samples (1 mg) were incubated with vehicle (3% DMSO) or C-terminally biotinylated NOXA SAHBs (30 μM) overnight in 1% CHAPS lysis buffer at

4 ºC. Biotin capture was accomplished by incubating the mixture with high-capacity streptavidin agarose (Thermo Scientific) for 2 hr at 4 ºC, followed by centrifugation and washing the pelleted beads three times with lysis buffer (1 mL). Bead-bound proteins were eluted by boiling in 10% SDS containing 10 mg/mL biotin for 10 min and then subjected to electrophoresis and western blotting using BFL-1 (Abcam, #125259) and MCL-1 (Rockland, #600-401-394S) antibodies.

tBID/Anti-Apoptotic Complex Disruption Assay. To evaluate the capacity of biotinylated NOXA SAHBs to compete with tBID for interactions with BFL-1 and MCL-1, 293T cells were transfected with either HA-BFL-1ΔC C4S/C19S or FLAG-MCL-1 in the p3XFLAG-CMV-10 vector (Sigma) as described above. After 24 hr, the transfected cells were trypsinized, washed with PBS, lysed in 1% CHAPS buffer, and the supernatant collected for protein concentration determination by BCA kit. Lysate samples (0.5 mg) were incubated with 0.25 μM recombinant tBID (R&D Systems) and 5 μM biotinylated NOXA SAHBs for 6 hr at room temperature. The mixtures were then subjected to HA or FLAG immunoprecipitation, followed by western analysis using 1:1000 dilutions of HA (Sigma-Aldrich, #12CA5), FLAG (Sigma-Aldrich, #F7425), and BID (Santa Cruz, #sc-11423) antibodies.

Competitive Fluorescence Polarization Binding Assay. Fluorescence polarization (FP) assays were performed as previously described. Briefly, direct binding curves were first generated by FITC-BID BH3 (25 nM) with serial dilutions of anti-apoptotic protein, and FP was measured at 5 min on a SpectraMax M5 microplate reader (Molecular

Devices). For competition assays, a serial dilution of acetylated or cysteine-reactive NOXA SAHB was added to the indicated recombinant protein at ~EC_{75} concentration, as determined by the direct binding assay. FITC-BID BH3 (25 nM) was then added and fluorescence polarization measured at 30 min. Nonlinear regression analysis of competitive binding curves was performed using Prism software (GraphPad).

BFL-1 Dependency and Co-Dependency Analysis. BFL-1 dependency analyses were performed using the reported genome-scale CRISPR-Cas9 loss-of-function screening dataset[16]. We defined 2,027 genes as likely pan-essential genes, whose dependency scores fall in the bottom 23% of gene scores in at least 90% of the cell lines evaluated. In addition to the published gene dependency scores, relative dependency Z-scores were calculated for each gene across all evaluated cancer cell lines using the median dependency score for each gene and the median average deviation. Pearson and Spearman correlation coefficients to BCL2A1 dependency were calculated using the R programming language across the gene dependencies within the 8 AML lines screened (MOLM13, MV411, NB4, NOMO1, P31FUJ, TF1, THP1, U937). Gene dependencies were selected for further consideration if at least 2 AML cell lines (1) showed evidence of dependency with scores of < -0.1, (2) the gene was expressed in at least 2 AML cell lines in the Cancer Cell Line Encyclopedia (CCLE: https://portals.broadinstitute.org/ccle) with transcripts per million (TPM) > 1, (3) the gene was not predicted to be one of the pan-essential genes noted above, and (4) the gene dependency was strongly correlated with coefficient > 0.9 by Pearson and Spearman correlations.

Cell Viability and Caspase-3/7 Activation Assays. U937 and MV4;11 AML cells cultured in RPMI containing 10% FBS and penicillin-streptomycin were plated in 96-well plates (5 x 10^3 cells per well) and, after overnight incubation, treated with the indicated concentrations of cysteine-reactive NOXA SAHBs and/or AZD0156 (Selleck Chemicals) in RPMI supplemented with 5% FBS for the indicated durations. Cell viability and caspase-3/7 activation was measured using CellTiter-Glo and Caspase-Glo 3/7 chemiluminescence reagents (Promega), respectively, and luminescence was detected by a Spectramax M5 microplate reader.

Phospho-signaling Analysis. U937 cells cultured in RPMI containing 10% FBS and penicillin-streptomycin were plated in 6-well plates (2 x 10^6 cells per well) and treated with the indicated concentrations of AZD0156 for 2 hr. Cells were then washed with PBS, lysed in 1% CHAPS buffer, and the supernatant collected for protein concentration determination by BCA kit. Samples were subjected to electrophoresis and western analysis using 1:1000 dilutions of phospho-ATM (S1981, Cell Signaling, #4526), ATM (Abcam, #ab78), phospho-CHK2 (Ser33/35, Cell Signaling, #2665), CHK2 (Cell Signaling, #2662), and actin (Sigma #A1978) antibodies.

RESULTS

Defining Sequence Composition and Optimal Staple Location

We used the NOXA BH3 sequence as our starting template for developing a BFL-1 selective inhibitor due to its relatively narrow anti-apoptotic binding spectrum compared to other BH3 domains. As a first step toward optimization, we shortened the NOXA BH3 sequence by eliminating N- and C-terminal residues that lacked critical interface contacts based on our review of the reported BFL-1/NOXA BH3 structure (PDB: 3MQP) (**Figures 3.1A and 3.1B**). We then conducted an *i, i+4* and *i, i+7* "staple scan" of the 15-amino acid sequence (NOXA BH3 amino acids 26-40), whereby all-hydrocarbon staples spanning one or two turns of the α-helix were sequentially substituted along the length of the peptide (**Figure 3.2**). For each construct, the N-terminus was capped with (R)-1 acryloylpiperidine-3-carboxamide, an acrylamide-bearing D-nipecotic acid derivative (D-NA) that we previously found to be optimally reactive with BFL-1/A1 C55 when incorporated into stapled BIM and NOXA BH3 helices[11].

We tested our library of D-NA-NOXA SAHBs for covalent reactivity with BFL-1 C55 by incubating each peptide with recombinant BFL-1ΔC C4S/C19S for 1 hour, followed by reducing and denaturing gel electrophoresis and Coomassie staining to monitor the change in the molecular weight of BFL-1 upon NOXA SAHB crosslinking. Strikingly, 14 of 20 constructs demonstrated complete (1-3, 6, 10-13, 15, 18-20) or near-complete (7, 9) conversion of BFL-1 to the covalent adduct, whereas NOXA SAHBs 4, 5, 8, 14, 16, and 17 exhibited impaired covalent reaction, consistent with replacement of amino acid residues critical to the BFL-1-binding interface (i.e. L29, R30, G33, and D34)

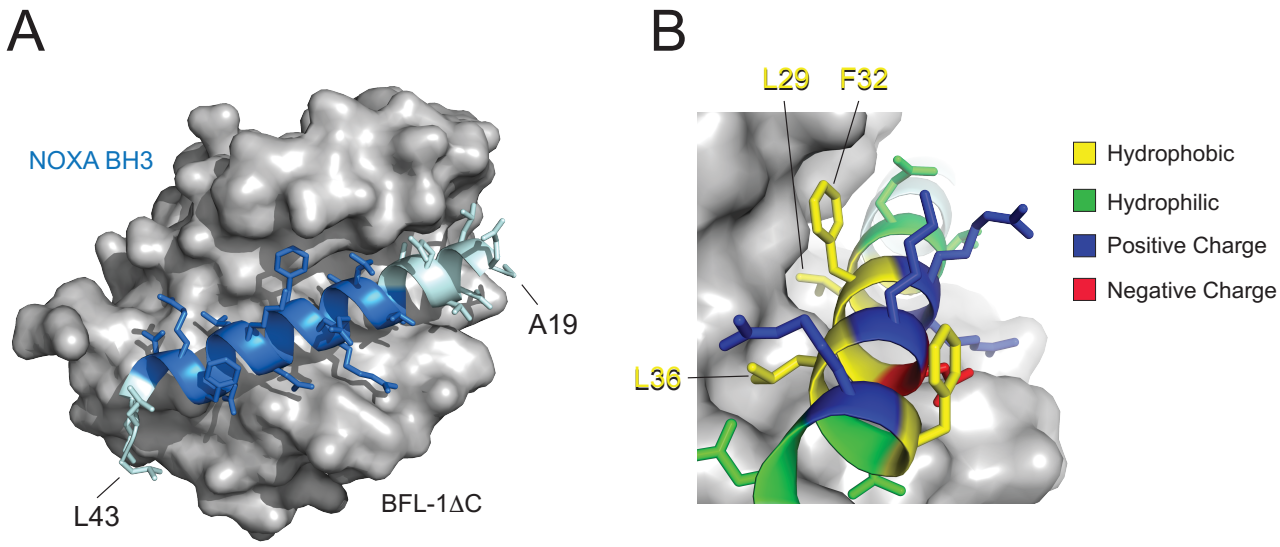

Figure 3.1 *Structural considerations in designing an optimized stapled NOXA BH3 peptide to covalently target BFL-1.*

(**A**) Structure of the NOXA BH3/BFL-1ΔC complex (PDB: 3MQP). The peptide region highlighted in dark blue was selected for staple scanning. (**B**) A view of the BH3-binding interface of the NOXA BH3/BFL-1ΔC complex demonstrates the hydrophilic and hydrophobic residues of the NOXA BH3 amphipathic helix that make critical contacts with the BFL-1 groove.

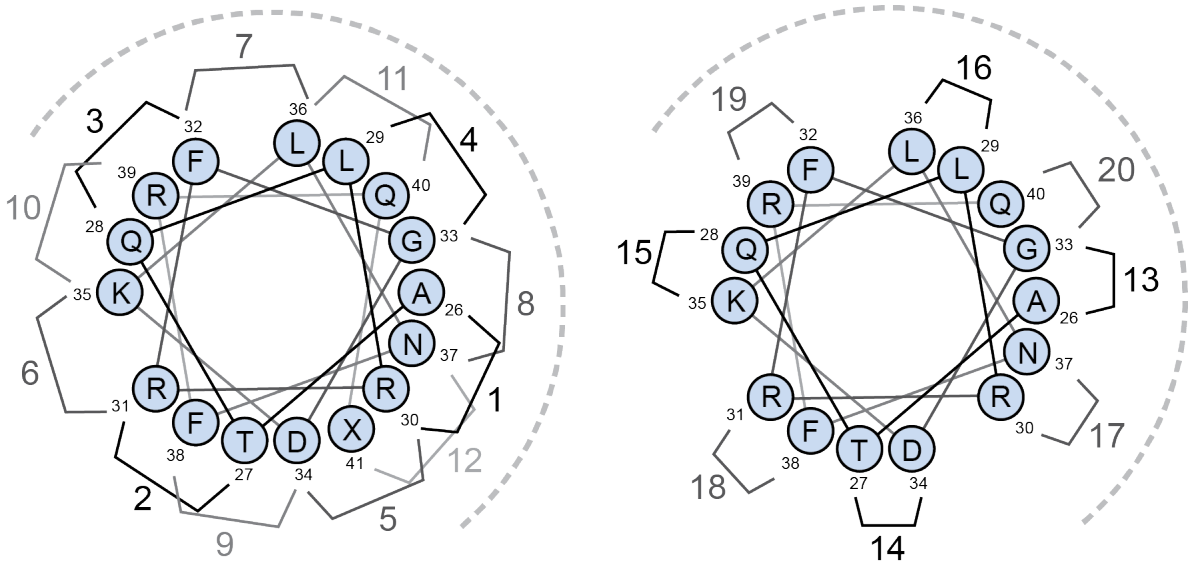

NOXA $BH3_{26-40}$	*ATQLRRFGDKLNFRQ
NOXA SAHB-1	*XTQLXRFGDKLNFRQ
NOXA SAHB-2	*AXQLRXFGDKLNFRQ
NOXA SAHB-3	*ATXLRRXGDKLNFRQ
NOXA SAHB-4	*ATQXRRFXDKLNFRQ
NOXA SAHB-5	*ATQLXRFGXKLNFRQ
NOXA SAHB-6	*ATQLRXFGDXLNFRQ
NOXA SAHB-7	*ATQLRRXGDKXNFRQ
NOXA SAHB-8	*ATQLRRFXDKLXFRQ
NOXA SAHB-9	*ATQLRRFGXKLNXRQ
NOXA SAHB-10	*ATQLRRFGDXLNFXQ
NOXA SAHB-11	*ATQLRRFGDKXNFRX
NOXA SAHB-12	*ATQLRRFGDKLXFRQX

NOXA SAHB-13	*8TQLRRFXDKLNFRQ
NOXA SAHB-14	*A8QLRRFGXKLNFRQ
NOXA SAHB-15	*AT8LRRFGDXLNFRQ
NOXA SAHB-16	*ATQ8RRFGDKXNFRQ
NOXA SAHB-17	*ATQL8RFGDKLXFRQ
NOXA SAHB-18	*ATQLR8FGDKLNXRQ
NOXA SAHB-19	*ATQLRR8GDKLNFXQ
NOXA SAHB-20	*ATQLRRF8DKLNFRX

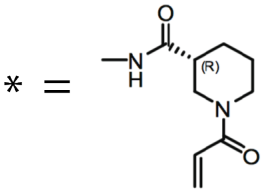

(R)-1 acryloylpiperidine-3-carboxamide

Figure 3.2 *Acrylamide-bearing shortened NOXA SAHB staple scan library.*

Helical wheel depiction and amino acid sequences of a NOXA BH3 staple scanning library. The stapled peptides were generated by inserting all-hydrocarbon *i, i+4* or *i, i+7* staples sequentially along the length of the NOXA BH3 peptide (amino acids 26-40) and the N-terminus capped with an acrylamide-derivatized D-nipecotic acid (D-NA) moiety.

with the bulky staple (**Figure 3.3A**). We then advanced a subset of the most reactive NOXA SAHB constructs to treatment (20 μM) of 293T cells expressing HA-BFL-1ΔC C4S/C19S. After a 6-hour exposure in serum-containing medium, the cells were washed, lysed, and protein supernatants analyzed by reducing and denaturing gel electrophoresis, followed by anti-HA western blotting. The appearance of a doublet is indicative of NOXA SAHB access to and covalent crosslinking of intracellular HA-BFL-1ΔC C4S/C19S at C55. Compared to BIM $SAHB_A$-3, the positive control and lead compound from our prior study[11] described in Chapter II, D-NA-NOXA SAHB-15 exhibited markedly enhanced activity (**Figure 3.3B**). Because select amphipathic peptides can disrupt cellular membranes, we screened D-NA-NOXA SAHB-15 in LDH release assays in advance of functional testing in cancer cells, and observed dose-responsive lysis of A375P melanoma cells cultured in 5% FBS after 30 minute treatment (**Figure 3.3C**). Thus, we sought a redesign strategy that would retain the favorable BFL-1-reactivity of D-NA-NOXA SAHB-15 yet enable intracellular access without cell membrane lysis.

Alternative Strategies for Eliminating Membrane Lysis and Preserving Bioactivity

We recently applied a stapled peptide library and unbiased statistical approach to discern the biophysical determinants for cellular uptake of stapled peptides and the risk factors in amino acid sequence composition for membrane lysis[17]. We observed that the combination of relatively high hydrophobic content and positive charge was the key determinant for nonspecific membrane disruption by amphipathic α-helices. In the case of a BIM SAHB library, for example, mutagenesis of a single glutamic acid to a

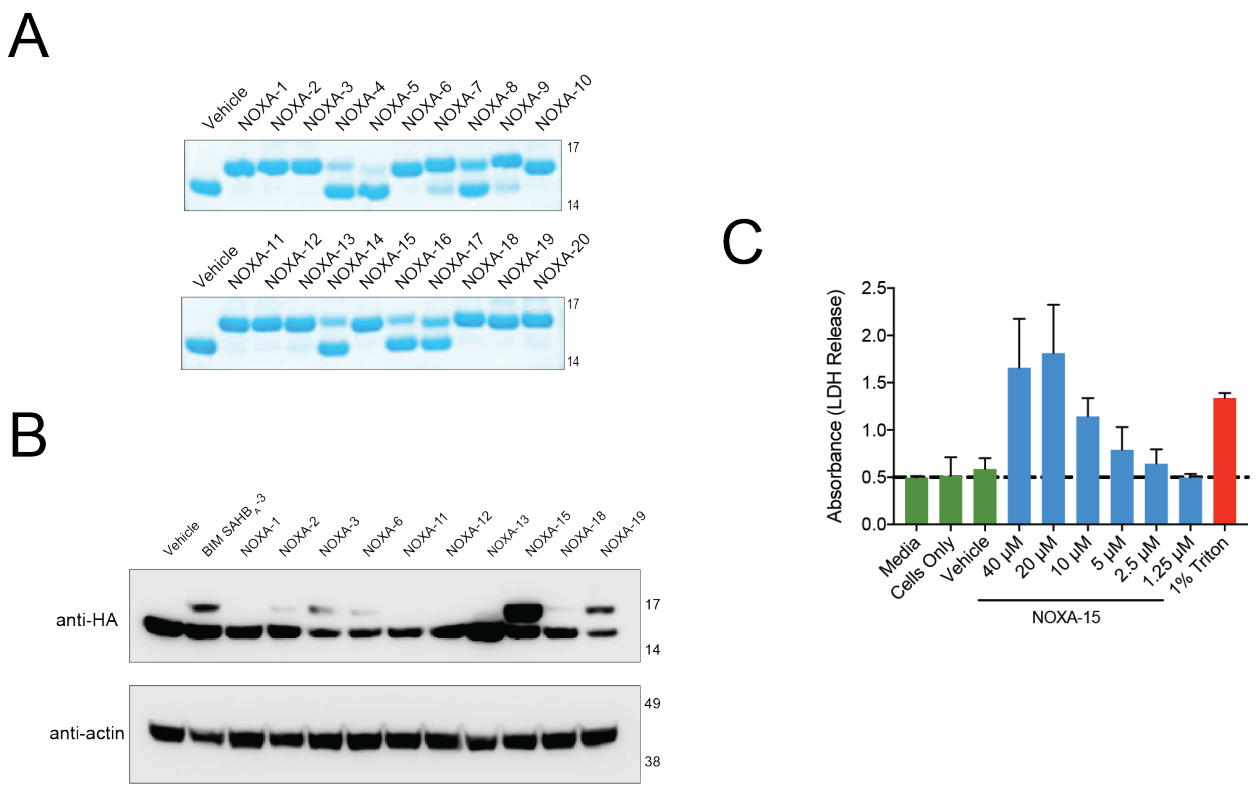

Figure 3.3 *Discovery of optimally-stapled NOXA BH3 peptides for covalent targeting of BFL-1.*

(**A**) Covalent reactivity of D-NA-NOXA SAHBs with C55 of BFL-1ΔC C4S/C19S, as detected by the shift in BFL-1 molecular weight following peptide/protein incubation, reducing and denaturing gel electrophoresis, and Coomassie staining. (**B**) Covalent reactivity of D-NA-NOXA SAHBs with HA-BFL-1ΔC C4S/C19S expressed in 293T cells, as detected by the shift in HA-BFL-1 molecular weight following cell treatment with NOXA SAHBs (20 μM) for 6 hours, lysate preparation, reducing and denaturing gel electrophoresis, and anti-HA western analysis. (**C**) Quantification of dose-responsive LDH release upon treatment of A375P cells with D-NA-NOXA SAHB-15 for 30 min. Data are mean ± SD for experiments performed in triplicate.

hydrophobic residue, such as leucine, selectively induced peptide-mediated membranolysis[17]. Based on these observations, we took a new two-pronged approach to mitigating the cellular lysis of D-NA-NOXA SAHB-15. First, we generated an alanine scanning library to assess the relative impact of point mutagenesis at each native residue of D-NA-NOXA SAHB-15. Of the thirteen constructs, three of the alanine mutations, L29A, F32A, and L36A, eliminated treatment-induced LDH release from A375P melanoma cells (**Figure 3.4A**). Interestingly, in each of these constructs, alanine mutagenesis resulted in decreasing the relative hydrophobicity of the mutated position. As a second strategy, we mutated discrete arginine residues to glutamic acid to lower the overall positive charge from +2 to 0, which likewise produced D-NA-NOXA SAHB-15 constructs with little to no LDH release activity (**Figure 3.5A**). Whereas the L/F to A mutations localized to the hydrophobic interaction face of the amphipathic NOXA BH3 helix, the R to E mutations resided on the hydrophilic surface (**Figures 3.4B and 3.5B**). To determine whether the constructs with point mutations that resolved the undesirable LDH release activity retained robust covalent BFL-1 reactivity, we incubated each mutant with BFL-1ΔC C4S/C19S as above, and monitored conversion of BFL-1 to the crosslinked species by Coomassie staining of electrophoresed samples. Whereas alanine mutagenesis of the highly conserved BH3 domain residues L29 and D34A led to incomplete reactivity toward BFL-1, all other mutants achieved complete conversion to the crosslinked species after a 1 hour incubation (**Figures 3.4C and 3.5C**). When applied to 293T cells expressing HA-BFL-1ΔC C4S/C19S, D-NA-NOXA SAHB-15 L29A showed no crosslinking, consistent with its impaired BFL-1 reactivity *in vitro*. In

Figure 3.4 *Site-specific reduction of peptide hydrophobicity eliminates membrane lysis and maintains effective covalent targeting of intracellular BFL-1.*

(**A**) LDH release from A375P cells upon treatment with an alanine scanning library of D-NA-NOXA SAHB-15 (40 μM peptide, 30 min). Data are mean ± SD for experiments performed in triplicate. (**B**) Structure of the NOXA BH3/BFL-1ΔC complex (PDB ID 3MQP), highlighting the (*i, i*+7) staple position #15 (red), and the alanine point mutants (green) that eliminated cellular lysis. (**C**) Covalent reactivity of an alanine scanning library of D-NA-NOXA SAHB-15 with C55 of BFL-1ΔC C4S/C19S, as detected by the shift in BFL-1 molecular weight following peptide/protein incubation, reducing and denaturing gel electrophoresis, and Coomassie staining. (**D**) Covalent reactivity of non-lytic alanine constructs of D-NA-NOXA SAHB-15 with HA-BFL-1ΔC C4S/C19S expressed in 293T cells, as detected by the shift in HA-BFL-1 molecular weight following cell treatment with NOXA SAHBs (20 μM) for 8 hr, lysate preparation, reducing and denaturing gel electrophoresis, and anti-HA western analysis.

Figure 3.4 (Continued)

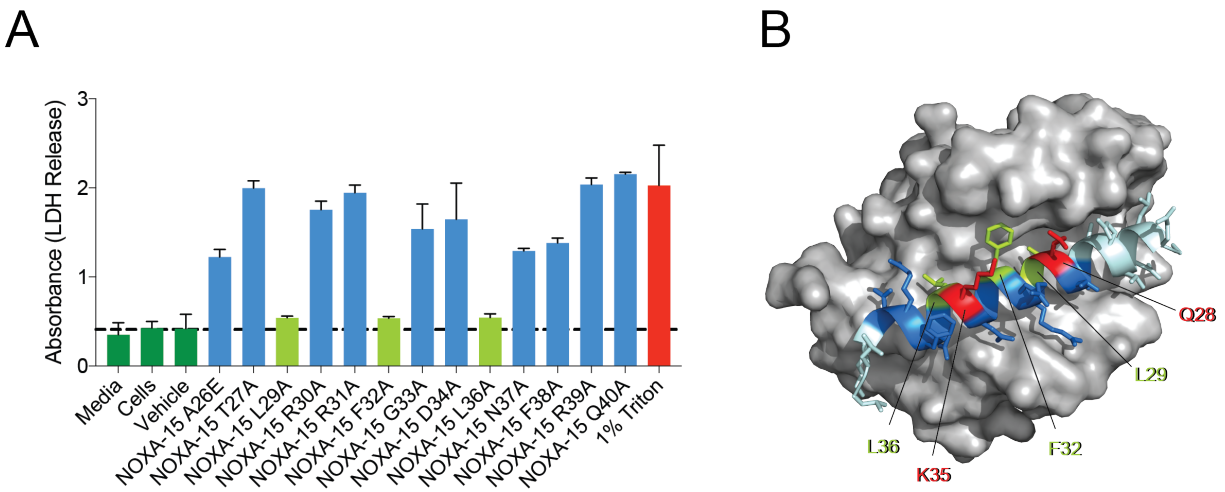

Figure 3.5 *Site-specific reduction of peptide positive charge as an alternative strategy to eliminating membrane lysis by covalent NOXA SAHBs.*

(**A**) LDH release from A375P cells upon treatment with Arg to Glu point mutants of D-NA-NOXA SAHB-15 (40 μM peptide, 30 min). Data are mean ± SD for experiments performed in triplicate. (**B**) Structure of the NOXA BH3/BFL-1ΔC complex (PDB ID 3MQP), highlighting the (*i, i+7*) staple position #15 (red), and the Arg to Glu point mutants (green) that eliminated cellular lysis. (**C**) Covalent reactivity of Arg to Glu point mutants of D-NA-NOXA SAHB-15 with C55 of BFL-1ΔC C4S/C19S, as detected by the shift in BFL-1 molecular weight following peptide/protein incubation, reducing and denaturing gel electrophoresis, and Coomassie staining. (**D**) Covalent reactivity of non-lytic Arg to Glu point mutant constructs of D-NA-NOXA SAHB-15 with HA-BFL-1ΔC C4S/C19S expressed in 293T cells, as detected by the shift in HA-BFL-1 molecular weight following cell treatment with NOXA SAHBs (20 μM) for 8 hr, lysate preparation, reducing and denaturing gel electrophoresis, and anti-HA western analysis.

Figure 3.5 (Continued)

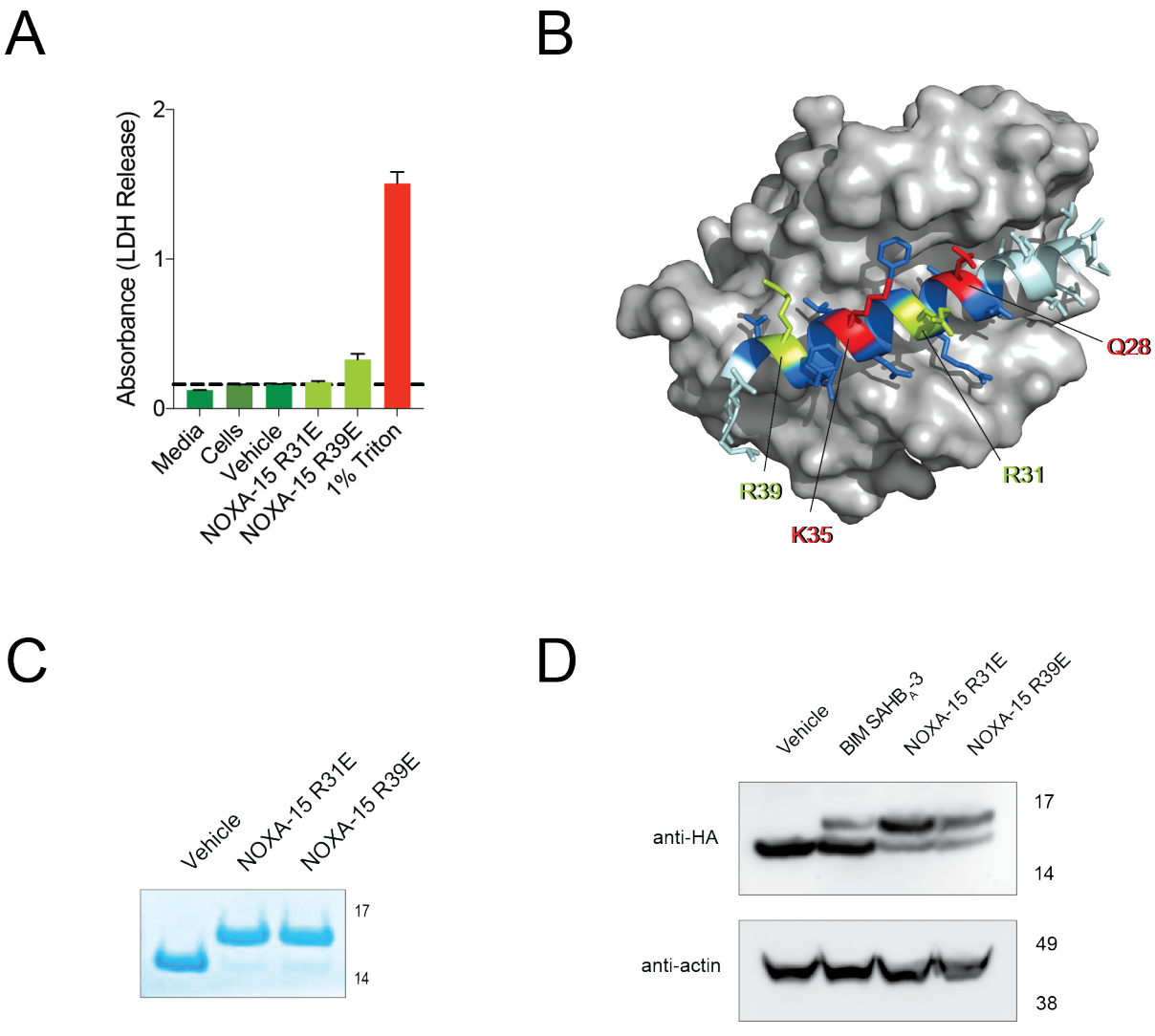

contrast, the F32A, L36A, R31E, and R39E mutants of D-NA-NOXA SAHB-15 achieved high level BFL-1 crosslinking that exceeded the performance of our previous lead compound, BIM $SAHB_A$-3, with D-NA-NOXA SAHB-15 F32A and D-NA-NOXA SAHB-15 R31E emerging as the most reactive constructs (**Figures 3.4D and 3.5D**). Thus, by reducing the hydrophobicity or overall positive charge of D-NA-NOXA SAHB-15, we effectively eliminated membrane lytic activity and achieved superior covalent targeting of BFL-1 in a cellular context.

Selectivity of Lead D-NA-NOXA SAHB-15 Peptides

Having generated lead cysteine-reactive NOXA SAHB constructs with an optimal staple location and non-lytic intracellular BFL-1 targeting activity, we next sought to assess their anti-apoptotic protein selectivity. We compared the competitive binding activity of C-terminally biotinylated D-NA-NOXA SAHB-15 F32A and R31E constructs, with and without the N-terminal D-nipecotic acid acrylamide (D-NA), in a 1:1:1 mixture of recombinant MCL-1ΔNΔC, BCL-X_LΔC, and BFL-1ΔC (all of which contain cysteines) by streptavidin pull-down assay. The Ac-NOXA SAHB-15 and D-NA-NOXA SAHB-15 peptides showed no interaction with BCL-X_L, little to no interaction with MCL-1, and robust crosslinking (input lanes) and pull-down of BFL-1 for the D-NA-derivatized NOXA SAHB-15 peptides only (**Figures 3.6A and 3.6B**). In the context of A375P cellular lysates, we observed enhanced native BFL-1 pull down by the cysteine-reactive NOXA SAHB-15 peptides as compared to the acetylated constructs, highlighting the benefit of covalent BFL-1 reactivity. We also detected a similar level of residual non-covalent

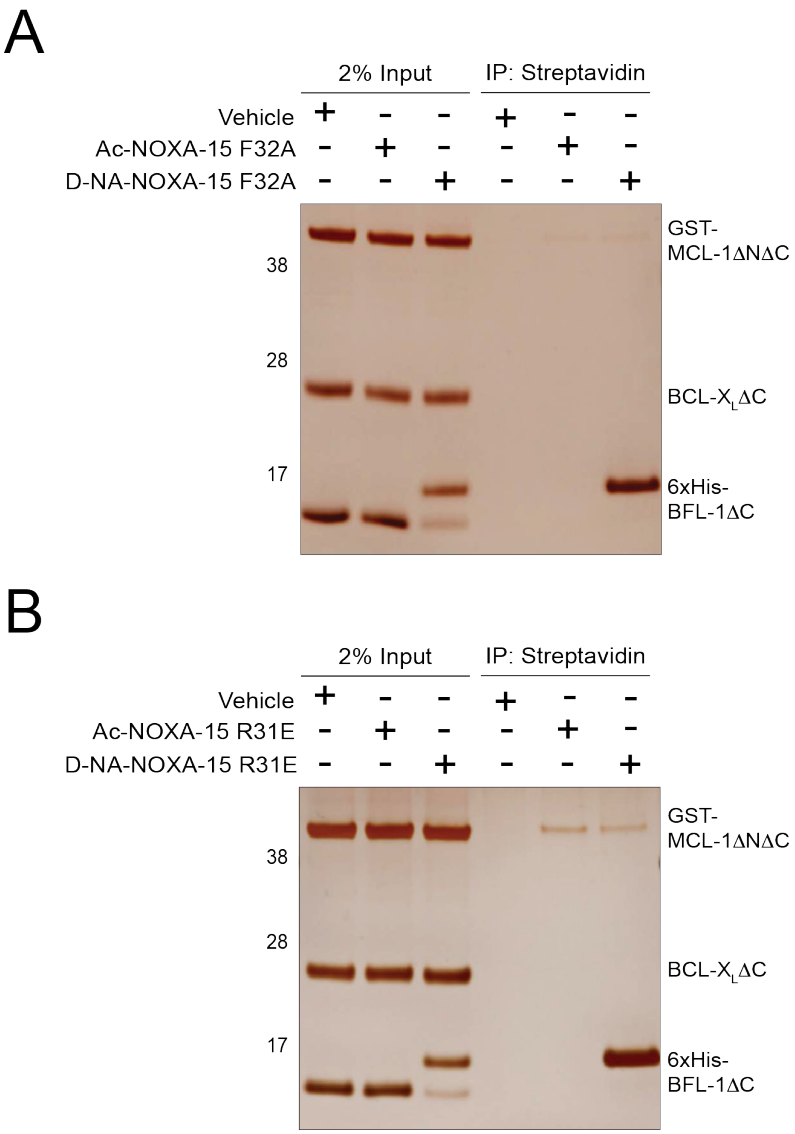

Figure 3.6 *The cysteine-reactive moiety of NOXA SAHB constructs enhances BFL-1 targeting in a mixture of recombinant anti-apoptotic proteins.*

(**A-B**) Incubation of C-terminally biotinylated NOXA SAHB-15 F32A (**A**) and NOXA SAHB-15 R31E (**B**) peptides bearing a D-NA or acetyl N-terminal caps with a mixture of recombinant MCL-1, BCL-X_L, and BFL-1 proteins demonstrates robust and selective covalent interaction of D-NA-NOXA SAHBs with BFL-1, as detected by silver stain of electrophoresed streptavidin pulldowns. No interaction between NOXA SAHBs and BCL-X_L, and little to no engagement of MCL-1, was observed.

interaction with native MCL-1 for both the Ac- and D-NA derivatized constructs (**Figures 3.7A and 3.7B**), which we sought to characterize further.

Since disruption of inhibitory heterodimeric complexes of anti-apoptotic and pro-apoptotic members underlies the functional activity of anti-apoptotic inhibitors[18], we compared the activity of Ac- and D-NA-derivatized NOXA SAHB-15 peptides in dissociating the complexes between pro-apoptotic tBID and anti-apoptotic HA-BFL-1 or FLAG-MCL-1, as assessed by co-immunoprecipitation and western analyses. D-NA-NOXA SAHB-15 F32A and R31E peptides effectively converted HA-BFL-1 to the crosslinked species, resulting in a marked decrease in tBID/HA-BFL-1 co-precipitation, whereas the corresponding acetylated constructs had no such effect (**Figures 3.8A and 3.8B**). Whereas we observed little to no non-covalent interaction between the NOXA SAHB-15 F32A and R31E constructs and recombinant MCL-1 protein (**Figure 3.6A and 3.6B**), and residual non-covalent interaction with native MCL-1 protein (**Figure 3.7A and 3.7B**), we found that neither the Ac- nor D-NA-derivatized NOXA SAHB-15 peptides were capable of dissociating the complex between tBID and FLAG-MCL-1 (**Figure 3.8C and 3.8D**). This result stands in contrast to the capacity of cysteine-reactive BIM $SAHB_A$-3 to disrupt both the tBID/HA-BFL-1 and tBID/FLAG-MCL-1 complexes by covalent and non-covalent targeting, respectively[11]. Thus, the novel D-NA-NOXA SAHB-15 compositions display a more precise BFL-1-selective functionality with respect to dissociating inhibitory anti-apoptotic complexes, which is the requisite pharmacologic feature of therapeutic inhibitors.

To verify this finding at the biochemical level, we conducted competitive fluorescence polarization binding analyses, comparing the ability of Ac- and D-NA-

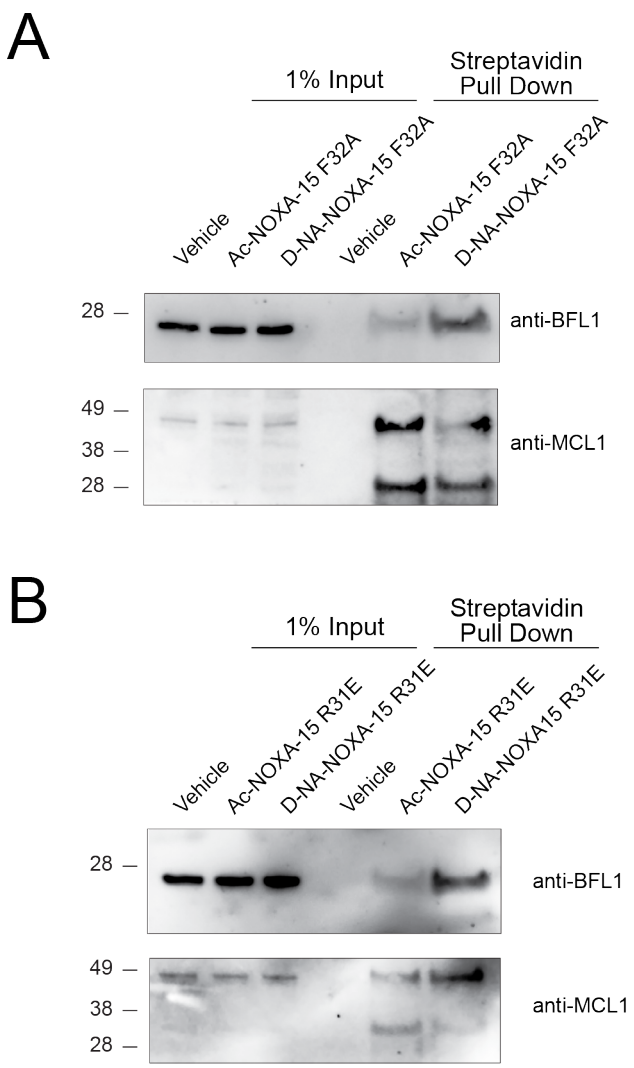

Figure 3.7 *Enhanced BFL-1 targeting in cell lysates upon incorporation of a cysteine-reactive moiety into NOXA SAHBs.*

(**A-B**) Cysteine-reactive NOXA SAHB-15 F32A (**A**) and NOXA SAHB-15 R31E (**B**) peptides display enhanced targeting of native BFL-1 compared to the corresponding acetylated derivatives, as assessed by streptavidin pulldown of treated A375P lysates and BFL-1 western analysis of electrophoresed eluates. Residual non-covalent interaction with MCL-1 is observed for both sets of NOXA SAHB-15 mutant constructs, as assessed by MCL-1 western analysis.

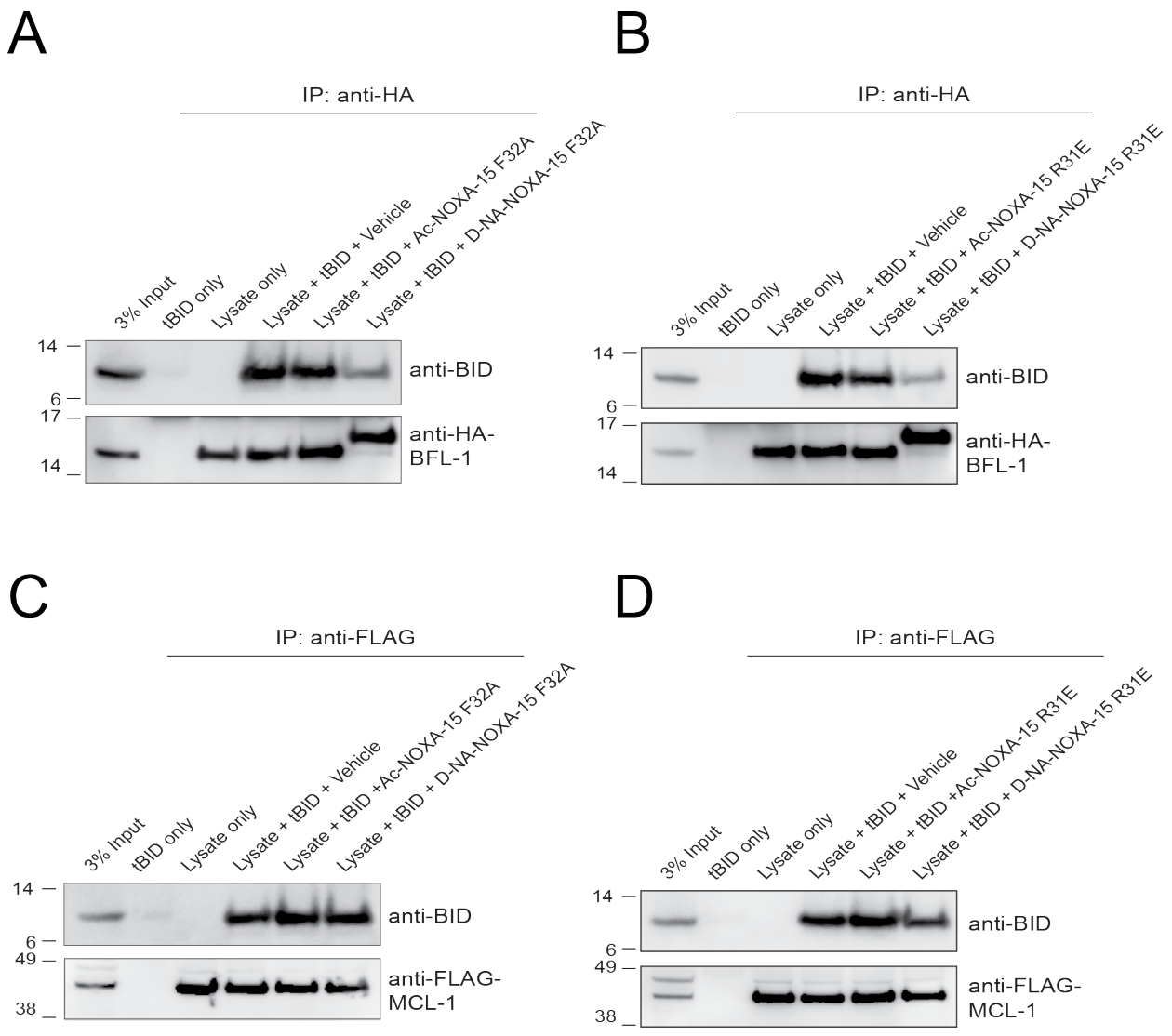

Figure 3.8 *Cysteine-reactive NOXA SAHBs selectively compete with tBID for BFL-1 but not MCL-1 interaction.*

(**A-D**) Cysteine-reactive, but not the acetylated, NOXA SAHB-15 F32A (**A**) and NOXA SAHB-15 R31E (**B**) peptides effectively targeted and dissociated the tBID/HA-BFL-1 complex and achieved robust covalent conjugation, whereas none of the NOXA SAHB-15 constructs dissociated the tBID/FLAG-MCL-1 complex (**C-D**).

derivatized NOXA SAHB-15 R31E peptides to disrupt anti-apoptotic interactions with the pro-apoptotic BID BH3 domain. Whereas Ac-NOXA SAHB-15 R31E showed essentially no capacity to compete with FITC-BID BH3 for BFL-1ΔC C4S/C19S interaction, the corresponding cysteine-reactive analog demonstrated dose-responsive and ultimately complete disruption of the complex (**Figure 3.9A**). Importantly, C55S mutagenesis of BFL-1 abrogated the competitive binding activity of D-NA-NOXA SAHB-15 R31E (**Figure 3.9B**). The corresponding Ac- and D-NA NOXA SAHB-15 R31E competition experiments using MCL-1 and BCL-X_L, anti-apoptotic proteins that contain cysteine residues but not in their BH3-binding grooves, showed little to no effect, respectively (**Figures 3.9C and 3.9D**). These data further confirmed that D-NA NOXA SAHB-15 peptides are especially effective at covalent targeting of BFL-1 and are finely tuned to selectively target the inhibitory complexes of BFL-1. Interestingly, competitive binding experiments performed with our original NOXA SAHB peptides of longer length (aa 19-43)[11] demonstrated significant non-covalent targeting of MCL-1 (**Figure 3.10**), indicating that shortening the NOXA SAHB-15 sequence contributed to narrowing its competitive binding spectrum to BFL-1.

Covalent Targeting of BFL-1 Synergizes with ATM Inhibition in AML

Cancer cells typically rely on the expression of one or more anti-apoptotic BCL-2 proteins to prevent mitochondrial apoptosis. To determine which cancers may be especially susceptible to targeted-inhibition of BFL-1, we queried the Dependency Map cancer cell line dependency database generated by screening the Avana CRISPR-Cas9 genome-scale library[19] and identified a spectrum of BFL-1 dependencies across human

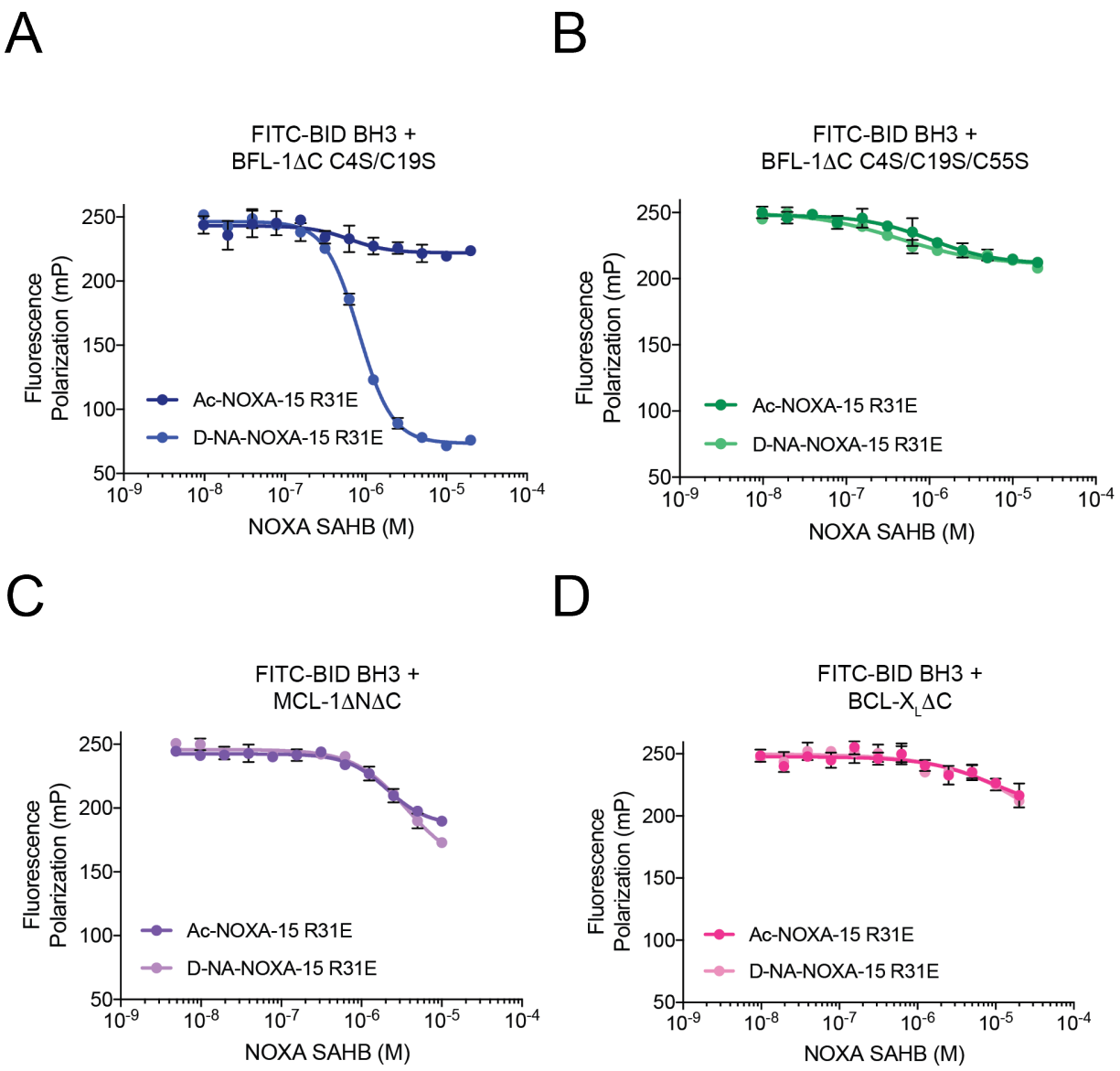

Figure 3.9 *A competitive fluorescence polarization binding assay confirmed selectivity of a cysteine-reactive NOXA SAHB for BFL-1.*

(**A-D**) Fluorescence polarization assays evaluating the capacity of D-NA- and Ac-NOXA SAHB-15 R31E peptides to compete with FITC-BID BH3 for interaction with BFL-1ΔC C4S/C19S (**A**), BFL-1ΔC C4S/C19S/C55S (**B**), MCL-1ΔNΔC (**C**), and BCL-X_LΔC (**D**). Data are mean ± SD for experiments performed in triplicate.

A

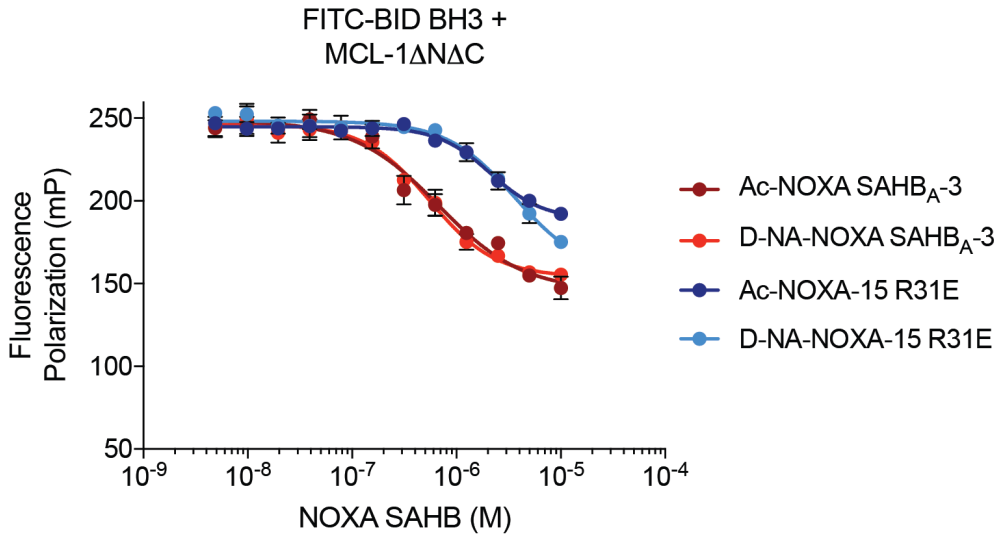

B

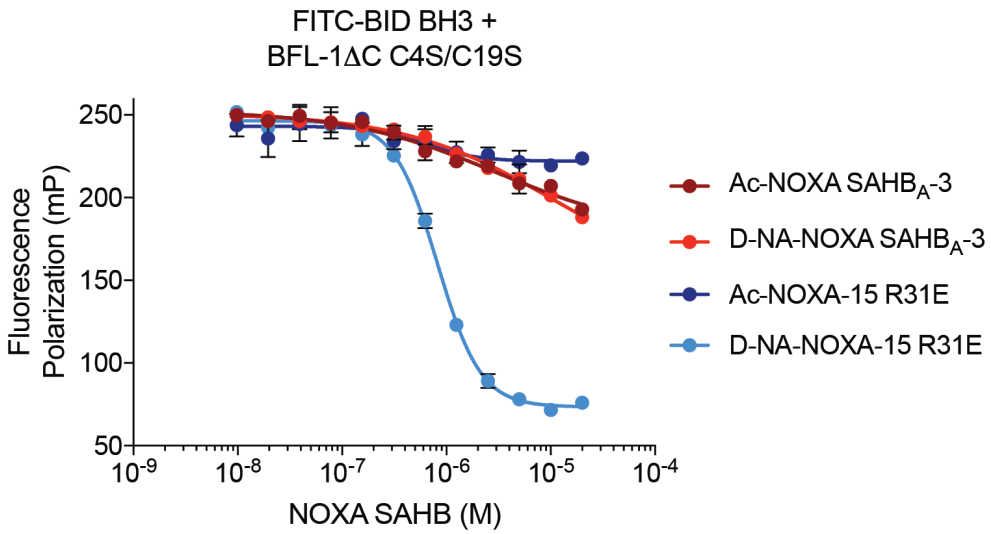

Figure 3.10 *Competitive BFL-1 and MCL-1 binding selectivities of D-NA-NOXA SAHBs*. (**A-B**) Comparative competitive binding activities of Ac- and D-NA-derivatized NOXA SAHB variants for the interaction between FITC-BID BH3 and BFL-1ΔC C4S/C19S (**A**) or MCL-1ΔNΔC (**B**), as assessed by fluorescence polarization assay. Data are mean ± SD for experiments performed in triplicate.

AML cell lines (**Figure 3.11A**). Cell lines with positive Z-score values exhibit little-to-no dependency on BFL-1 (e.g. MV4-11), whereas progressively negative Z-scores (especially < -2) reflect increasing dependency on BFL-1 (e.g. U937). Because resistant cancer cells harness multiple signaling pathways to reinforce their immortality, we further evaluated co-dependencies of BFL-1 in AML. Unexpectedly, the Ataxia Telangiectasia mutated (ATM) serine/threonine kinase, which is activated by DNA double-strand breaks, emerged as the most highly BFL-1 co-dependent gene in AML (**Figure 3.11B, Table 3.1**). The availability of small molecule ATM inhibitors such as AZD0156, which is currently being tested in Phase 1 clinical trials for patients with advanced malignancies (NCT02588105), enabled us to examine whether the genetic findings of BFL-1 dependency and ATM co-dependency in AML could inform an effective combination treatment.

We treated the U937 AML cell line that demonstrated the strongest BFL-1 dependency score with serial dilutions of D-NA-NOXA SAHB-15 R31E and AZD0156[20], as single agents and in combination, and performed CalcuSyn analysis[21] to monitor for synergy. Whereas each compound demonstrated dose-responsive, moderate impairment of U937 cell viability, the combination was strongly synergistic, as reflected by a log(CI) value of < -0.22 (**Figures 3.12A and 3.12B**). Monitoring caspase-3/7 activation over time likewise revealed prominent synergistic activity of the D-NA-NOXA SAHB-15 R31E/AZD0156 combination (**Figure 3.12C**). To confirm that AZD0156 was effectively targeting ATM at the applied doses, we treated U937 cells with the ATM inhibitor for 2 hr and monitored ATM auto-phosphorylation at Ser1981 and

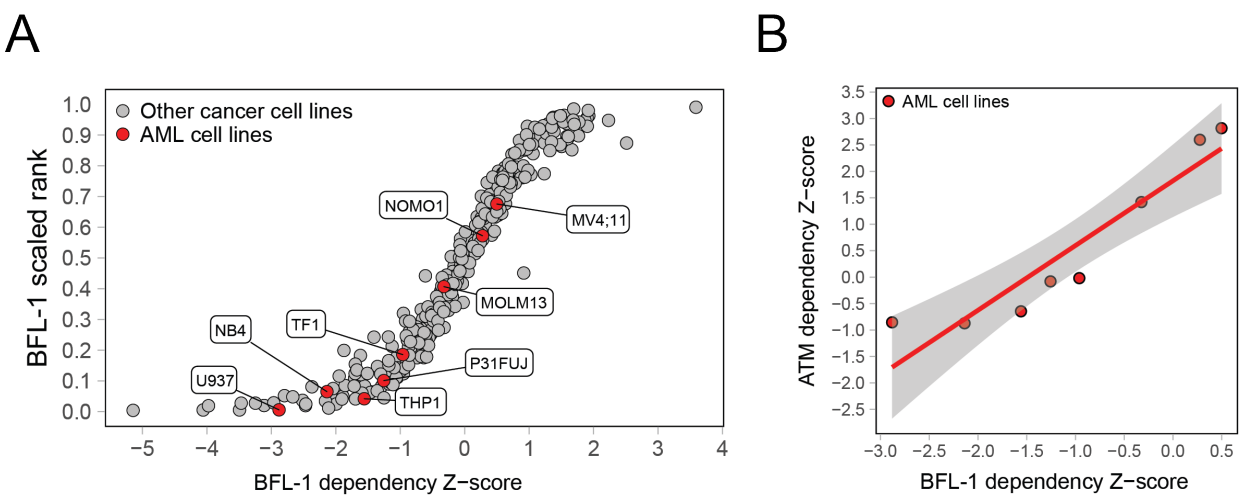

Figure 3.11 *CRISPR-Cas9 screening reveals oncogenic dependencies in human AML cell lines.*

(**A**) A scatter plot demonstrates the variable, relative dependency on BFL-1 among cancer cell lines subjected to genome-scale CRISPR-Cas9 screening. Among the human AML cell lines (red), U937 and MV4;11 cells demonstrate the highest and lowest BFL-1 dependency scores, respectively. For each cell line, the gene's dependency rank and dependency score are plotted on the y and x axis, respectively. (**B**) A plot depicting the strong correlation between BFL-1 and ATM dependencies in the human AML cell lines (Pearson and Spearman correlation coefficients of 0.94 and 0.98, respectively).

Table 3.1 *BFL-1 co-dependencies in human AML cell lines.*

Pearson and Spearman correlations for BFL-1 co-dependencies in AML cell lines subjected to a genome-scale CRISPR-Cas9 screen and identified based on the following criteria: (1) gene scored as a potential dependency in at least 2 AML cell lines (score < -0.1), (2) gene is expressed in at least 2 AML cell lines (TPM >1), (3) gene is not predicted to be a pan-lethal gene, and (4) Pearson and Spearman correlations are both > 0.9.

	Pearson Correlation Coefficient	Spearman Correlation Coefficient
BFL1	1	1
DCTPP1	0.94110259	0.928571429
ATM	0.937773368	0.976190476
GEN1	0.936089024	0.904761905
ASCC1	0.934906261	0.928571429
NSUN6	0.916185332	0.904761905
FBXO42	0.911441405	0.904761905
DYNC2LI1	0.907170948	0.904761905
JRKL	0.904267905	0.928571429
C3orf62	0.902864788	0.904761905

Figure 3.12 *BFL-1-dependent cytotoxicity of cysteine-reactive NOXA SAHB-15 mutants and synergy with ATM inhibition in human AML cells.*

(**A-F**) Cell viability, Calcusyn dose-effect plots, and caspase-3/7 activation for U937 (**A-C**) and MV4;11 (**D-F**) cells treated with D-NA-NOXA SAHB-15 R31E, ATM inhibitor AZD0156, or the combination at the indicated doses. Data are mean ± SD for experiments performed in triplicate, normalized to vehicle control (0.4% DMSO), and repeated twice with independent cell cultures with similar results. CI, combination index. *, $p<0.01$ by two-tailed Student's t test.

Figure 3.12 (Continued)

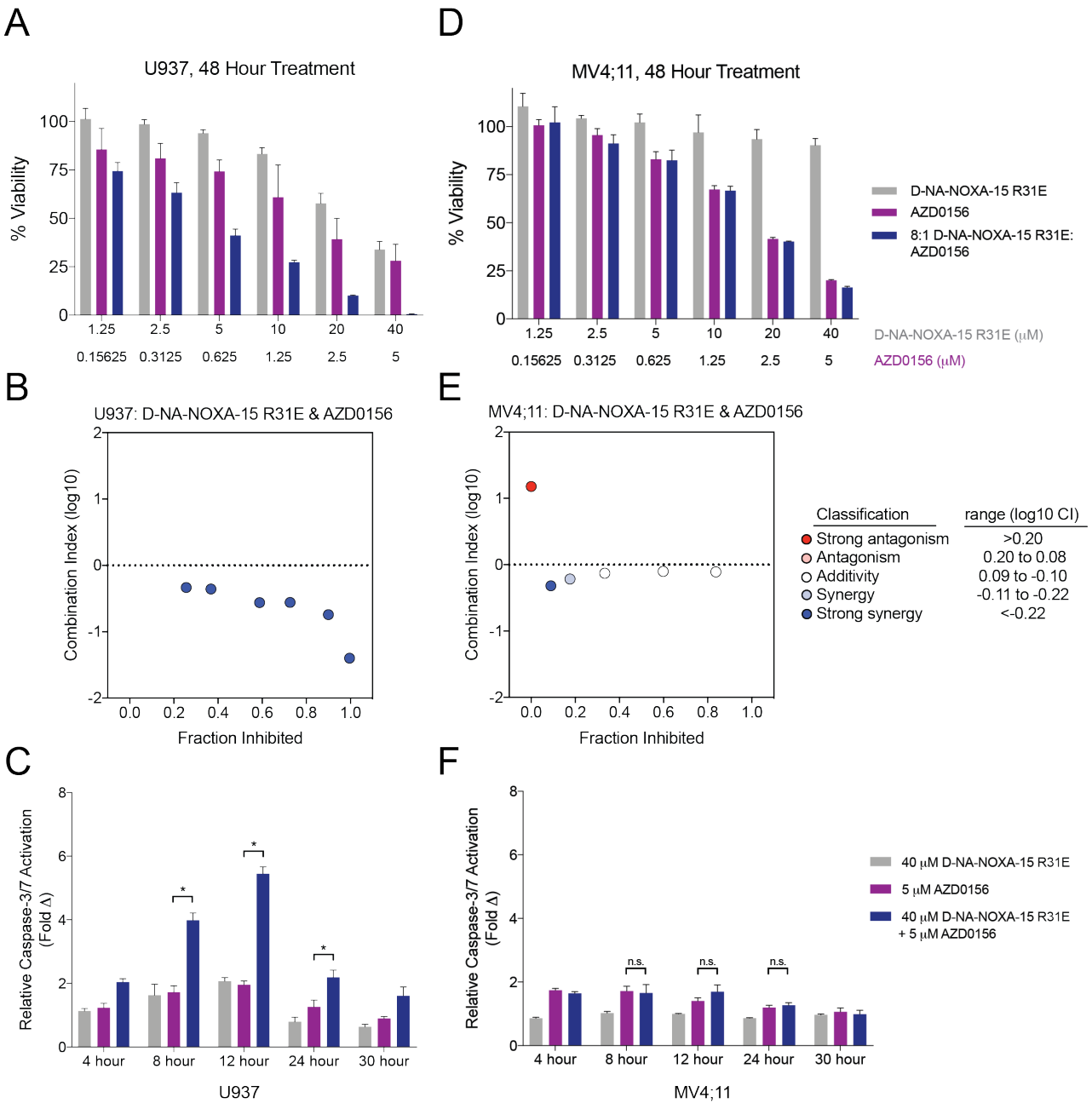

downstream CHK2 phosphorylation at Ser33/35 by western blot. Indeed, we observed dose-responsive inhibition of S1981 auto-phosphorylation, which was otherwise constitutively elevated in U937 cells, and potent blockade of CHK2 phosphorylation even at the lowest treatment dose (**Figure 3.13**). As a further measure of the specificity of observed BFL-1/ATM inhibitory synergy, we repeated the analysis using the MV4;11 AML cell line, which showed no evidence of BFL-1 dependency in the CRISPR-Cas9 screen (**Figure 3.11A**). In this cellular context, D-NA-NOXA SAHB-15 R31E had no cytotoxic activity, AZD0156 impaired viability with similar potency as observed in U937 cells, and no synergistic activity was evident for the combination in viability or caspase-3/7 activation assays (**Figures 3.12D, 3.12E, and 3.12F**). Thus, the selective cytotoxicity of D-NA-NOXA SAHB-15 R31E in U937 vs. MV4;11 AML cells corresponds to the differential BFL-1 dependencies observed by CRISPR-Cas9 screen (**Figure 3.11A, 3.12A and 3.12B**). In addition, the genetic co-dependency of BFL-1 and ATM in AML informed a new, synergistic combination treatment.

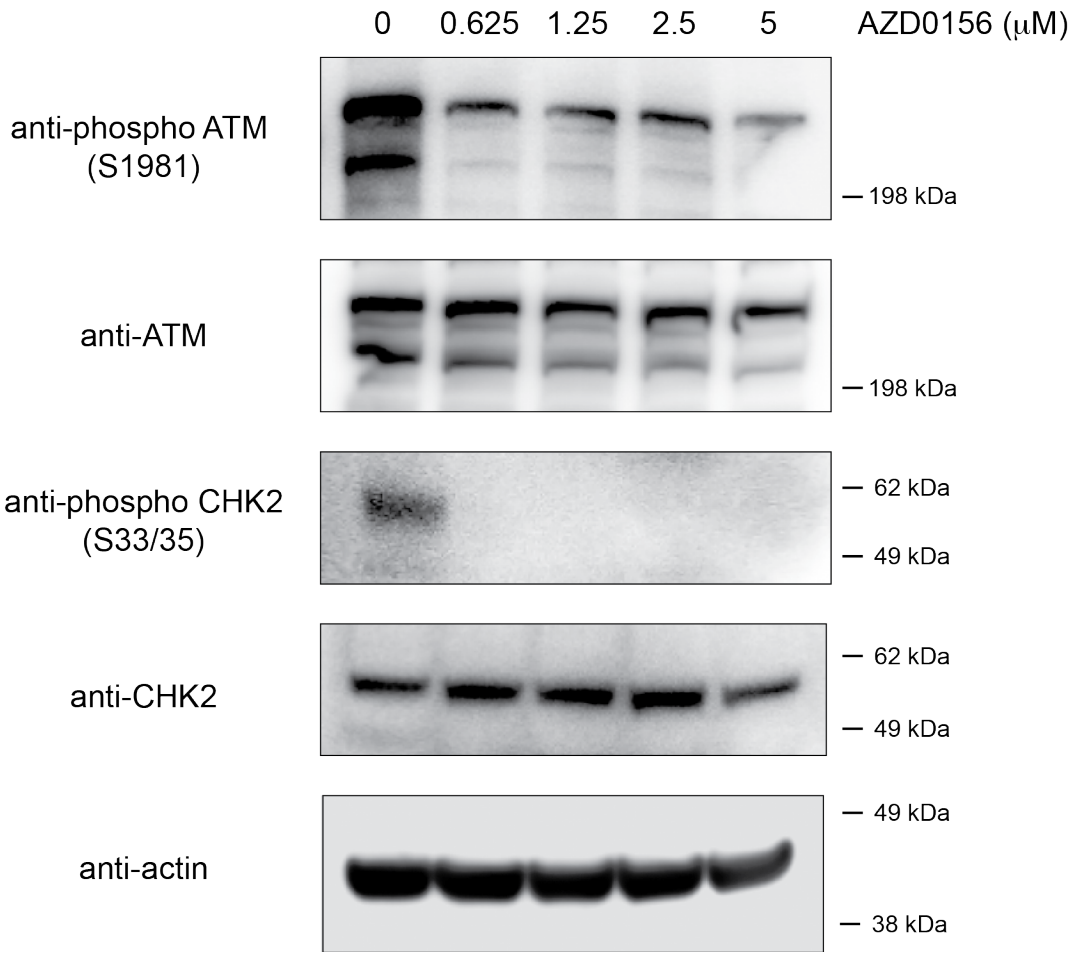

Figure 3.13 *AZD0156 inhibition of ATM kinase activity in U937 cells.*

U937 cells were treated with the indicated doses of AZD0156 for 2 hr and the phosphorylation status of ATM S1981 and CHK2 S33/35 monitored by western blot.

DISCUSSION

The therapeutic efficacy of targeted inhibition of BCL-2 by venetoclax in human cancer has triggered renewed interest in pharmacologic modulation of BCL-2 family proteins for clinical benefit in cancer and potentially other diseases of pathologic cell survival. Whereas venetoclax is now FDA-approved for 17p-deleted CLL and a series of small molecule MCL-1 inhibitors have recently entered Phase 1 testing, BFL-1 remains undrugged, motivating our efforts to develop selective and multimodal compounds that include BFL-1 in their binding spectrum. The principle of small molecule discovery for targeted inhibition of BCL-2 family proteins is based on mimicry of the BH3 α-helix[6,22]. We have taken the alternative approach of harnessing the natural binding spectra and biological activities of native BH3 domain α-helices to advance modulators of individual, subsets, and all BCL-2 family proteins[7,11,23,24]. That is, we use the natural amino acid composition of diverse BH3 sequences but insert all-hydrocarbon, structurally-stabilizing staples to remedy the traditional liabilities of peptide therapeutics, including loss of bioactive shape, proteolytic instability, and limited cell penetrance[25]. Our analyses of the biophysical, structural, and biological properties of stapled peptide libraries have revealed several guiding principles in designing constructs that optimally recapitulate bioactive structure, avoid the membrane-lytic risk factor associated with select amphipathic peptides, and achieve on-mechanism activity in cells and tissues[17,25]. Among the benefits of designing stapled peptides for targeting protein-protein interactions is the capacity to arrive at a lead peptide composition relatively rapidly based on harnessing natural peptide sequences as the synthetic starting point. The

clinical potential of stapled peptides as a new drug modality is currently being evaluated in Phase 1 and 2 clinical trials, with encouraging early results[10].

Because cancer cells rarely rely on one survival factor to achieve immortality, the benefits of targeting individual anti-apoptotic proteins could be fleeting, as evidenced by the capacity of cancer cells to rewire their anti-apoptotic dependence on BCL-2 proteins that lie outside the binding spectrum of selective molecular inhibitors[26]. However, the concern that anti-apoptotic inhibitors with broader targeting spectra could increase the potential for unwanted side-effects, such as the on-mechanism thrombocytopenia observed for the dual BCL-2/BCL-X_L inhibitor ABT-737[27], has led to prioritization of selective anti-apoptotic inhibitors[6,24,28]. In seeking a strategy for precision-targeting of BFL-1, we discovered a unique cysteine in its BH3-binding pocket, allowing for selective covalent targeting of BFL-1 by stapled BH3 peptides bearing an acrylamide moiety[11]. Whereas our lead compound BIM $SAHB_A$-3 manifested dual features of covalent BFL-1 and non-covalent MCL-1 inhibition, resulting in apoptosis induction of BFL-1 and MCL-1 co-expressing melanoma cells (Chapter 2, **Figure 2.11** and **Figure 2.12**), here we sought to tune the binding specificity to BFL-1 only based on optimizing the design of NOXA BH3-based stapled peptides. To achieve this goal, we synthesized a staple scanning library of a NOXA BH3 template that was shortened to emphasize the predominant α-helical binding interface. Then, our peptide characterization workflow identified a lead construct based on optimal biochemical reactivity with BFL-1 C55, but also key liabilities, including lack of cell penetrance and membrane-lytic activity. We effectively overcame these drawbacks by alanine scanning mutagenesis, which revealed an opportunity to maximize cell uptake and abrogate cell membrane lysis by

lowering the relative hydrophobicity of specific amino acid positions. Alternatively, reducing the overall peptide positive charge by converting select arginine residues to glutamic acid residues, achieved the same goal. Ultimately, we developed cysteine-reactive NOXA SAHBs capable of robust covalent reaction with BFL-1, cell penetrance in the absence of membrane lysis, selective disruption of inhibitory BFL-1 complexes, and specific, BFL-1-dependent cytotoxicity in human AML cells.

Although cancer cells can indeed demonstrate preferred dependencies on individual anti-apoptotic proteins[29,30], the potential for resistance based on expression of alternate BCL-2 proteins motivated us to explore BFL-1 co-dependencies in human cancer. Analysis of a cancer cell dependency database derived from CRISPR/Cas9 screening[19] revealed both a spectrum of BFL-1 dependency in human AML and a striking and unexpected co-dependency on the ATM kinase, which can promote cancer cell survival by mitigating DNA replicative stress[31,32]. We tested the fidelity of these genetic results against our precision BFL-1 inhibitor and the clinical-grade ATM kinase inhibitor AZD0156, both as single agents and in combination. We found that D-NA-NOXA SAHB R31E was selectively cytotoxic as a single agent, and synergized with ATM inhibition, exclusively in the context of BFL-1 dependence. Taken together, our stapled peptide design and characterization workflow provide novel compositions with tailored BFL-1 targeting capability and inform an unanticipated combination treatment for BFL-1-dependent human AML.

REFERENCES

1. Sattler, M. *et al.* Structure of Bcl-xL-Bak Peptide Complex: Recognition Between Regulators of Apoptosis. *Science* **275,** 983–986 (1997).

2. Llambi, F. *et al.* A unified model of mammalian BCL-2 protein family interactions at the mitochondria. *Molecular Cell* **44,** 517–531 (2011).

3. Letai, A. *et al.* Distinct BH3 domains either sensitize or activate mitochondrial apoptosis, serving as prototype cancer therapeutics. *Cancer Cell* **2,** 183–192 (2002).

4. Davids, M. S. *et al.* Phase I First-in-Human Study of Venetoclax in Patients With Relapsed or Refractory Non-Hodgkin Lymphoma. *J. Clin. Oncol.* **35,** 826–833 (2017).

5. Roberts, A. W. *et al.* Targeting BCL2 with Venetoclax in Relapsed Chronic Lymphocytic Leukemia. *N Engl J Med* **374,** 311–322 (2016).

6. Kotschy, A. *et al.* The MCL1 inhibitor S63845 is tolerable and effective in diverse cancer models. *Nature* 1–20 (2016).

7. Walensky, L. D. *et al.* Activation of apoptosis in vivo by a hydrocarbon-stapled BH3 helix. *Science* **305,** 1466–1470 (2004).

8. Bernal, F. *et al.* A Stapled p53 Helix Overcomes HDMX-Mediated Suppression of p53. *Cancer Cell* **18,** 411–422 (2010).

9. Chang, Y. S. *et al.* Stapled α-helical peptide drug development: a potent dual inhibitor of MDM2 and MDMX for p53-dependent cancer therapy. *Proc. Natl. Acad. Sci. U.S.A.* **110,** E3445–54 (2013).

10. Meric-Bernstam, F. *et al.* Phase I trial of a novel stapled peptide ALRN-6924 disrupting MDMX- and MDM2-mediated inhibition of WT p53 in patients with solid tumors and lymphomas. *JCO* **35,** 2505–2505 (2017).

11. Huhn, A. J., Guerra, R. M., Harvey, E. P., Bird, G. H. & Walensky, L. D. Selective Covalent Targeting of Anti-Apoptotic BFL-1 by Cysteine-Reactive Stapled Peptide Inhibitors. *Cell Chem Biol* **23,** 1123–1134 (2016).

12. Harvey, E. P. *et al.* Crystal Structures of Anti-apoptotic BFL-1 and Its Complex with a Covalent Stapled Peptide Inhibitor. *Structure* **26,** 153–160.e4 (2018).

13. Bird, G. H., Bernal, F., Pitter, K. & Walensky, L. D. Synthesis and biophysical characterization of stabilized alpha-helices of BCL-2 domains. *Meth. Enzymol.* **446,** 369–386 (2008).

14. Bird, G. H., Crannell, W. C. & Walensky, L. D. Chemical synthesis of hydrocarbon-stapled peptides for protein interaction research and therapeutic targeting. *Curr Protoc Chem Biol* **3,** 99–117 (2011).

15. Pitter, K., Bernal, F., LaBelle, J. & Walensky, L. D. Dissection of the BCL-2 family signaling network with stabilized alpha-helices of BCL-2 domains. *Meth. Enzymol.* **446,** 387–408 (2008).

16. Meyers, R. M. *et al.* Computational correction of copy-number effect improves specificity of CRISPR-Cas9 essentiality screens in cancer cells. *bioRxiv* 1–15 (2017).

17. Bird, G. H. *et al.* Biophysical determinants for cellular uptake of hydrocarbon-stapled peptide helices. *Nature Chemical Biology* **12,** 845–852 (2016).

18. Certo, M. *et al.* Mitochondria primed by death signals determine cellular addiction to antiapoptotic BCL-2 family members. *Cancer Cell* **9,** 351–365 (2006).

19. Tsherniak, A. *et al.* Defining a Cancer Dependency Map. *Cell* **170,** 564–570.e16 (2017).

20. Degorce, S. L. *et al.* Discovery of Novel 3-Quinoline Carboxamides as Potent, Selective, and Orally Bioavailable Inhibitors of Ataxia Telangiectasia Mutated (ATM) Kinase. *J. Med. Chem.* **59,** 6281–6292 (2016).

21. Chou, T. C. & Talalay, P. Quantitative analysis of dose-effect relationships: the combined effects of multiple drugs or enzyme inhibitors. *Adv. Enzyme Regul.* **22,** 27–55 (1984).

22. Oltersdorf, T. *et al.* An inhibitor of Bcl-2 family proteins induces regression of solid tumours. *Nature* **435,** 677–681 (2005).

23. LaBelle, J. L. *et al.* A stapled BIM peptide overcomes apoptotic resistance in hematologic cancers. *J. Clin. Invest.* **122,** 2018–2031 (2012).

24. Stewart, M. L., Fire, E., Keating, A. E. & Walensky, L. D. The MCL-1 BH3 helix is an exclusive MCL-1 inhibitor and apoptosis sensitizer. *Nature Chemical Biology* **6,** 595–601 (2010).

25. Walensky, L. D. & Bird, G. H. Hydrocarbon-Stapled Peptides: Principles, Practice, and Progress. *J. Med. Chem.* **57,** 6275–6288 (2014).

26. Yecies, D., Carlson, N. E., Deng, J. & Letai, A. Acquired resistance to ABT-737 in lymphoma cells that up-regulate MCL-1 and BFL-1. *Blood* **115,** 3304–3313 (2010).

27. Mason, K. D. *et al.* Programmed anuclear cell death delimits platelet life span. *Cell* **128,** 1173–1186 (2007).

28. Souers, A. J. *et al.* ABT-199, a potent and selective BCL-2 inhibitor, achieves antitumor activity while sparing platelets. *Nat Med* **19,** 202–208 (2013).

29. Anderson, M. A. *et al.* The BCL2 selective inhibitor venetoclax induces rapid onset apoptosis of CLL cells in patients via a TP53-independent mechanism. *Blood* **127,** 3215–3224 (2016).

30. Haq, R., Yokoyama, S. & Hawryluk, E. B. BCL2A1 is a lineage-specific antiapoptotic melanoma oncogene that confers resistance to BRAF inhibition. P*roc. Natl. Acad. Sci. U.S.A.* **110,** 4321-4326 (2013).

31. Morgado-Palacin, I. *et al.* Targeting the kinase activities of ATR and ATM exhibits antitumoral activity in mouse models of MLL-rearranged AML. *Sci Signal* **9,** ra91–ra91 (2016).

32. Ghelli Luserna di Rora, A., Iacobucci, I. & Martinelli, G. The cell cycle checkpoint inhibitors in the treatment of leukemias. *J Hematol Oncol* **10,** 77 (2017).

CHAPTER IV

Conclusions and Future Directions

Discussion of Results

Rationale for Covalent Stapled Peptide Inhibition of BFL-1

BFL-1 is an anti-apoptotic protein that has emerged as a contributory factor to the development, maintenance, and chemoresistance of human melanoma, lymphoma, and leukemia, yet it remains undrugged[1-4]. With the small molecule BCL-2 inhibitor venetoclax having gained FDA approval in 2016 for the treatment of 17p-deleted CLL, it remains a high priority goal to develop inhibitors of individual members or subsets of BCL-2 family anti-apoptotic proteins. This is particularly important because cancer cells can upregulate anti-apoptotic proteins such as BFL-1 and MCL-1 as a resistance mechanism to selective BCL-2 inhibition[2,5-7]. Here, we discovered and exploited a unique cysteine in the BH3-binding groove of BFL-1 to develop selective covalent inhibitors by combining the high-affinity non-covalent interactions of a structurally-reinforced BH3 helix with the irreversible blockade afforded by covalent reaction.

By installing an all-hydrocarbon crosslink spanning one or two helical turns of the naturally-occurring BH3 sequence, peptide stapling technology stabilizes helical structure and imparts beneficial pharmacological properties including protease resistance and cellular uptake[8]. These Stabilized Alpha-Helices of BCL-2 domains (SAHBs) are ideal tools to modulate and dissect protein-protein interaction networks involving α-helical interacting domains, including the BCL-2 family and beyond[9]. Furthermore, stapled peptides have emerged as prototype therapeutics, with the stapled p53 helix ALRN-6924 advancing to Phase 2 clinical trials for the treatment of relapsed solid and hematological cancers bearing wild-type p53 (NCT02264613)[10,11]. Since α-helices mediate numerous pathologic protein-protein interactions throughout

biology, stapled peptides represent a promising approach to targeting otherwise "undruggable" protein targets in human disease[12]. Key benefits of stapled peptides include their ability to engage large and shallow binding surfaces, mimic bioactive structures, and achieve cellular uptake, thus bridging the gap between small molecules and biologics[13].

To expand the arsenal of drug modalities for protein targeting, we combined focally-reactive warhead moieties with BCL-2 family-targeting SAHBs to create novel chimeric stapled peptides to reactivate apoptosis in BFL-1-dependent cancer. Covalent inhibition has historically been avoided in drug discovery due to safety and off-target concerns, however there has been a resurgence of interest in covalent strategies in recent years. Many commonly used drugs, such as acetaminophen and certain proton pump inhibitors, are covalent inhibitors, yet their molecular mechanisms were not uncovered until long after their clinical utility was established[14]. Traditional drug discovery platforms were designed to avoid covalent inhibitors, due to concerns about non-specific reactivity and toxic drug metabolites[15]. Nevertheless, covalent inhibitors have several advantages that specifically derive from the irreversible nature of their binding interaction, including the ability to compete with high levels of endogenous substrate, prolonged duration of action, and the potential to target shallow binding sites[15]. These attractive properties have been leveraged in recent years to develop covalent inhibitors of kinases implicated in oncogenesis. The success of this approach is exemplified by the FDA approval of such covalent inhibitors as ibrutinib to inhibit Bruton's tyrosine kinase in leukemias and lymphomas, and afatinib to target EGFR in certain non-small cell lung cancers[16,17].

While a major concern of covalent inhibitors is potential off-target reactivity, which could result in unwanted toxicity, optimized non-covalent affinity of a drug for its target can efficiently and selectively template the covalent reaction, whose efficiency is then dictated by the reactivity of the electrophile and proximity to a nucleophile on the protein surface[18]. Thus, it is possible to fine-tune the selectivity and reactivity of a covalent inhibitor by modulating its non-covalent interaction with a target and selecting an optimal electrophile. Given their large non-covalent binding surface as compared to small molecules, stapled peptides represent an ideal starting point to develop covalent inhibitors with reduced off-target reactivity. Indeed, we demonstrated that acrylamide-bearing stapled peptides target Cys55 in BFL-1 with exquisite selectivity, and display no reactivity with structurally-similar BCL-2 family proteins. What's more, we observe little to no non-specific reactivity with other members of the proteome (Chapter II).

Given the frequency with which α-helices mediate PPIs, particularly in the context of human disease, cysteine-reactive stapled peptide inhibitors represent a potentially widely applicable drug development strategy for clinically-relevant, helix-mediated PPIs whose targets contain a cysteine in or around the critical binding site. Indeed, there are many examples of native cysteines adjacent to the regulatory helix-in-groove binding surfaces of therapeutic targets, including the FAS/FADD, RASSF1C/DAXX, and tryptophanyl-tRNA synthetase homodimer interactions[19-21] (**Figure 4.1**). Additionally, acquired cysteine mutations in cancer have been exploited as covalent handles for mutant-selective drugs, increasing their selectivity for the mutant over wild-type form of the protein[22]. One notable example is $KRAS^{G12C}$, which is located in close proximity to the protein's regulatory interface with an α-helix of the

Figure 4.1 *Exemplary Helix-in-Groove Interactions Bearing Native Cysteines for Covalent Stapled Peptide Targeting.*

(**A-E**) A diversity of regulatory binding surfaces that involve α-helical ligands inserting into surface grooves contain targetable cysteines, as exemplified by the (**A**) SOS1/KRAS G12C (PDB: 1NVU), (**B**) Mediator of RNA Polymerase II transcription subunit 11/Mediator of RNA polymerase II transcription subunit 22 (PDB: 4H62), (**C**) Tryptophanyl-tRNA synthetase homodimer (PDB: 1ULH), (**D**) FAS/FADD (PDB: 3EZQ), and (**E**) RASSF1C/ DAXX (PDB: 2KZU) interactions (α-helical ligand, cyan; cysteine-proximal residue on α-helix, orange sticks; protein target, grey; cysteine on protein target, orange surface).

Figure 4.1 (Continued)

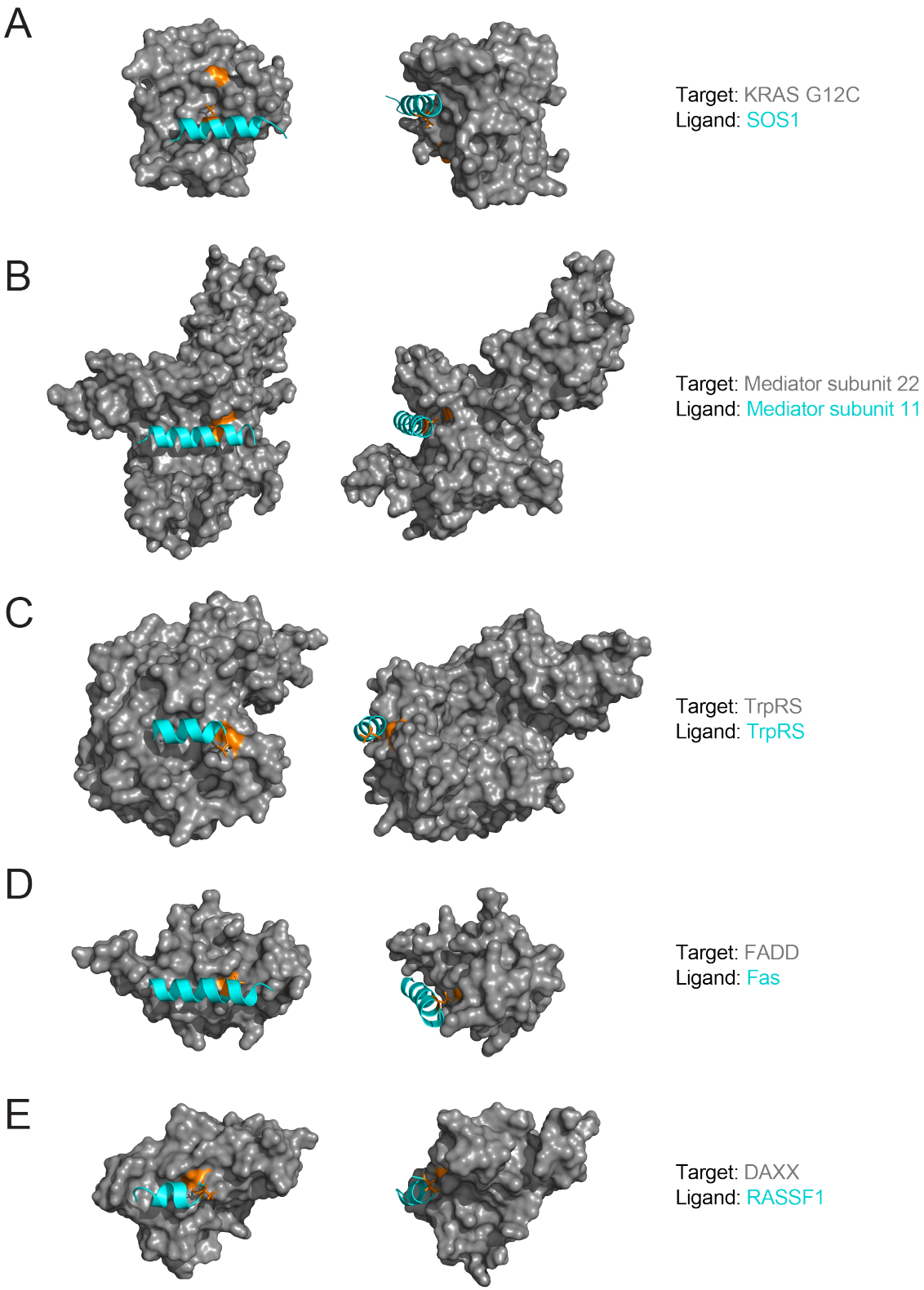

guanine-nucleotide exchange factor SOS1[23] (**Figure 4.1A**). Stapled peptides modeled after the SOS1 helix have been shown to directly bind wild-type and mutant KRAS, and inhibit nucleotide exchange and downstream signaling[24]. Given the increased interest in developing covalent inhibitors of $KRAS^{G12C}$, transforming SOS1 stapled peptides into covalent inhibitors could represent an alternative approach to neutralizing oncogenic $KRAS^{G12C}$.

Molecular Strategy for BFL-1 Targeting at Cys55

The BH3-binding groove is a highly conserved structural feature of BCL-2 family proteins, yet the unique cysteine residue in the BFL-1 hydrophobic pocket proved to be a selectivity factor and molecular handle for covalent targeting with acrylamide-bearing stapled BH3 peptides. Since our initial discovery, additional groups have pursued similar strategies to covalently target BFL-1 Cys55 with peptide inhibitors[25,26]. Though stapled peptides display therapeutic potential and are currently being evaluated in clinical trials, small molecules remain the most widely adopted drug class. The recent success of venetoclax has fueled efforts to develop small molecule inhibitors of other anti-apoptotic targets, with new MCL-1-selective compounds recently advanced to Phase 1 testing in cancer[27,28]. The mechanistic and targeting insights that derived from our covalent stapled peptide inhibitor studies suggest that BFL-1 may also be selectively targeted by small molecule covalent inhibitors. NMR-based fragment screening was effectively applied to discover small molecule inhibitors of BCL-2, BCL-X_L, and BCL-w, and later MCL-1, however the application of this methodology to develop BFL-1 inhibitors has not been reported to date[28-30]. Fluorescence polarization-

based high-throughput screening approaches have yielded compounds with only modest potency and selectivity for BFL-1[7,31]. The unique cysteine in the BH3-binding groove of BFL-1 could provide a new opportunity to address this target by covalent drug discovery.

We have adopted disulfide-fragment-based screening in an effort to identify molecular inhibitors that specifically target Cys55. This disulfide tethering-based screening methodology was pioneered by Dr. James Wells, and relies on the formation of a disulfide bond between a thiol-containing fragment and the protein target[32]. The cysteine-containing protein of interest is screened against a library of fragments under partially reducing conditions, and if any fragment has even weak affinity for the protein, binding will be stabilized by disulfide bond formation, allowing for subsequent mass spectrometry-based hit identification[32]. This strategy was successfully applied to oncogenic $KRAS^{G12C}$, and medicinal chemistry optimization of the original hits yielded drug candidates with potent *in vivo* efficacy[33-36]. Having validated covalent targeting of BFL-1 Cys55 as an effective strategy, we have undertaken a tethering screen approach to identify small molecule fragments that might similarly engage and inhibit BFL-1.

In addition to potentially identifying small molecule covalent inhibitors of BFL-1, the tethering approach could allow us to investigate the minimal essential drug size required to functionally block the BH3-binding groove of BFL-1. Indeed, significant truncation of our lead cysteine-reactive NOXA SAHB did not reduce covalent affinity or inhibitory activity (Chapter III). As another example, the Aileron stapled p53 peptide currently being tested in clinical trials, primarily engages HDMX via three critical residues at the helical surface[37]. Likewise, X-ray crystallography has shown that the

small molecule BCL-2/BCL-X_L inhibitor, ABT-737, mimics the BCL-X_L-binding of three key residues of the α-helical BAK BH3 domain[29]. Cysteine-reactive small molecules identified by a tethering-based screen for BFL-1 inhibitors could be compared to our covalent stapled peptides to provide insight into the key determinants for BFL-1 interaction. We anticipate that these ongoing efforts will inform our understanding of the molecular binding components that are sufficient for effective BFL-1 inhibition, and how target engagement is influenced by covalent reaction.

Future Directions

In vivo Efficacy Testing of Covalent Stapled Peptide Inhibitors of BFL-1

The clinical success of venetoclax has catalyzed efforts to develop inhibitors to target the spectrum of anti-apoptotic proteins, and thereby subvert apoptotic resistance in cancer. We have pursued an alternative approach to targeting these proteins by taking nature's blueprint for BCL-2 family inhibition and transforming endogenous interacting helical domains into structurally-reinforced peptides with promising pharmacological properties. In addition to providing proof-of-concept for selective covalent targeting of a BCL-2 family protein using chimeric stapled peptides, our studies provide a springboard for developing cysteine-reactive SAHBs as a therapeutic strategy to inhibit BFL-1 and reactivate apoptosis in cancer. This work has yielded two constructs with distinct properties that could be leveraged as therapeutic agents in different disease contexts: BIM $SAHB_A$-3, which displays covalent reactivity towards BFL-1 and retains non-covalent affinity for MCL-1 (Chapter II), and D-NA-NOXA SAHB-15 R31E, which demonstrates exclusive, covalent selectivity for BFL-1 (Chapter III).

These stapled peptide inhibitors expand the chemical toolbox for modulating BCL-2 family proteins for therapeutic benefit in cancer by targeting individual or multiple family members.

Given the striking increase in melanoma cell apoptosis observed in response to a cysteine-reactive versus non-covalent BIM SAHB (Chapter II), we plan to compare the efficacy of BIM SAHB$_A$-3 to BIM SAHB$_{A1}$ in an A375P xenograft model. Although BIM and BID SAHBs have demonstrated anti-tumor activity in various mouse xenograft models of hematologic cancer[38,39], the efficacy of BCL-2 family-targeting stapled peptides has not been evaluated in solid tumors to date. Indeed, the evaluation of single-agent activity of BIM SAHB$_A$-3 versus BIM SAHB$_{A1}$ in inhibiting melanoma tumor progression could provide compelling evidence in support of further preclinical development of the chimeric stapled peptide strategy. An *in vivo* study that includes toxicology analysis would also serve to validate the specificity of cysteine-reactive BIM SAHB$_A$-3, which showed little off-target activity in cultured cells. Comparing the pharmacokinetics and biodistribution of BIM SAHB$_A$-3 to BIM SAHB$_{A1}$ would also provide insight into the relative pharmacologic benefits and liabilities of non-covalent versus covalent targeting *in vivo*. We envision extending these studies to assess stapled peptide combinations with other anti-melanoma agents such as the BRAF inhibitor vemurafanib, since BFL-1 upregulation has been implicated as the mechanism underyling chemoresistance to BRAF inhibition in BRAF^{V600E}-mutant melanoma cells[1].

Based on our discovery of a BFL-1/ATM co-dependency in AML (Chapter III), we also plan to test our lead covalent stapled peptide inhibitors of BFL-1 in combination with a small molecule ATM inhibitor to assess for synergy in AML xenograft models. For

example, an initial *in vivo* experiment could involve measuring the anti-tumor activity of D-NA-NOXA SAHB-15 R31E and the ATM inhibitor AZD0156[40] in a U937 xenograft model, both singly and in combination. Given the increasing use of venetoclax to target BCL-2 in cancer, it is prudent to anticipate chemoresistance by upregulation of MCL-1 and/or BFL-1, which is frequently observed in cell culture upon prolonged treatment with ABT-737[2,5]. Thus, studies that evaluate our new BFL-1 inhibitors as single agents and in combination in mouse cancer models will be important to address potential venetoclax resistance. Such studies would also serve to validate cancer target co-dependencies, as informed by genome-wide CRISPR-Cas9 dependency screening[41], and determine if drug synergies predicted by the Cancer Dependency Map and observed in cell culture co-treatments extend to the *in vivo* context. Thus, advancing covalent SAHBs to *in vivo* testing marks the critical next step in evaluating the clinical translation potential of covalent stapled peptide inhibitors for cancer treatment.

Physiological Role of BFL-1 Cys55 as a Redox Sensor

The presence of a unique cysteine in the canonical BH3-binding groove of BFL-1 provided a selectivity factor for precision covalent targeting by acrylamide-bearing stapled peptide inhibitors. However, the biological significance of this fortuitous juxtaposition between cysteines in NOXA and BFL-1 remains unknown. The proximity of BFL-1 Cys55 to Cys25 of the NOXA BH3 domain, as well as the ability of a NOXA SAHB to form a disulfide bond with BFL-1 *in vitro* (Chapter II), raises the question of whether this disulfide interaction can form under physiological conditions and whether it serves a regulatory function. Although a disulfide bond was not observed in the crystal

structure of the BFL-1/NOXA BH3 complex (PDB: 3MQP), the experimental conditions included a reducing agent, which would preclude disulfide bond formation. Our results prompted us to hypothesize that reactive oxygen species (ROS) could potentially induce apoptosis by enforcing disulfide bond formation between NOXA and BFL-1, thereby inhibiting the anti-apoptotic activity of a key BCL-2 family protein. Indeed, this mechanism could provide a link between ROS sensing and apoptosis at the level of the mitochondria.

Reactive oxygen species (ROS) can serve as second messengers in diverse cellular contexts and can influence the apoptotic response[42]. For example, hydrogen peroxide (H_2O_2) is generated as a normal byproduct of aerobic respiration, and is also produced by exogenous insults, such as radiation and chemical exposure[43]. H_2O_2 signaling can trigger seemingly contradictory outcomes depending on its concentration and biological context; whereas low levels of H_2O_2 have been shown to stimulate anti-oxidants to protect against DNA damage, high levels of H_2O_2 trigger the expression of pro-oxidants, leading to apoptosis induction[44]. On a molecular level, H_2O_2 acts as a secondary messenger through chemical modification of free cysteine residues, promoting either direct oxidation or inducing disulfide bond formation, which in turn alters protein function[45].

The influence of ROS on apoptotic regulation and cellular responses has been examined across a broad range of ROS levels[42,45]. For example, ROS can exert a pro-apoptotic effect through the oxidation of cardiolipin, resulting in dissociation of cytochrome *c* and disulfide bond formation between APAF-1 and pro-caspase-9, which in turn leads to auto-activation and cleavage[42,43]. High levels of ROS can activate

signaling pathways upstream of the BCL-2 family, such as the JNK, ATM, and AMPK pathways, which can upregulate pro-apoptotic proteins like NOXA, PUMA, and BAX, and also directly phosphorylate and thereby modulate BCL-2 family proteins[42,45]. Whether or not ROS can directly regulate BCL-2 family proteins through oxidation has not been fully explored.

A number of findings point to a link between ROS and BFL-1 regulation. Sub-lethal doses of H_2O_2 have been shown to upregulate BFL-1 mRNA and protein levels in Jurkat cells via the NF-κB pathway, protecting against Fas-mediated apoptosis[46]. This signaling response could represent a physiological defensive mechanism in T cells, which are often exposed to ROS through granulocyte-derived H_2O_2 in the inflammatory microenvironment[47]. Nevertheless, cells succumb to apoptosis in response to higher doses of H_2O_2 even though elevated BFL-1 expression is sustained, suggesting that once a certain threshold of oxidative stress is breached, BFL-1 can no longer maintain cell survival. Whereas elevated ROS levels can induce the expression of pro-apoptotic proteins[48], it is plausible that oxidative stress could also promote disulfide bond formation between NOXA BH3 Cys25 and BFL-1 Cys55, resulting in a stably-inhibited complex. Intriguingly, NOXA expression is induced by hypoxia and ROS, and NOXA is required for H_2O_2-induced apoptotic cell death[49,50].

Although we observe disulfide bond formation between recombinant BFL-1 and NOXA SAHBs, capturing a covalent complex between NOXA and BFL-1 *in situ* requires exploration. One experimental approach could involve expressing HA-tagged full-length BFL-1, bearing either the wild-type C55 or a C55S mutation, in Jurkat T cells, followed by treatment with low and high doses of H_2O_2 to simulate a range of oxidative stress

conditions. The cells could then be harvested, lysed, and subjected to HA-immunoprecipitation followed by Western blotting for NOXA under non-reducing and non-denaturing conditions. If present, a disulfide bond between BFL-1 and NOXA would remain intact, and Western blotting would reveal an additional NOXA-reactive band at a higher molecular weight due to the covalent complex with BFL-1. As a measure of specificity, such findings would not be expected for the HA-BFL-1 C55S condition. Capturing the native complex using immunoprecipitation and mass spectrometry methods, in diverse cell types and stress conditions, would also be important to confirm physiologic relevance. If proven correct, an ROS-induced and disulfide-based mechanism for BFL-1 inhibition would represent a novel mode of BCL-2 family regulation under conditions of oxidative stress.

In addition to intermolecular disulfide bond formation between BFL-1 and NOXA BH3, it is conceivable that BFL-1 could be further regulated by an intramolecular disulfide bond between C55 and a cysteine residue within its C-terminal helix. The C-terminal α9 helix of BFL-1 has not been fully characterized, although it displays significant amphipathic character and appears critical for BFL-1 localization to the mitochondria[51]. In pro-apoptotic BAX and anti-apoptotic BCL-w and BCL-X_L, the C-terminal helices can be sequestered in the canonical BH3-binding groove, enforcing a cytosolic localization[52-54]. Indeed, BFL-1 has been reported to toggle between cytosolic and mitochondrial localizations; the mechanistic basis for these findings may derive from alternate BFL-1 conformations, one with the C-terminal helix occupying the hydrophobic groove (cytosol) and the other with the helix released and inserted into the mitochondrial outer membrane (mitochondria)[51]. The full-length structure of BFL-1 has

yet to be solved but HADDOCK[55] protein docking of the C-terminal helix modeled by FlexPep[56] into the apo BFL-1ΔC crystal structure (PDB: 5WHI) aligns the α9 helix in the BH3-binding groove and predicts a juxtaposition between Cys175 and Cys55 at a distance of 5.6 Å, which could support disulfide bond formation (**Figure 4.2**). Of note, the C-terminal helix binds in the opposite N-to-C terminus orientation in the groove compared to the observed BH3 domain interactions. Although mostly amphipathic, the BFL-1 α9 helix contains numerous hydrophilic residues that may interrupt its proposed hydrophobic interaction surface, potentially lowering interaction affinity compared to BH3 domain binding and allowing for toggling between cytosolic and mitochondrial conformations.

To determine whether such an auto-inhibitory mechanism for BFL-1 regulation exists, biochemical and cellular experiments will be geared toward determining whether intramolecular disulfide bond formation is chemically feasible, and if so, whether covalent interaction regulates BFL-1 localization and/or anti-apoptotic activity. By analogy to the development of NOXA SAHBs to examine intermolecular disulfide bond formation with BFL-1 (Chapter II), stapled peptides modeled after the C-terminal helix of BFL-1, containing C175 or a C175S mutation, can be synthesized to evaluate disulfide bond formation *in vitro*. If *in vitro* disulfide bond formation indeed occurs, the hypothesis could then be explored in a cellular context using GFP-BFL-1 constructs bearing C55, C55S, C175S, or C55S/C175S residues. Fluorescence microscopy analysis could be used to compare the intracellular localization of the distinct GFP-BFL-1 constructs at baseline and upon exposure to oxidative stress. In this manner, a potential role of intramolecular disulfide bond formation between α9 and the BH3-binding groove in

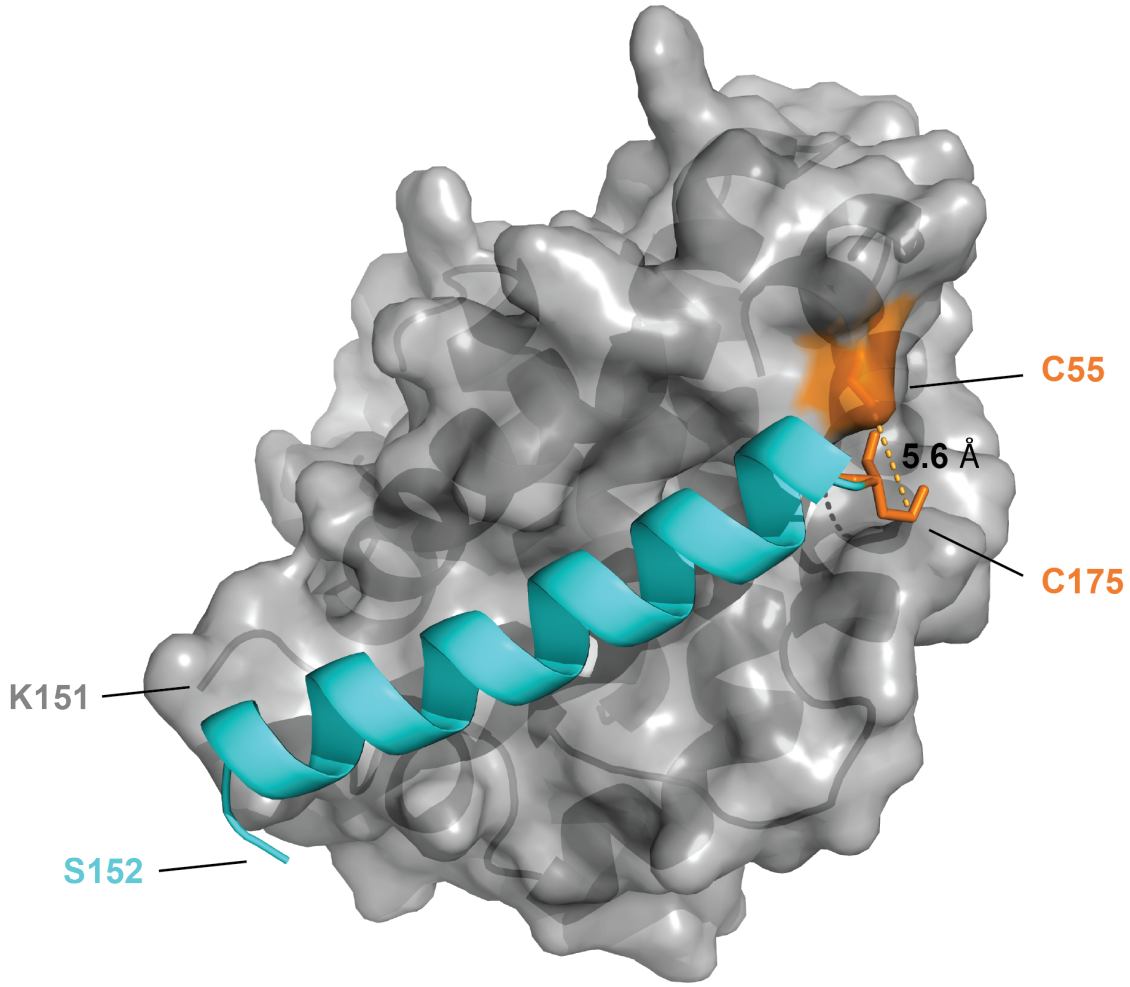

Figure 4.2 *Disposition of the BFL-1 α9 helix upon computational docking into the canonical BH3-binding groove of BFL-1.*

HADDOCK and FlexPep docking of the C-terminal α9 helix of BFL-1 into the crystal structure of BFL-1ΔC (PDB: 5WHI) predicts an alignment of C175 with C55 that may be amenable to intramolecular disulfide bond formation.

regulating BFL-1 localization could be explored. In addition, the relative capacity of the individual constructs to protect against oxidative stress-induced apoptosis could potentially link intracellular localization with anti-apoptotic activity. Whereas expression of cysteine-mutant BFL-1 would be expected to confer a survival advantage, BFL-1 auto-inhibition through oxidative stress-induced intramolecular disulfide bond formation would be expected to impair anti-apoptotic activity. Thus, investigating the potential physiologic significance of inter- and intra-molecular disulfide bond formation involving C55 could reveal a new dimension of anti-apoptotic regulation by BFL-1 (**Figure 4.3**).

Conclusions

In summary, we have taken a novel approach to selective targeting of BFL-1, a BCL-2 family protein linked to the pathogenesis and chemoresistance of melanoma, leukemia, and lymphoma. Given the clinical success of BCL-2 targeting in cancer, advancing therapeutic strategies to block BFL-1 remains a high priority. By combining the advantages of stapled peptide α-helices modeled after natural pro-apoptotic domains with the cysteine-targeting efficiency of electrophilic warheads, we developed the first exquisitely selective, covalent inhibitors of BFL-1. Using multidisciplinary approaches, we demonstrated the selective targeting, cellular penetrance, and pro-apoptotic activity of our novel constructs in BFL-1-driven melanoma and AML. In uncovering a novel BFL-1/ATM co-dependency in AML, we further informed the potential utility of combining BFL-1 and ATM inhibitors to synergistically subvert apoptotic resistance in AML. Whereas renewed interest in small-molecule covalent inhibitors has successfully led to a series of new drugs to block the deep hydrophobic pockets of oncogenic kinases,

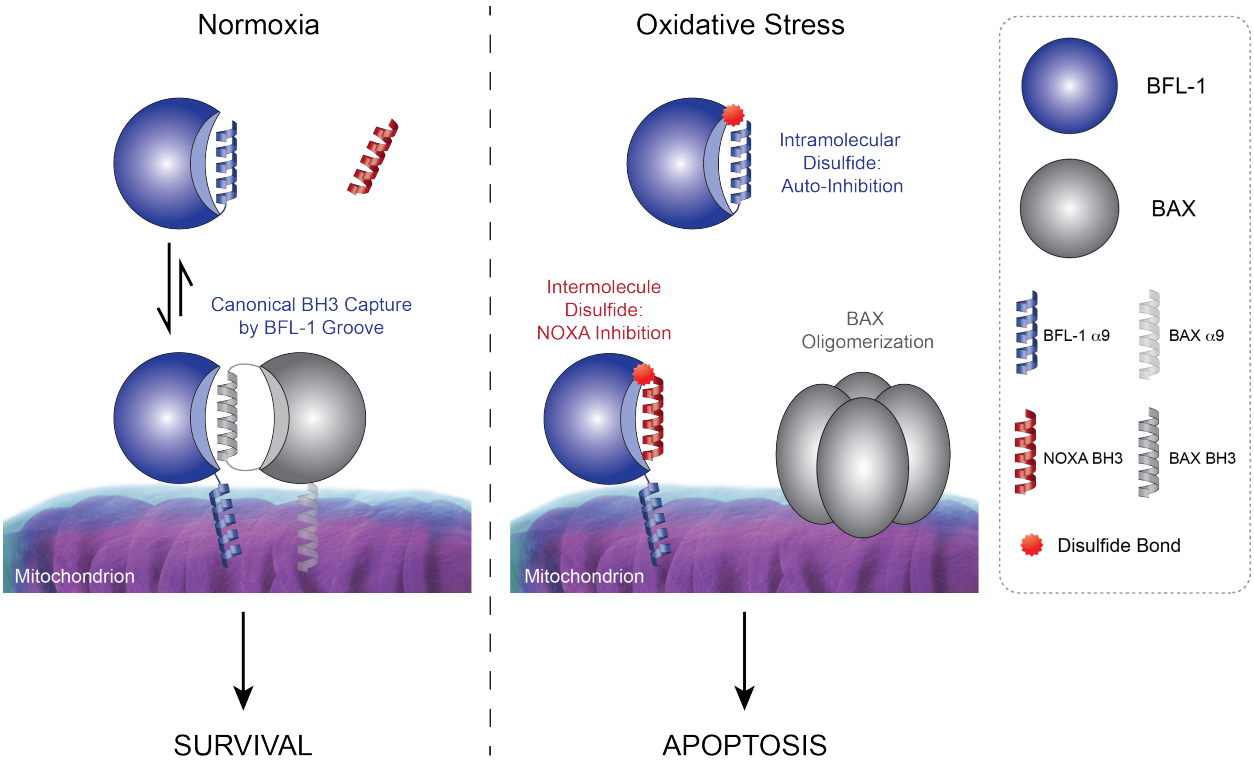

Figure 4.3 *Model of BFL-1 regulation by oxidative stress*.

BFL-1 localization and anti-apoptotic activity could be regulated by inter- and intramolecular disulfide bond formation in response to oxidative stress. Under normoxic conditions, BFL-1 may toggle between cytosolic and mitochondrial localizations based on the disposition of its C-terminal helical domain. Under conditions of oxidative stress, BFL-1 could potentially be inhibited by two mechanisms: (1) intermolecular disulfide bond formation between BFL-1 C55 and NOXA C25 at the mitochondria and (2) intramolecular disulfide bond formation between BFL-1 C55 and C175 in the cytosol.

covalent stapled peptide inhibitors have the potential to address a series of large and previously undruggable protein interfaces with strikingly selective reactivity, as exemplified here by covalent inhibition of anti-apoptotic BFL-1 by electrophilic warhead-bearing stapled BH3 peptides.

REFERENCES

1. Haq, R. *et al.* BCL2A1 is a lineage-specific antiapoptotic melanoma oncogene that confers resistance to BRAF inhibition. *Proc. Natl. Acad. Sci. U.S.A.* **110,** 4321–4326 (2013).

2. Yecies, D., Carlson, N. E., Deng, J. & Letai, A. Acquired resistance to ABT-737 in lymphoma cells that up-regulate MCL-1 and BFL-1. *Blood* **115,** 3304–3313 (2010).

3. Mahadevan, D. *et al.* Transcript profiling in peripheral T-cell lymphoma, not otherwise specified, and diffuse large B-cell lymphoma identifies distinct tumor profile signatures. *Mol. Cancer Ther.* **4,** 1867–1879 (2005).

4. Fan, G. *et al.* Defective ubiquitin-mediated degradation of antiapoptotic Bfl-1 predisposes to lymphoma. *Blood* **115,** 3559–3569 (2010).

5. Vogler, M. *et al.* Concurrent up-regulation of BCL-XL and BCL2A1 induces approximately 1000-fold resistance to ABT-737 in chronic lymphocytic leukemia. *Blood* **113,** 4403–4413 (2009).

6. Lucas, K. M. *et al.* Modulation of NOXA and MCL-1 as a Strategy for Sensitizing Melanoma Cells to the BH3-Mimetic ABT-737. *Clinical Cancer Research* **18,** 783–795 (2012).

7. Mathieu, A.-L. *et al.* Identification of Small Inhibitory Molecules Targeting the Bfl-1 Anti-Apoptotic Protein That Alleviates Resistance to ABT-737. *J Biomol Screen* **19,** 1035–1046 (2014).

8. Bird, G. H., Bernal, F., Pitter, K. & Walensky, L. D. Synthesis and biophysical characterization of stabilized alpha-helices of BCL-2 domains. *Meth. Enzymol.* **446,** 369–386 (2008).

9. Pitter, K., Bernal, F., LaBelle, J. & Walensky, L. D. Dissection of the BCL-2 family signaling network with stabilized alpha-helices of BCL-2 domains. *Meth. Enzymol.* **446,** 387–408 (2008).

10. Meric-Bernstam, F. *et al.* Phase I trial of a novel stapled peptide ALRN-6924 disrupting MDMX- and MDM2-mediated inhibition of WT p53 in patients with solid tumors and lymphomas. *JCO* **35,** 2505–2505 (2017).

11. Chang, Y. S. *et al.* Stapled α-helical peptide drug development: a potent dual inhibitor of MDM2 and MDMX for p53-dependent cancer therapy. *Proc. Natl. Acad. Sci. U.S.A.* **110,** E3445–54 (2013).

12. Verdine, G. L. & Walensky, L. D. The Challenge of Drugging Undruggable Targets in Cancer: Lessons Learned from Targeting BCL-2 Family Members. *Clinical Cancer Research* **13,** 7264–7270 (2007).

13. Cromm, P. M., Spiegel, J. & Grossmann, T. N. Hydrocarbon Stapled Peptides as Modulators of Biological Function. *ACS Chem. Biol.* **10,** 1362–1375 (2015).

14. Singh, J., Petter, R. C., Baillie, T. A. & Whitty, A. The resurgence of covalent drugs. *Nat Rev Drug Discov* **10,** 307–317 (2011).

15. Bauer, R. A. Covalent inhibitors in drug discovery: from accidental discoveries to avoided liabilities and designed therapies. *Drug Discovery Today* **20,** 1061–1073 (2015).

16. Burger, J. A. *et al.* Ibrutinib as Initial Therapy for Patients with Chronic Lymphocytic Leukemia. *N Engl J Med* **373,** 2425–2437 (2015).

17. Solca, F. *et al.* Target binding properties and cellular activity of afatinib (BIBW 2992), an irreversible ErbB family blocker. *Journal of Pharmacology and Experimental Therapeutics* **343,** 342–350 (2012).

18. Singh, J., Petter, R. C., Baillie, T. A. & Whitty, A. The resurgence of covalent drugs. *Nat Rev Drug Discov* **10,** 307–317 (2011).

19. Allen, B. L. & Taatjes, D. J. The Mediator complex: a central integrator of transcription. *Nat Rev Mol Cell Biol* **16,** 155–166 (2015).

20. Kise, Y. *et al.* A short peptide insertion crucial for angiostatic activity of human tryptophanyl-tRNA synthetase. *Nat Struct Mol Biol* **11,** 149–156 (2004).

21. Kitagawa, D. *et al.* Release of RASSF1C from the nucleus by Daxx degradation links DNA damage and SAPK/JNK activation. *The EMBO Journal* **25,** 3286–3297 (2006).

22. Visscher, M., Arkin, M. R. & Dansen, T. B. Covalent targeting of acquired cysteines in cancer. *Curr Opin Chem Biol* **30,** 61–67 (2016).

23. Margarit, S. M., Sondermann, H., Hall, B. E. & Nagar, B. Structural evidence for feedback activation by Ras· GTP of the Ras-specific nucleotide exchange factor SOS. *Cell* **112,** 685–695 (2003).

24. Leshchiner, E. S. *et al.* Direct inhibition of oncogenic KRAS by hydrocarbon-stapled SOS1 helices. *Proc. Natl. Acad. Sci. U.S.A.* **112,** 1761–1766 (2015).

25. de Araujo, A. D., Lim, J., Good, A. C., Skerlj, R. T. & Fairlie, D. P. Electrophilic Helical Peptides That Bond Covalently, Irreversibly, and Selectively in a Protein-Protein Interaction Site. *ACS Med. Chem. Lett.* **8,** 22–26 (2017).

26. Barile, E. *et al.* hBfl-1/hNOXA Interaction Studies Provide New Insights on the Role of Bfl-1 in Cancer Cell Resistance and for the Design of Novel Anticancer Agents. *ACS Chem. Biol.* **12,** 444–455 (2017).

27. Souers, A. J. *et al.* ABT-199, a potent and selective BCL-2 inhibitor, achieves antitumor activity while sparing platelets. *Nat Med* **19,** 202–208 (2013).

28. Kotschy, A. *et al.* The MCL1 inhibitor S63845 is tolerable and effective in diverse cancer models. *Nature* **538,** 477–482 (2016).

29. Oltersdorf, T. *et al.* An inhibitor of Bcl-2 family proteins induces regression of solid tumours. *Nature* **435,** 677–681 (2005).

30. Bruncko, M. *et al.* Studies Leading to Potent, Dual Inhibitors of Bcl-2 and Bcl-xL. *J. Med. Chem.* **50,** 641–662 (2007).

31. Zhai, D. *et al.* High-Throughput Fluorescence Polarization Assay for Chemical Library Screening against Anti-Apoptotic Bcl-2 Family Member Bfl-1. *J Biomol Screen* **17,** 350–360 (2012).

32. Erlanson, D. A. *et al.* Site-directed ligand discovery. *Proc. Natl. Acad. Sci. U.S.A.* **97,** 9367–9372 (2000).

33. Ostrem, J. M., Peters, U., Sos, M. L., Wells, J. A. & Shokat, K. M. K-Ras(G12C) inhibitors allosterically control GTP affinity and effector interactions. *Nature* **503,** 548–551 (2013).

34. Ostrem, J. M. L. & Shokat, K. M. Direct small-molecule inhibitors of KRAS: from structural insights to mechanism-based design. *Nat Rev Drug Discov* **15,** 771–785 (2016).

35. Patricelli, M. P. *et al.* Selective Inhibition of Oncogenic KRAS Output with Small Molecules Targeting the Inactive State. *Cancer Discovery* **6,** 316–329 (2016).

36. Janes, M. R. *et al.* Targeting KRAS Mutant Cancers with a Covalent G12C-Specific Inhibitor. *Cell* **172,** 578–589.e17 (2018).

37. Chang, Y. S. *et al.* Stapled α-helical peptide drug development: a potent dual inhibitor of MDM2 and MDMX for p53-dependent cancer therapy. *Proc. Natl. Acad. Sci. U.S.A.* **110,** E3445–54 (2013).

38. Walensky, L. D. *et al.* Activation of apoptosis in vivo by a hydrocarbon-stapled BH3 helix. *Science* **305,** 1466–1470 (2004).

39. LaBelle, J. L. *et al.* A stapled BIM peptide overcomes apoptotic resistance in hematologic cancers. *J. Clin. Invest.* **122,** 2018–2031 (2012).

40. Degorce, S. L. *et al.* Discovery of Novel 3-Quinoline Carboxamides as Potent, Selective, and Orally Bioavailable Inhibitors of Ataxia Telangiectasia Mutated (ATM) Kinase. *J. Med. Chem.* **59,** 6281–6292 (2016).

41. Meyers, R. M. *et al.* Computational correction of copy-number effect improves specificity of CRISPR-Cas9 essentiality screens in cancer cells. *bioRxiv* 1–15 (2017).

42. Wu, C.-C. & Bratton, S. B. Regulation of the Intrinsic Apoptosis Pathway by Reactive Oxygen Species. *Antioxidants & Redox Signaling* **19,** 546–558 (2013).

43. Galadari, S., Rahman, A., Pallichankandy, S. & Thayyullathil, F. Reactive oxygen species and cancer paradox: To promote or to suppress? *Free Radical Biology and Medicine* **104,** 144–164 (2017).

44. Veal, E. A., Day, A. M. & Morgan, B. A. Hydrogen Peroxide Sensing and Signaling. *Molecular Cell* **26,** 1–14 (2007).

45. Lennicke, C., Rahn, J., Lichtenfels, R., Wessjohann, L. A. & Seliger, B. Hydrogen peroxide – production, fate and role in redox signaling of tumor cells. *Cell Communication and Signaling* 1–19 (2015).

46. Kim, H., Kim, Y.-N., Kim, H. & Kim, C.-W. Oxidative stress attenuates Fas-mediated apoptosis in Jurkat T cell line through Bfl-1 induction. *Oncogene* **24,** 1252–1261 (2004).

47. Schmielau, J. & Finn, O. J. Activated granulocytes and granulocyte-derived hydrogen peroxide are the underlying mechanism of suppression of T-cell function in advanced cancer patients. *Cancer Research* **61,** 4756–4760 (2001).

48. Montero, A. J. & Jassem, J. Cellular redox pathways as a therapeutic target in the treatment of cancer. *Drugs* **71,** 1385–1396 (2011).

49. Guikema, J. E., Amiot, M. & Eldering, E. Exploiting the pro-apoptotic function of NOXA as a therapeutic modality in cancer. *Expert Opinion on Therapeutic Targets* **21,** 767–779 (2017).

50. Aikawa, T., Shinzawa, K., Tanaka, N. & Tsujimoto, Y. Noxa is necessary for hydrogen peroxide-induced caspase-dependent cell death. *FEBS Letters* **584,** 681–688 (2010).

51. Brien, G. *et al.* C-terminal residues regulate localization and function of the antiapoptotic protein Bfl-1. *J. Biol. Chem.* **284,** 30257–30263 (2009).

52. Denisov, A. Y. *et al.* Solution Structure of Human BCL-w. *Journal of Biological Chemistry* **278,** 21124–21128 (2003).

53. Suzuki, M., Youle, R. J. & Tjandra, N. Structure of Bax: coregulation of dimer formation and intracellular localization. *Cell* **103,** 645–654 (2000).

54. Yao, Y. *et al.* Conformation of BCL-XL upon Membrane Integration. *Journal of Molecular Biology* **427,** 2262–2270 (2015).

55. van Zundert, G. C. P. *et al.* The HADDOCK2.2 Web Server: User-Friendly Integrative Modeling of Biomolecular Complexes. *Journal of Molecular Biology* **428,** 720–725 (2016).

56. London, N., Raveh, B., Cohen, E., Fathi, G. & Schueler-Furman, O. Rosetta FlexPepDock web server--high resolution modeling of peptide-protein interactions. *Nucleic Acids Res.* **39,** W249–53 (2011).

Appendix

Supplemental Information

Supplemental Table 1. *Stapled peptide compositions utilized in Chapter II.*

Peptide	N-terminus	Sequence	C-terminus	MW	(M+3)/3	Figures
NOXA SAHB$_A$ WT (aa 19-43)	FITC-βAla-	AELEVECATQLRXJGDXLNFRQKLL		3403.1	1135.3	2.3
NOXA SAHB$_A$ WT	Btn-PEG-βAla-	AELEVECATQLRXFGDXLNFRQKLL		3556.0	1186.3	2.2
NOXA SAHB$_A$ C25S	FITC-βAla-	AELEVESATQLRXFGDXLNFRQKLL		3387.0	1130.1	2.3
NOXA SAHB$_A$ C25S	Btn-PEG-βAla-	AELEVESATQLRXFGDXLNFRQKLL		3539.9	1181.1	2.2
NOXA SAHB$_A$-1	1	EVESATQLRXFGDXLNFRQKLLK		2892.6	965.3	2.4
NOXA SAHB$_A$-2	2	EVESATQLRXFGDXLNFRQKLLK		2906.6	970.0	2.4
NOXA SAHB$_A$-3	3	EVESATQLRXFGDXLNFRQKLL		2778.4	927.2	2.4, 2.6
NOXA SAHB$_A$-3	3	EVESATQLRXFGDXLNFRQKLL	Lys(biotin)	3132.6	1045.2	2.5, 2.7, 2.8
NOXA SAHB$_A$-4	4	EVESATQLRXFGDXLNFRQKLLK		2906.6	969.9	2.4
NOXA SAHB$_A$-5	5	EVESATQLRXFGDXLNFRQKLLK		2892.6	965.2	2.4
NOXA SAHB$_A$-6	6	EVESATQLRXFGDXLNFRQKLLK		2892.6	965.3	2.4
NOXA SAHB$_A$-7	7	EVESATQLRXFGDXLNFRQKLLK		2852.5	951.8	2.4
NOXA SAHB$_A$-8	8	EVESATQLRXFGDXLNFRQKLLK		2795.4	932.9	2.4
NOXA SAHB$_A$ (aa 22-43)	Ac	EVESATQLRXFGDXLNFRQKLL		2655.3	886.0	2.6
NOXA SAHB$_A$	Ac	EVESATQLRXFGDXLNFRQKLL	Lys(biotin)	3009.4	1004.2	2.5, 2.7
BIM SAHB$_A$-1	1	IAQELRXIGDXFNAYYARK		2428.0	810.5	2.4
BIM SAHB$_A$-2	2	IAQELRXIGDXFNAYYARK		2442.0	815.0	2.4
BIM SAHB$_A$-3	3	IAQELRXIGDXFNAYYARR		2469.3	824.4	2.4, 2.6, 2.7-12
BIM SAHB$_A$-3	3	IAQELRXIGDXFNAYYARR	Lys(biotin)	2823.5	942.3	2.5, 2.7-8, 2.13
BIM SAHB$_A$-4	4	IAQELRXIGDXFNAYYARK		2442.0	815.0	2.4
BIM SAHB$_A$-5	5	IAQELRXIGDXFNAYYARK		2428.0	810.3	2.4
BIM SAHB$_A$-6	6	IAQELRXIGDXFNAYYARK		2428.0	810.3	2.4
BIM SAHB$_A$-7	7	IAQELRXIGDXFNAYYARK		2388.0	797.1	2.4
BIM SAHB$_A$-8	8	IAQELRXIGDXFNAYYARK		2330.9	778.0	2.4
BIM SAHB$_A$ (aa 148-166)	Ac	IAQELRXIGDXFNAYYARR		2346.9	783.3	2.7
BIM SAHB$_A$	Ac	IAQELRXIGDXFNAYYARR	Lys(biotin)	2701.1	901.4	2.5, 2.7-8, 2.13
BIM SAHB$_A$ (aa 146-166)	FITC-βAla-	IWIAQELRXIGDXFNAYYARR		3064.3	1022.4	2.8
BIM SAHB$_A$-3	FITC-Cyste-3-	IAQELRXIGDXFNAYYARR		2935.5	979.8	2.8, 2.13
BIM SAHB$_{A1}$ (aa 146-166)	Ac	IWIAQELRXIGDXFNAYYARR		2646.3	883.1	2.10-2.12

1: (S)-1-acryloylpyrrolidine-3-carboxamide; **2**: 1-acryloylpiperidine-4-carboxamide; **3**. (R)-1 acryloylpiperidine-3-carboxamide; **4**: (S)-1-acryloylpiperidine-3- carboxamide; **5**: (S)-1-acryloylpyrrolidine-2- carboxamide; **6**: (R)-1-acryloylpyrrolidine-2- carboxamide; **7**: (E)-4-(dimethylamino)but-2-enamide; **8**: acrylamide.

Supplemental Table 2. *Stapled peptide compositions utilized in Chapter III*.

Peptide	N-terminus	Sequence	C-terminus	MW	(M+3)/3	Figures
NOXA SAHB-1	D-NA	XTQLXRFGDKLNFRQ		2037	679.8	3.3
NOXA SAHB-2	D-NA	AXQLRXFGDKLNFRQ		2007	669.8	3.3
NOXA SAHB-3	D-NA	ATXLRRXGDKLNFRQ		1989	663.8	3.3
NOXA SAHB-4	D-NA	ATQXRRFXDKLNFRQ		2094	698.9	3.3
NOXA SAHB-5	D-NA	ATQLXRFGXKLNFRQ		1993	665.2	3.3
NOXA SAHB-6	D-NA	ATQLRXFGDXLNFRQ		1979	660.8	3.3
NOXA SAHB-7	D-NA	ATQLRRXGDKXNFRQ		2003	668.8	3.3
NOXA SAHB-8	D-NA	ATQLRRFXDKLXFRQ		2093	698.5	3.3
NOXA SAHB-9	D-NA	ATQLRRFGXKLNXRQ		2001	668.1	3.3
NOXA SAHB-10	D-NA	ATQLRRFGDXLNFXQ		1981	661.5	3.3
NOXA SAHB-11	D-NA	ATQLRRFGDKXNFRX		2022	675.1	3.3
NOXA SAHB-12	D-NA	ATQLRRFGDKLXFRQX		2150	717.5	3.3
NOXA SAHB-13	D-NA	8TQLRRFXDKLNFRQ		2178	726.9	3.3
NOXA SAHB-14	D-NA	A8QLRRFGXKLNFRQ		2090	697.5	3.3
NOXA SAHB-15	D-NA	AT8LRRFGDXLNFRQ		2050	684.2	3.3
NOXA SAHB-16	D-NA	ATQ8RRFGDKXNFRQ		2080	694.2	3.3
NOXA SAHB-17	D-NA	ATQL8RFGDKLXFRQ		2036	679.5	3.3
NOXA SAHB-18	D-NA	ATQLR8FGDKLNXRQ		2002	668.5	3.3
NOXA SAHB-19	D-NA	ATQLRR8GDKLNFXQ		2002	668.5	3.3
NOXA SAHB-20	D-NA	ATQLRRF8DKLNFRX		2121	707.9	3.3
NOXA SAHB-15 A26E	D-NA	ET8LRRFGDXLNFRQ		2108	703.5	3.4
NOXA SAHB-15 T27A	D-NA	AA8LRRFGDXLNFRQ		2020	674.2	3.4
NOXA SAHB-15 L29A	D-NA	AT8ARRFGDXLNFRQ		2008	670.2	3.4
NOXA SAHB-15 R30A	D-NA	AT8LARFGDXLNFRQ		1964	655.8	3.4
NOXA SAHB-15 R31A	D-NA	AT8LRAFGDXLNFRQ		1964	655.8	3.4
NOXA SAHB-15 F32A	D-NA	AT8LRRAGDXLNFRQ		1973	658.8	3.4, 3.8-10, 3.12
NOXA SAHB-15 G33A	D-NA	AT8LRRFADXLNFRQ		2064	688.9	3.4
NOXA SAHB-15 D34A	D-NA	AT8LRRFGAXLNFRQ		2006	669.5	3.4
NOXA SAHB-15 L36A	D-NA	AT8LRRFGDXANFRQ		2008	670.2	3.4
NOXA SAHB-15 N37A	D-NA	AT8LRRFGDXLAFRQ		2007	669.9	3.4
NOXA SAHB-15 F38A	D-NA	AT8LRRFGDXLNARQ		1974	659.0	3.4
NOXA SAHB-15 R39A	D-NA	AT8LRRFGDXLNFAQ		1965	656.0	3.4
NOXA SAHB-15 Q40A	D-NA	AT8LRRFGDXLNFRA		1993	665.2	3.4
NOXA SAHB-15 R31E	D-NA	AT8LREFGDXLNFRQ		2025	675.8	3.5, 3.8
NOXA SAHB-15 R39E	D-NA	AT8LRRFGDXLNFEQ		2025	675.8	3.5
NOXA SAHB-15 R31E	Ac	AT8LREFGDXLNFRQ	Lys(biotin)	2250	751.0	3.6, 3.7
NOXA SAHB-15 R31E	D-NA	AT8LREFGDXLNFRQ	Lys(biotin)	2374	792.3	3.6, 3.7
NOXA SAHB-15 F32A	Ac	AT8LRRAGDXLNFRQ	Lys(biotin)	2201	734.7	3.6, 3.7
NOXA SAHB-15 F32A	D-NA	AT8LRRAGDXLNFRQ	Lys(biotin)	2325	776.0	3.6, 3.7
BID BH3	FITC-βAla	DIIRNIARHLAQVGDSBDRSI		2820	941.1	3.9, 3.10
NOXA $SAHB_A$	Ac	EVESATQLRXFGDXLNFRQKLL		2655	886.0	3.10
NOXA $SAHB_A$-3	D-NA	EVESATQLRXFGDXLNFRQKLL		2779	927.2	3.10

D-NA: D-nipecotic acid acrylamide, or (R)-1 acryloylpiperidine-3-carboxamide; **Ac**: acetyl; **X**: S-pentenyl alanine; **8**: R-octenyl alanine.